Sutherland, R., Dickens, G.R., Blum, P., and the Expedition 371 Scientists
Proceedings of the International Ocean Discovery Program Volume 371
publications.iodp.org

https://doi.org/10.14379/iodp.proc.371.101.2019

Expedition 371 summary[1]

R. Sutherland, G.R. Dickens, P. Blum, C. Agnini, L. Alegret, G. Asatryan, J. Bhattacharya, A. Bordenave, L. Chang, J. Collot, M.J. Cramwinckel, E. Dallanave, M.K. Drake, S.J.G. Etienne, M. Giorgioni, M. Gurnis, D.T. Harper, H.-H.M. Huang, A.L. Keller, A.R. Lam, H. Li, H. Matsui, H.E.G. Morgans, C. Newsam, Y.-H. Park, K.M. Pascher, S.F. Pekar, D.E. Penman, S. Saito, W.R. Stratford, T. Westerhold, and X. Zhou[2]

Keywords: International Ocean Discovery Program, IODP, *JOIDES Resolution*, Expedition 371, Site U1506, Site U1507, Site U1508, Site U1509, Site U1510, Site U1511, Tasman Frontier, Zealandia, Reinga, Challenger, Eastern Australian Current, Lord Howe, Murihiku, New Caledonia, Norfolk, Northland, Pacific, Ring of Fire, Tasman, Taranaki, Tonga, Kermadec, Waka Nui, Wanganella, subduction, Early Eocene Climatic Optimum, EECO, Middle Eocene Climatic Optimum, MECO, biogenic bloom, stratigraphy, diagenesis, compaction, volcanism

Contents

Abstract

International Ocean Discovery Program (IODP) Expedition 371 drilled six sites (U1506–U1511) in the Tasman Sea, southwest Pacific, between 27 July and 26 September 2017. The primary goal was to understand Tonga-Kermadec subduction initiation through recovery of Paleogene sediment records. Secondary goals were to understand regional oceanography and climate through intervals of the Cenozoic, especially the Eocene. We recovered 2506 m of cored sediment and volcanic rock in 36.4 days of on-site drilling over a total expedition length of 58 days. The ages of strata at the base of each site were middle Eocene to Late Cretaceous. The cored intervals at five sites (U1506–U1510) sampled mostly nannofossil and foraminiferal ooze or chalk that contained volcanic or volcaniclastic intervals with variable clay content. Paleocene and Cretaceous sections at Site U1509 also contain calcareous clay and claystone. At Site U1511, a sequence of abyssal clay and diatomite was recovered with only minor amounts of carbonate. Wireline logs were collected at Sites U1507 and U1508.

Our results provide the first firm basis for correlating lithostratigraphic units across a substantial part of northern Zealandia, including ties to onshore geology in New Caledonia and New Zealand. All six sites provide new stratigraphic and paleogeographic information that can be put into context through regional seismic stratigraphic interpretation and hence provide constraints on geodynamic models of subduction zone initiation. Evidence from Site U1507 suggests the northern New Caledonia Trough formed during an early stage of Paleogene tectonic change (before 44 Ma). Paleowater depth estimates from Site U1509 indicate that the Cretaceous Fairway-Aotea-Taranaki Basin dramatically deepened (~2000 m) at a similar time. Northern Lord Howe Rise at Site U1506 rose to sea level at ~50 Ma and subsided back to bathyal depths (600–1000 m) by 45 Ma. In contrast, southern Lord Howe Rise, at least near Site U1510, experienced its peak of transient uplift at ~40–30 Ma. A pulse of convergent plate failure took place across the southern part of the region (Sites U1508–U1511) between 45 and 35 Ma. Uplift of Lord Howe Rise was associated with intraplate volcanism, whereas volcanic activity on Norfolk Ridge near Site U1507 started at ~38 Ma and may relate to subduction.

Shipboard observations made using cores and logs represent a substantial gain in fundamental knowledge about northern Zealandia. Prior to Expedition 371, only Deep Sea Drilling Project Sites 206, 207, and 208 had penetrated beneath upper Eocene strata in the region. Our samples and results provide valuable new constraints on geodynamic models of subduction initiation because they reveal the timing of plate deformation, the magnitude and timing of vertical motions, and the timing and type of volcanism. Secondary drilling objectives focused on paleoclimate topics were not fully completed, but significant new records were obtained that should contain information on Cenozoic oceanography and climate in the southwest Pacific.

Introduction

The Tasman Frontier encompasses an extensive, geologically complex, and underexplored area of the ocean between Australia, New Zealand, and New Caledonia (Figure **F1**). It includes a vast

[1] Sutherland, R., Dickens, G.R., Blum, P., Agnini, C., Alegret, L., Asatryan, G., Bhattacharya, J., Bordenave, A., Chang, L., Collot, J., Cramwinckel, M.J., Dallanave, E., Drake, M.K., Etienne, S.J.G., Giorgioni, M., Gurnis, M., Harper, D.T., Huang, H.-H.M., Keller, A.L., Lam, A.R., Li, H., Matsui, H., Morgans, H.E.G., Newsam, C., Park, Y.-H., Pascher, K.M., Pekar, S.F., Penman, D.E., Saito, S., Stratford, W.R., Westerhold, T., Zhou, X., 2019. Expedition 371 summary. *In* Sutherland, R., Dickens, G.R., Blum, P., and the Expedition 371 Scientists, *Tasman Frontier Subduction Initiation and Paleogene Climate*. Proceedings of the International Ocean Discovery Program, 371: College Station, TX (International Ocean Discovery Program). https://doi.org/10.14379/iodp.proc.371.101.2019

[2] **Expedition 371 Scientists' affiliations.**

MS 371-101: Published 2 February 2019

submerged portion of the Zealandia continent (Mortimer et al., 2017) and lies west of the prominent Tonga-Kermadec Trench system. The primary goal of International Ocean Discovery Program (IODP) Expedition 371 was to understand Tonga-Kermadec subduction initiation through recovery of Paleogene sediment records at six new sites across the Tasman Frontier (Figures **F1**, **F2**, **F3**, **F4**).

Subduction systems are primary drivers of plate motions, mantle dynamics, and global geochemical cycles, but little is known about how subduction starts. What are the initial conditions? How do forces and kinematics evolve? What are the short-term consequences and surface signatures: uplift, subsidence, deep-water sedimentary basins, convergence, extension, and volcanism? The early Eocene onset of subduction in the western Pacific was accompanied by a profound global reorganization of tectonic plates, with known plate motions before and after the change (Billen and Gurnis, 2005; Sharp and Clague, 2006; Steinberger et al., 2004; Whittaker et al., 2007). The Izu-Bonin-Mariana (e.g., IODP Expeditions 350, 351, and 352) and Tonga-Kermadec systems contain complementary information about subduction initiation (Figure **F1**), but the southwest Pacific has had little relevant drilling.

Eocene tectonic change occurred at a turning point in Cenozoic climate. Long-term global warming through the Paleocene–Eocene transition culminated in the Early Eocene Climatic Optimum (EECO; ~53–49 Ma), which was followed by overall cooling through the remainder of the Cenozoic (Figure **F5**) (Zachos et al., 2008; Westerhold et al., 2018). The Paleocene and Eocene were also punctuated by an unknown number of geologically brief events of extreme warmth, biological turnover, and geochemical change commonly referred to as "hyperthermals" (Zachos et al., 2008; Westerhold et al., 2018).

Figure F1. Location of Izu-Bonin-Mariana and Tonga-Kermadec subduction systems in western Pacific.

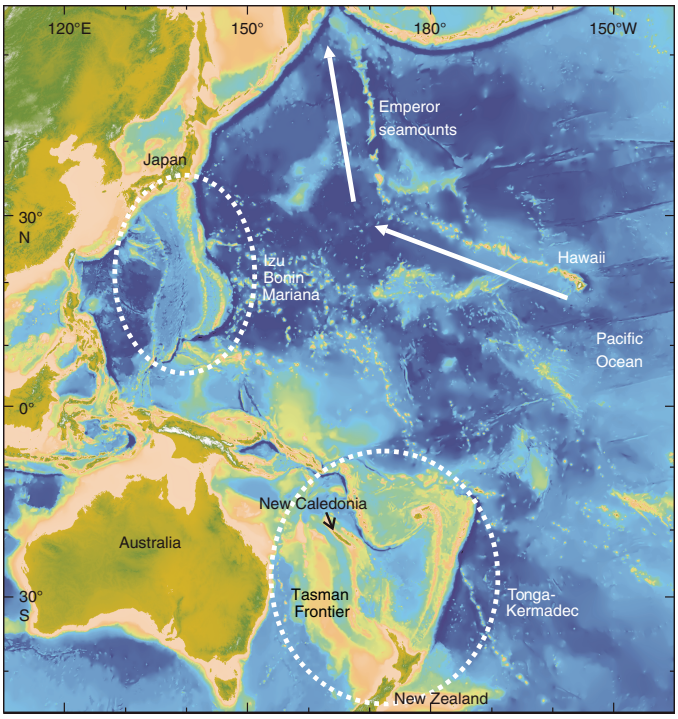

Figure F2. Location of Sites U1506–U1511 (stars) in the southwest Pacific. Dots = relevant DSDP and ODP sites. The expedition departed from Townsville and returned to Hobart. Dashed line = approximate location of Zealandia (Mortimer et al., 2017).

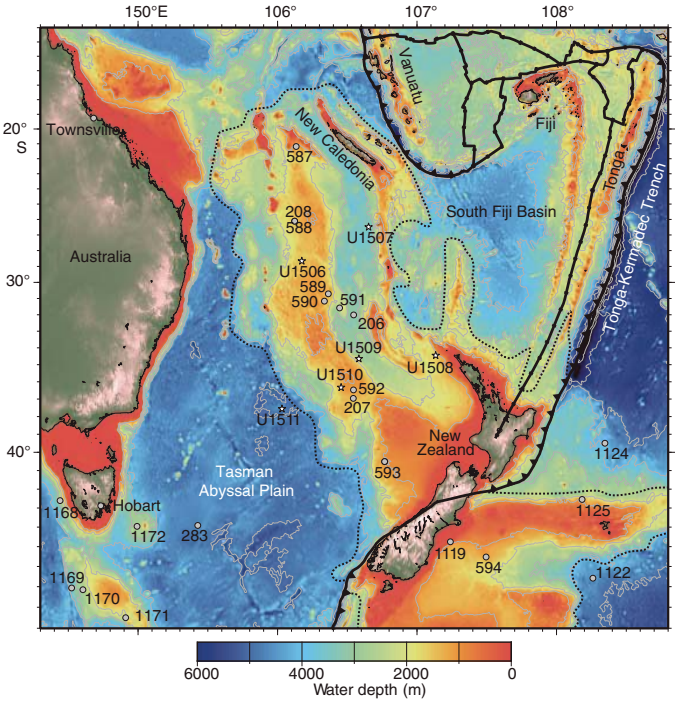

Figure F3. Location of Sites U1506 and U1507 (stars) in the northern part of Tasman Frontier in relation to New Caledonia, submarine physiographic features, and DSDP sites (dots).

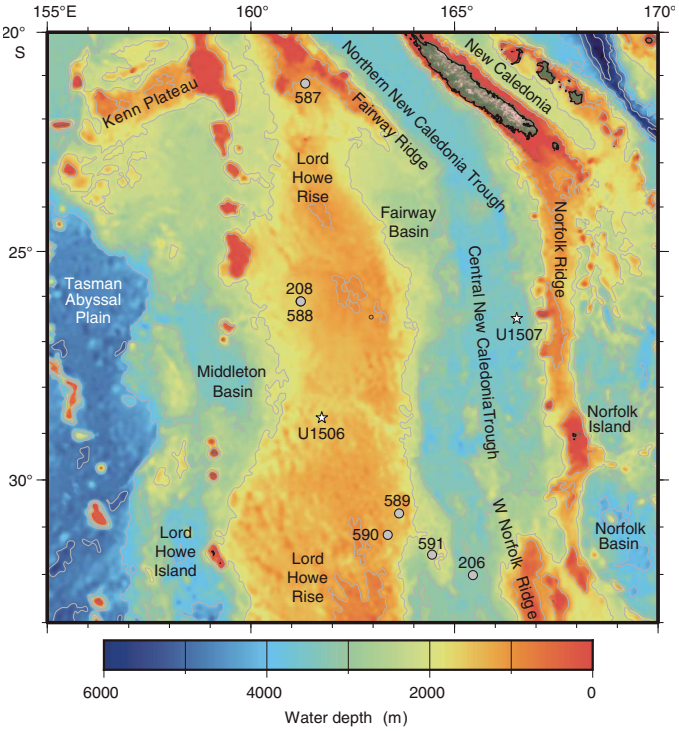

Figure F4. Location of Sites U1508–U1511 (stars) in the southern part of Tasman Frontier in relation to New Zealand, submarine physiographic features, and DSDP sites (gray dots). White dots = petroleum boreholes.

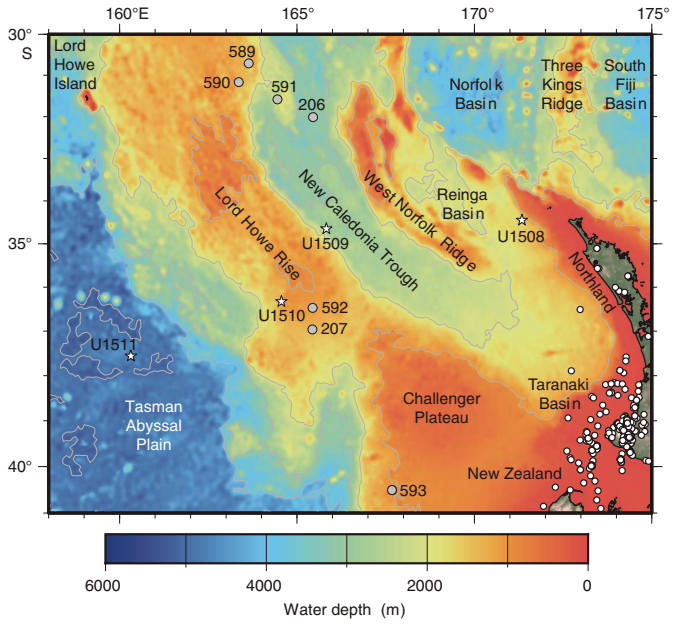

A secondary scientific goal of Expedition 371 was to better understand the long-term and short-term transitions during the early Paleogene. Why did Earth's climate move between multimillion-year greenhouse and icehouse climate states? Was this related to tectonic change, particularly as expressed by widespread initiation of subduction zones in the western Pacific? How do the hyperthermal events fit into broader early Cenozoic change? The Tasman Frontier is a special location to address such questions. Under very high pCO_2 conditions or high climate sensitivity, global climate models can reasonably simulate early Eocene warming in many regions (Huber and Caballero, 2011; Lunt et al., 2012) but not the extreme warmth previously reported in the southwest Pacific and Southern Ocean (Bijl et al., 2009; Hollis et al., 2009, 2012; Pross et al., 2012; Douglas et al., 2014). Moreover, the EECO and most of the established hyperthermals are exposed in several uplifted marine sections of New Zealand (Nicolo et al., 2007; Hollis et al., 2009, 2012; Slotnick et al., 2012).

The Eocene–Oligocene transition and Neogene paleoceanography have been subjects of numerous scientific drilling expeditions, including Deep Sea Drilling Project (DSDP) Legs 21, 29, and 90 (Figure F2). Results from these three previous expeditions in the Tasman Sea were highly influential in the development of ideas that connected regional oceanography with thermal isolation and glaciation of Antarctica and hence global climate change (Burns and Andrews, 1973; Kennett, 1977; Kennett et al., 1975; Kennett and von

Figure F5. Stable carbon and oxygen isotope compositions of Cenozoic benthic foraminifers (Zachos et al., 2008) compared with global climate/ocean events and regional tectonism. Note that the long-term decrease in $\delta^{18}O$, interpreted to be global cooling and greater continental ice volume, begins during the EECO at ~53–49 Ma and thus coincides with significant tectonic change around the Tasman Sea. Oi1 = Oligocene isotope Event 1. NZ = New Zealand.

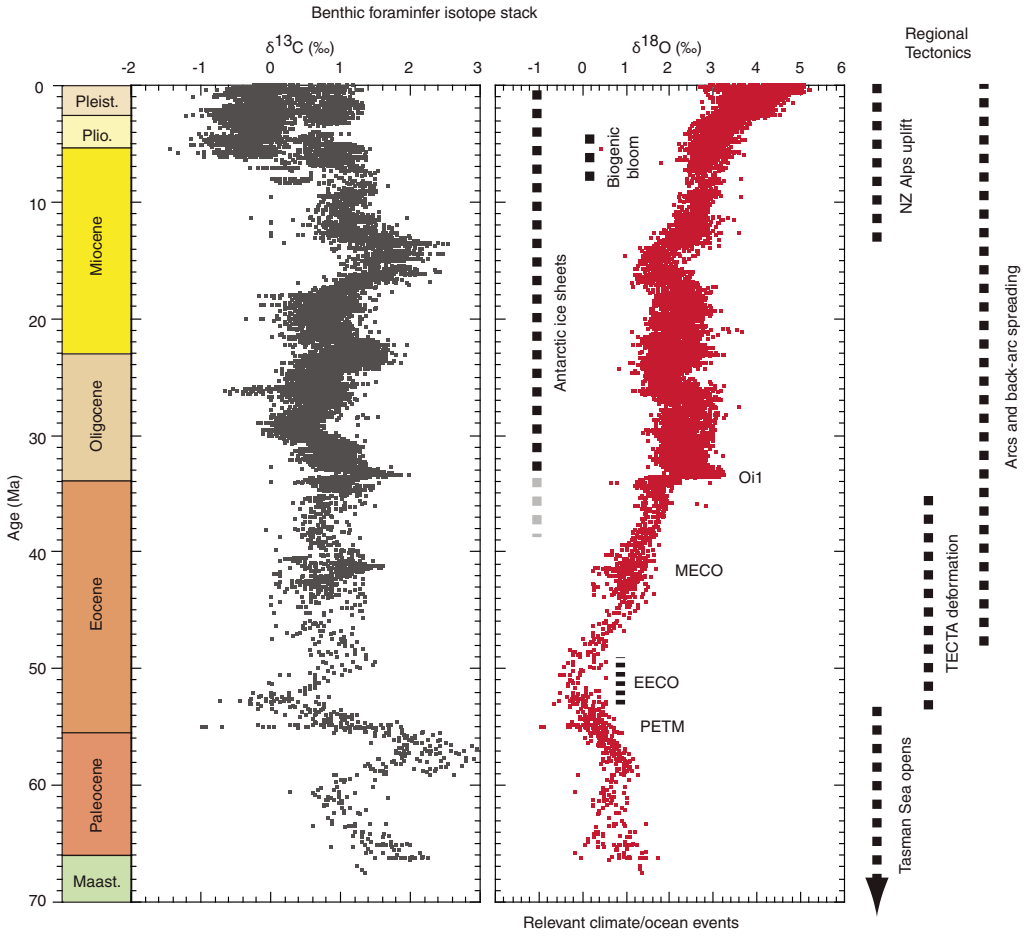

der Borch, 1986). Ocean Drilling Program (ODP) Legs 181 and 189 further investigated the Eocene–Oligocene opening of the southern Tasman Sea gateway (Carter et al., 2004; Exon et al., 2004b). A key line of evidence for this history revolves around the presence of widespread unconformities in the Tasman Sea. However, regional vertical tectonics or local faulting has not been considered (Sutherland et al., 2010, 2017). Records from the Tasman Sea may also offer insights into understanding pan-Pacific paleoceanography during the Neogene (Grant and Dickens, 2002; Karas et al., 2011).

Scientific background

Subduction initiation and global plate tectonics

Subduction initiation and changes in plate motion are linked because the largest driving and resisting tectonic forces occur in subduction zones (Becker and O'Connell, 2001; Buffett, 2006; Lithgow-Bertelloni and Richards, 1998; Stadler et al., 2010). Subduction initiation models have two end-member classes: induced or spontaneous (Stern, 2004) (Figure **F6**). In the spontaneous model, oceanic lithosphere ages, cools, increases in density and gravitational instability, and sinks into the mantle under its own weight (Stern and Bloomer, 1992; Turcotte et al., 1977). In the induced model, externally applied compressive stress and convergence is necessary to overcome lithospheric strength before convective instability can grow and subduction initiates (McKenzie, 1977; Toth and Gurnis, 1998).

Half of all presently active subduction zones on Earth began during the Cenozoic (Gurnis et al., 2004), so it is possible to assemble observations to address the question of how and why these margins evolved into self-sustaining subduction zones. Recent drilling results from Expedition 351 shed light on this question, and new models suggest juxtaposition of a transcurrent fault and relict arc could have led to Izu-Bonin-Mariana subduction initiation just before 50 Ma (Leng and Gurnis, 2015). Subduction initiation at a passive continental margin has received considerable attention through the concept of a Wilson cycle (a class of the spontaneous model), but no known Cenozoic examples of passive margins evolving into subduction zones exist (Stern, 2004). Spontaneous and induced models predict different states of stress and vertical motions during their early stages, and recovering evidence to distinguish these states underpinned our drilling strategy.

The largest change in global plate motions since 84 Ma (the only period with precisely known plate kinematics) is manifest as the Emperor-Hawaii seamount chain bend (Figure **F1**). Geochronology shows the Emperor-Hawaii bend started at ~50 Ma and may have occurred over ~8 My (Sharp and Clague, 2006). The onset of Pacific plate motion change corresponds to the timing of Pacific/Farallon plate boundary rearrangement (Caress et al., 1988) and termination of spreading in the Tasman Sea (Gaina et al., 1998), followed by a change in direction and rapid increase in rate of Australia-Antarctic spreading with consequent northward acceleration of Australia (Müller et al., 2000; Seton et al., 2012; Whittaker et al., 2007) and initiation of Australia-Pacific spreading south of New Zealand (Keller, 2003; Sutherland, 1995; Wood et al., 1996). Eocene emplacement of ophiolites and deformed flysch may record the onset of convergence in New Caledonia (Aitchison et al., 1995). Reconfiguration of plate boundaries in Antarctica (Cande et al., 2000), the Indian Ocean (Cande et al., 2010), and Asia (Aitchison et al., 2007) confirms the global extent of tectonic change.

The westward swerve in Pacific plate motion occurred at about the same time as subduction zones initiated throughout the western Pacific (Gurnis et al., 2004; Hall et al., 2003; Steinberger et al., 2004). Reconstructing what happened in the western Pacific is of fundamental significance for understanding subduction initiation and hence the physics of plate tectonics and mantle flow.

Early Paleogene greenhouse

Sediment records from the early Paleogene provide insights into Earth surface systems (e.g., climate, oceanography, biotic evolution, and geochemical cycling) when average temperatures across the globe were much warmer than present day and the poles were largely free of ice (Zachos et al., 2008; Pearson et al., 2009; Pagani et al., 2011). For example, during the EECO, mean annual sea-surface temperatures (SSTs) may have exceeded 38°C in the tropics and 20°C at latitudes greater than 50° north and south (Pearson et al., 2009; Huber and Caballero, 2011; Cramwinckel et al., 2018). The extreme warmth especially manifests in records from the southwest Pacific region (Bijl et al., 2009; Hollis et al., 2012; Pross et al., 2012).

Figure F6. Induced vs. spontaneous subduction initiation models with possible examples (adapted from Stern, 2004; Arculus et al., 2015a).

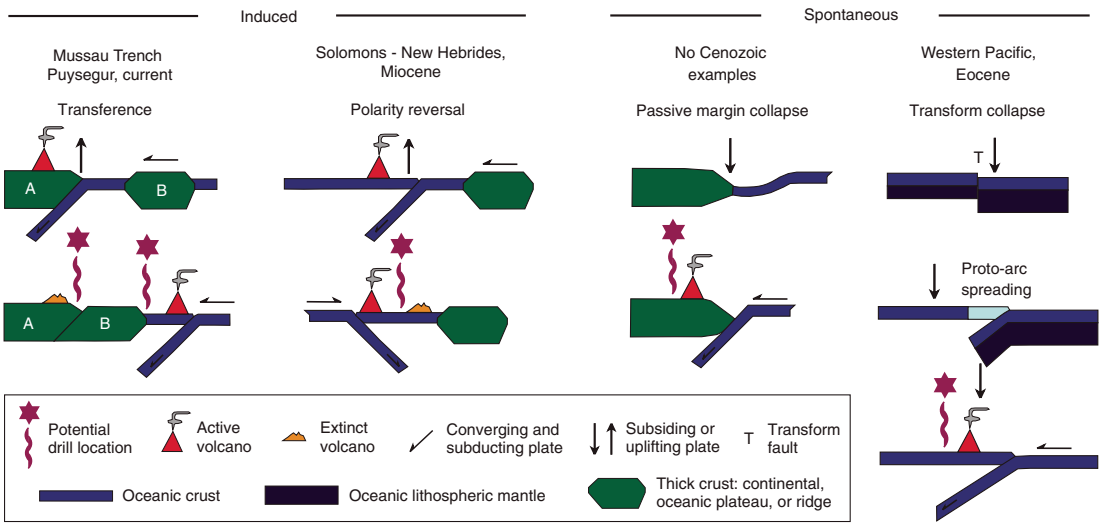

Theory and models link the much higher global temperatures to elevated atmospheric greenhouse gas concentrations (Shaffer et al., 2016). Available evidence supports this idea because atmospheric pCO_2 levels during the early Paleogene and especially the EECO likely exceeded 1000 parts per million by volume (ppmv) (e.g., Pearson and Palmer, 2000; Pagani et al., 2011; Beerling and Royer, 2011). As evidenced by prominent negative excursions in $\delta^{13}C$ records and coincident carbonate dissolution at deep seafloor locations, massive additions of carbon to the ocean and atmosphere also occurred during some of the hyperthermals (Dickens et al., 1997; Zachos et al., 2005; Lauretano et al., 2016; Westerhold et al., 2018). Indeed the most prominent hyperthermal, the Paleocene/Eocene Thermal Maximum (PETM; ~56 Ma) has been suggested as the outstanding past analog for understanding current and future climate change caused by humans (e.g., Dickens et al., 1997; Pagani et al., 2006; McInerney and Wing, 2011; Zeebe and Zachos, 2013).

Studying intervals of the early Paleogene should inform our understanding of Earth's behavior under elevated temperatures and high greenhouse gas conditions. Climate model simulations using either very high greenhouse gas radiative forcing or very high climate sensitivity yield mean annual temperatures consistent with abundant data for the early Eocene (Huber and Caballero, 2011; Lunt et al., 2012). However, at several sites in the southwest Pacific, both on and off shore (e.g., from Leg 189), multiple proxies yield SSTs 5°–10°C warmer than predicted by model simulations (Hollis et al., 2012; Pross et al., 2012). One possibility is that modeled SST predictions are too low because the region was influenced by a warm southward-flowing current system (Hollis et al., 2012) unaccounted for in climate models. Another possibility is that paleobathymetry has not been depicted accurately because parts of the Tasman Frontier were much shallower during the early Eocene compared with present day (Sutherland et al., 2010; Baur et al., 2014).

A fundamental geoscience question remains after decades of research: why did Earth's climate generally cool since the late early Eocene (~49 Ma)? Most hypotheses have invoked changes in the amount of volcanism or weathering (e.g., Raymo and Ruddiman, 1992; Berner and Kothavala, 2001; Kent and Muttoni, 2008), which would affect carbon addition to or carbon removal from the ocean and atmosphere (Berner, 1994; Ridgwell and Zeebe, 2005). An emergent alternative view is that Eocene tectonic change drove long-term Cenozoic climate change (Lee et al., 2013; Reagan et al., 2013). Prior to the early Eocene, most volcanic arcs were continental, where rising magma can react with carbonate-rich crust and generate voluminous CO_2. However, initiation of widespread island-arc subduction systems around the Pacific during the early Eocene created a network of submarine plate boundaries that may have first increased and later decreased CO_2 fluxes to the atmosphere.

The warming trend of the late Paleocene through early Eocene, the hyperthermal events of the early Eocene, the EECO, and subsequent cooling can be found in uplifted marine sedimentary successions of eastern New Zealand (Dallanave et al., 2015; Hancock et al., 2003; Hollis, 2006; Hollis et al., 2005; Nicolo et al., 2007; Slotnick et al., 2012) and New Caledonia (Dallanave et al., 2018). Comparable lower Paleogene stratigraphic records should lie across the Tasman Frontier and provide valuable insights to the magnitude and extent of past global warmth, as well as possible causes.

Post-Eocene climate evolution

Initial reports for Legs 21 and 29 (Burns and Andrews, 1973; Kennett et al., 1975) laid foundations for understanding the interplay between tectonic and oceanographic events in the region, including opening of the Tasman Sea and separation of Australia and New Zealand from Antarctica (Andrews et al., 1975; Andrews and Ovenshine, 1975; Edwards, 1973, 1975; Kennett et al., 1975; Kennett and Shackleton, 1976).

Stable isotope records generated from Leg 29 (DSDP Sites 277 and 279) sediment revealed a general cooling trend over the Cenozoic, with evidence for a pronounced cooling step across the Eocene–Oligocene transition. A series of landmark publications from these legs proposed that ocean circulation was a primary driver of regional and global climate through the early Cenozoic, and the role of circumpolar gateways in the evolution of Antarctic ice sheets and global climate was first hypothesized (Kennett, 1977; Kennett and Shackleton, 1976; Nelson and Cooke, 2001).

Leg 189 focused on the ocean gateway hypothesis and generated a wealth of data and debate (Exon et al., 2004a; Kennett and Exon, 2004). Some continue to argue that opening of the Tasmanian gateway and subsequent development of the Antarctic Circumpolar Current (ACC) played a crucial role in southwest Pacific oceanography and climate (Kennett and Exon, 2004), whereas others link late Paleogene cooling and ice sheet growth to a tectonically driven decline in atmospheric CO_2 (DeConto and Pollard, 2003; Huber et al., 2004).

Drilling in the broad Indo-Pacific area has documented a phenomenon coined the late Miocene–early Pliocene "biogenic bloom" (Farrell et al., 1995; Dickens and Owen, 1999). Between about 9 and 4 Ma, the accumulation of biogenic components (e.g., carbonate, biosilica, and barite) increased significantly at many sites beneath regions of modern surface water divergence. This increase is especially obvious along the Equator in the eastern Pacific (van Andel et al., 1975; Farrell et al., 1995), in the far North Pacific (Rea et al., 1995), and along the Oman margin (Brummer and van Eijden, 1992). Eastern flow of the Eastern Australian Current (EAC) from Australia toward New Zealand leads to an east–west zone of surface water divergence referred to as the Tasman Front. At DSDP Site 590, which lies beneath the Tasman Front (Figure **F7**), carbonate accumulation rates doubled between the late Miocene and early Pliocene, consistent with the biogenic bloom phenomenon (Grant and Dickens, 2002). The coincidence of elevated export production at numerous locations suggests far-field oceanographic teleconnections during the Neogene, such as via an acceleration of Indo-Pacific upwelling and nutrient delivery to the photic zone.

Geological setting

The seafloor beneath the Tasman Frontier represents a fascinating large-scale submarine area because a substantial portion consists of bathymetric highs and lows that lie between 750 and 3500 m water depth (Figures **F1**, **F2**). Nowhere else on Earth does such an extensive region sit on the global hyposmetric curve. This is because the bathymetric highs, the islands of New Zealand and New Caledonia, and perhaps the New Caledonia Trough represent the northern part of a submerged continent referred to as Zealandia (Mortimer et al., 2017). Unlike other continents, most of Zealandia lies underwater because the continental crust is relatively thin (~20 km on average).

Figure F7. Primary ocean currents (C), fronts (F), and gyres (G) of the Southern Ocean (after Rintoul et al., 2001). The Tasman Sea sector is affected by the ACC and EAC.

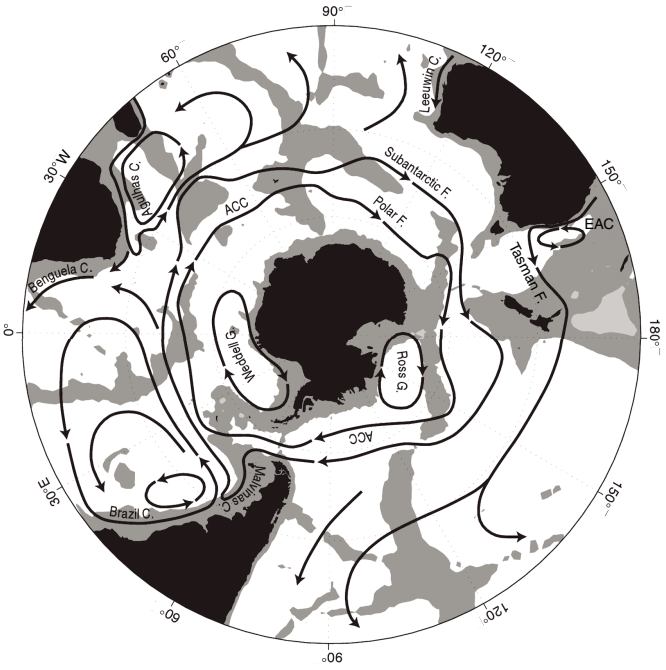

A lengthy subduction system lies east of northern Zealandia and includes the Tonga and Kermadec Trenches (Figure **F1**). This Tonga-Kermadec system has been studied much less than the Izu-Bonin-Mariana system but is complementary and has the following advantages for investigation by drilling: (1) the Tonga-Kermadec system formed adjacent to thin continental crust that early back-arc spreading isolated from later complication by faulting or volcanism; (2) persistent submarine conditions and moderate water depths led to preservation of fossil-rich bathyal sediment records in many places; (3) seismic reflection data demonstrate the existence of Eocene tectonic signals of change, including compression, uplift/subsidence, and volcanism; and (4) relative motions of the Australian and Pacific plates are precisely known (Cande and Stock, 2004; Sutherland, 1995).

The tectonic history of the Tasman Frontier can be simplified into four phases with approximate ages:

- >350–100 Ma: subduction along the eastern Gondwana margin.
- 100–80 Ma: continental rifting in the Tasman Sea region.
- 80–50 Ma: oceanic rifting and opening of the Tasman Sea.
- 50–0 Ma: Tonga-Kermadec subduction and related deformation.

Continental "basement" beneath bathymetric rises in the region is inferred to be similar to rocks found in New Zealand, New Caledonia, and eastern Australia; this inference is supported by limited dredge samples and drilling (DSDP Site 207), seismic velocity, and gravity and magnetic anomalies (Collot et al., 2012; Klingelhoefer et al., 2007; Mortimer, 2004a, 2004b; Mortimer et al., 2008; Sutherland, 1999; Tulloch et al., 1991; Wood and Woodward, 2002). Lord Howe Rise and Challenger Plateau (Figures **F3**, **F4**) are probably composed of quartzose metasedimentary rocks and granitoids of Paleozoic age that represent the eastern edge of Gondwana (Mortimer et al., 2017). High-amplitude magnetic anomalies and a single dredge sample from the West Norfolk Ridge suggest a fossil arc of late Paleozoic and Mesozoic age (formed along the active margin of Gondwana) underlies the southern New Caledonia Trough (Mortimer et al., 1998; Sutherland, 1999). The geology of New Caledonia and northern New Zealand suggests that Norfolk Ridge is underlain by Mesozoic fore-arc accretionary rocks formed at the convergent margin of Gondwana (Adams et al., 2009; Aitchison et al., 1998; Cluzel et al., 2010; Cluzel and Meffre, 2002; Mortimer, 2004b). Based on comparison with eastern New Zealand (Davy et al., 2008), a "fossil" Gondwana trench lay along the northeast side of the Norfolk Ridge system and the ancient slab dipped southwest beneath Lord Howe Rise during the Mesozoic.

The tectonic regime along the Tasman sector of the Gondwana margin changed during the Cretaceous from subduction and convergence to widespread rifting and extension. Igneous activity was widespread and of variable type and chemistry during the Cretaceous. Calc-alkaline and adakitic (high Sr/Y) activity with a subduction-related signature is characteristic of the early phase (130–110 Ma) in New Zealand and New Caledonia, whereas an intraplate rift setting characterizes later activity after ~105–100 Ma and is also recorded on Lord Howe Rise (Bryan et al., 1997; Cluzel et al., 2010; Higgins et al., 2011; Mortimer et al., 1999; Tulloch et al., 2009). Late Cretaceous rift basins contain coastal sandstone facies overlain by transgressive marine sandstones and mudstones in New Zealand, eastern Australia, and New Caledonia and are likely present in the Tasman Frontier region (Collot et al., 2009; Herzer et al., 1999; King and Thrasher, 1996; Uruski and Wood, 1991; Uruski, 2008). The end of widespread rifting in New Zealand, New Caledonia, and Australia and the subsequent transition to passive margin conditions were contemporaneous with the onset of seafloor spreading in the Tasman Sea at ~80 Ma, but local normal fault activity is known to have continued to ~60 Ma in Taranaki and northern South Island, New Zealand (King and Thrasher, 1996; Laird, 1993).

Late Cretaceous to early Cenozoic seafloor spreading in the Tasman Basin is inferred from magnetic anomalies (Hayes and Ringis, 1973; Weissel and Hayes, 1977). The earliest seafloor spreading may predate Chron C33r (84–80 Ma) east of Tasmania (Royer and Rollet, 1997), but marginal seafloor along much of the western edge of Lord Howe Rise probably formed during Chron C33r (Gaina et al., 1998; Sutherland, 1999). Seafloor spreading ceased in the central Tasman Sea during Chron C24 (53–52 Ma) or very shortly afterward (Gaina et al., 1998).

Deformation, exhumation, and emplacement of ultramafic, mafic, and sedimentary allochthons occurred in New Caledonia during the middle and late Eocene (Aitchison et al., 1995; Cluzel et al., 2001). The peak of high-pressure metamorphism in northern New Caledonia was at 44 Ma, and exhumation was largely complete by 34 Ma (Baldwin et al., 2007). Seismic stratigraphic evidence shows that the New Caledonia Trough either formed or was substantially modified during this event, although Cretaceous sedimentary basins beneath the trough escaped Cenozoic convergent deformation in most places (Collot et al., 2008; Sutherland et al., 2010). Regional deformation and emplacement of allochthons in northern New Zealand occurred later than in New Caledonia or the Norfolk Ridge system, with the onset of tectonic activity during the late Oligocene and early Miocene (~30–20 Ma) (Bache et al., 2012; Herzer, 1995; Herzer et al., 1997; Rait et al., 1991; Stagpoole and Nicol, 2008).

Relative motion between the Australia and Pacific plates is precisely known for the period since Chron C20 (43 Ma) because the plate boundary south of New Zealand was extensional and a plate

Figure F8. Australia-Pacific relative plate motion history plotted on Tasman Frontier bathymetric features (NC = New Caledonia, R = ridge) (after Bache et al., 2012). Australian plate points are reconstructed relative to a fixed Pacific plate at 1 My intervals. Dashed lines = relocated positions of Norfolk Ridge at 5 My intervals, revealing that plate motion rates were low in New Zealand during the interval 45–25 Ma.

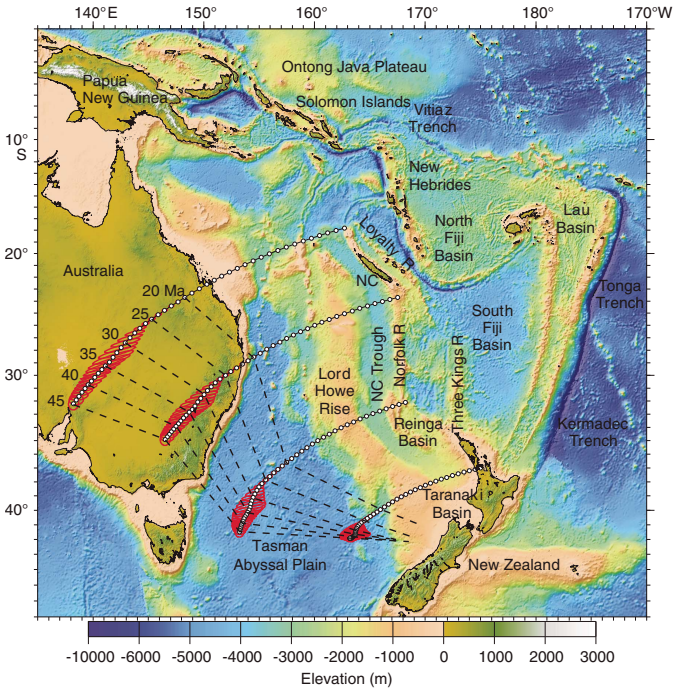

circuit through Antarctica can be followed to provide additional constraints (Cande and Stock, 2004; Keller, 2003; Sutherland, 1995). Eocene convergence rates varied from <1 cm/y in New Zealand to 10 cm/y near New Caledonia (Figure **F8**). Late Eocene to Holocene subduction zone roll-back has produced back-arc basins (Loyalty, Norfolk, South Fiji, North Fiji, Havre, and Lau) and ridges interpreted to be fossil and active arcs east of the Norfolk Ridge system (Loyalty, Three Kings, Lau-Colville, Tonga-Kermadec, and Vanuatu) (Crawford et al., 2003; Herzer et al., 2009; Herzer and Mascle, 1996; Mortimer et al., 2007; Schellart et al., 2006). The complexity of basin opening makes local determination of past plate boundary configurations and rates difficult. This back-arc region has now mostly isolated the submerged continental part of the Tasman Frontier region from Cenozoic subduction-related deformation and volcanism.

A variety of tectonic models have been proposed to explain how Eocene–Miocene arcs and back-arc basins formed between the Tonga-Kermadec Trench and Norfolk Ridge (Cluzel et al., 2006; Crawford et al., 2003; Herzer et al., 2009; Mortimer et al., 2007; Schellart et al., 2006). General agreement exists that the modern Tonga-Kermadec system evolved from a boundary lying near the Norfolk Ridge and New Caledonia in the middle Eocene. However, ideas about the exact geometry of that boundary or the nature of Cretaceous to middle Eocene plate boundaries northeast of Norfolk Ridge (Whattam et al., 2008) vary because the region has either been subducted or deformed and intruded. The region is also sparsely sampled.

The oldest Cenozoic volcanic rocks from the southwest Pacific with clear subduction affinities were dredged from the Tonga-Kermadec fore arc and have ages in the range of 52–48 Ma (Meffre et al., 2012). In New Caledonia, dikes with subduction affinities cut ophiolitic rocks and are interpreted to be approximately synchronous with felsic dikes that are dated at ~53 Ma (Cluzel et al., 2006), representing the earliest evidence for subduction and predating the peak of high-pressure metamorphism at 44 Ma (Baldwin et al., 2007) and nappe emplacement in New Caledonia (Aitchison et al., 1995; Maurizot, 2012). Given that magnetic anomaly interpretations suggest seafloor spreading in the Tasman Basin ceased at ~52–50 Ma (Gaina et al., 1998), strong evidence exists for Pacific-wide synchronicity in major plate reorganization. More generally, the age of the Emperor-Hawaii bend, the inception of Izu-Bonin-Mariana subduction, and a change from extension to compression occurred in the Tasman Frontier.

Scientific objectives

Expedition 371 was designed to address the following questions.

1. *How and why does subduction initiation occur?*
   a. Did plate convergence and a period of high horizontal stress with convergent failure precede and induce subduction initiation, or did subduction initiation happen spontaneously with early extensional stresses?
   b. What vertical stresses occurred during subduction initiation, and when and where was this manifest as uplift or subsidence?
2. *Was the Eocene southwest Pacific anomalously warm, and why?*
   a. What were surface water temperatures during the early Cenozoic across the region, and if anomalous, do they link to local physiographic or oceanographic changes?
   b. Can early Eocene changes in paleoceanography and carbon cycling as found in the Tasman Frontier be linked to major changes in regional tectonics?
3. *How does post-Eocene oceanography and climate compare with elsewhere in the Pacific?*
   a. When did the modern ocean circulation system develop as evidenced in the Tasman Frontier?
   b. Are pole-Equator climate teleconnections manifested in the Tasman Sea during the late Cenozoic?

Drilling strategy

Our drill sites were chosen foremost to test geodynamic model predictions. Periods of time in the past that had high horizontal stress may be recorded as faulted or folded strata. Anomalous vertical stress in the past, such as stress caused by traction or buoyancy, would have been balanced by surface uplift or subsidence and should manifest as changes in paleodepths of the seafloor. Furthermore, past changes in thermal or chemical anomalies in the crust or mantle may be recorded by characteristic volcanic products. We aimed to collect sedimentary records with these signals.

The timing and style of faulting and folding can be determined from stratigraphic relationships tied to seismic reflection data. In general, three units constrain the timing of a tectonic event: faulted strata are older than the event, unfaulted strata are younger than the event, and syntectonic growth strata record progressive faulting during the event. Growth strata are typically identified from thickness changes in a sedimentary unit that drapes faulted units, and seismic reflectors in the syntectonic unit may exhibit fanning geometries close to faults.

The only practical way of measuring elevation of the crust through time is against a sea level reference frame. Flat unconformities with regional consistency on seismic reflection data often represent surfaces produced by sea level–modulated erosional processes. Certain sediment components, particularly fossils of neritic organisms, can provide independent evidence for vertical positions. Samples dredged from >1500 m water depth in the Reinga Basin during the TAN1312 expedition contain Paleogene bioclastic limestone with shallow-marine fossils, supporting the hypothesis that large (>1 km) vertical motions were associated with subduction initiation (Browne et al., 2016). We aimed to recover shallow-water (<400 m) fossils, either in place or reworked by sediment gravity flows, at several locations to provide direct evidence of past vertical positions at precisely dated times. Importantly, sediment records targeted for tectonic research objectives align with paleoceanographic goals. Analyses of microfossil assemblages and sediment geochemistry can be used to reconstruct a variety of past ocean conditions, such as water temperature.

Our strategy was to obtain information on transects parallel and perpendicular to where subduction initiated to constrain the different physical processes involved in subduction zone initiation (Figure **F9**). The proximal ridge includes New Caledonia, Norfolk Ridge, Reinga Basin, and northwest New Zealand (Figures **F2**, **F3**, **F4**). Sediment and rocks in this region are deformed, presumably during the initial phase of surface convergence (Sutherland et al., 2017). Knowledge from New Caledonia, Sites U1507 and U1508, and New Zealand produce a proximal boundary–parallel transect that progressively samples initial rates of predicted convergence (Bache et al., 2012).

Sites U1506 and U1507, combined with knowledge from New Caledonia and regional seismic reflection interpretation, should provide a boundary-perpendicular transect in the northern region (Figure **F3**), where Eocene convergence rates are thought to have been highest (Figure **F8**). Sites U1508–U1511, combined with knowledge from New Zealand and Australia, provide a southern transect (Figure **F4**) that has clear signs of an extended period of plate failure (Sutherland et al., 2017).

Figure F9. Scales of observation in relation to physical processes. Timing of events relative to each other, to plate motion parameters, and to global events will be used as a discriminator between alternate tectonic models. Arrows = drill site locations.

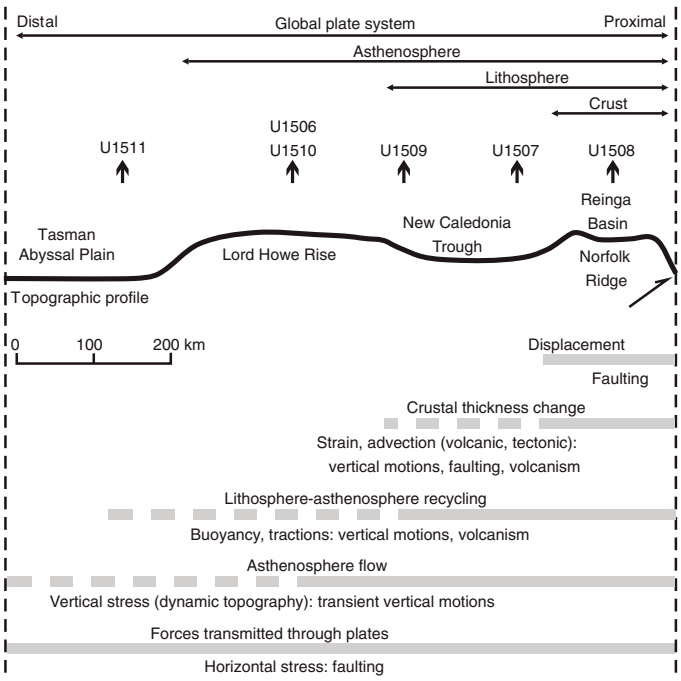

We aimed to test the hypothesis that the proximal basin, the New Caledonia Trough, subsided >2 km during the Paleogene, even though it was only subjected to minor convergent deformation (Sutherland et al., 2010). Sites U1507 and U1509 were chosen to constrain the magnitude and timing of subsidence in relation to other events. In addition, the New Caledonia Trough contains a record of detrital products derived from ridges on either side and so records the timing of deformation and emergence of those ridges (Etienne et al., 2018; Bache et al., 2014a).

The distal ridge, Lord Howe Rise, shows signs of minor Eocene convergent deformation, volcanism, and significant erosion surfaces (Sutherland et al., 2010). Sites U1506 and U1510 were chosen to determine the timing and magnitude of vertical motions and hence constrain the history of dynamic topography (upper mantle flow), lithospheric buoyancy, and/or tractions related to shear zones. Different geodynamic model classes make very different predictions of vertical motion.

The distal basin, the Tasman Abyssal Plain, shows signs of local convergent deformation (Sutherland et al., 2017). The force transmitted through the tectonic plate must have been large enough to stop seafloor spreading and cause failure of the lithosphere. Site U1511 was chosen to determine the timing of this change in stress state and how it relates to other tectonic events. The timing and magnitude of force transmitted through a plate is a powerful discriminator: an induced subduction model predicts a larger and earlier compressive force than a spontaneous subduction model (Gurnis et al., 2004).

The Australia-Pacific convergence rate during the time of interest was much faster near New Caledonia than near New Zealand (Figure **F8**). Geodynamic models predict that stresses in an initiating subduction system evolve in response to the total convergence experienced (Gurnis et al., 2004), so models predict along-strike changes in timing that can be tested using biostratigraphy. The absolute timing of observables can also be compared with known plate motions. This ability to track total convergence precisely through space and time is special to the Tonga-Kermadec system. Most subduction systems have imprecisely known kinematic histories because the rock record has been subducted.

Site summaries

Site U1506 (northern Lord Howe Rise)

Background and objectives

Site U1506 (proposed Site LHRN-3A) is located on the northern Lord Howe Rise, ~290 km south of DSDP Sites 208 and 588 and where geophysical surveys image a regional unconformity (Sutherland et al., 2016). At Sites 208 and 588, the unconformity corresponds to a break between foraminiferal and nannofossil chalk of early Oligocene age and siliceous microfossil–bearing chalk, radiolarite, and diatomite of middle Eocene age. The primary scientific objective at Site U1506 was to test the hypothesis that the northern Lord Howe Rise uplifted to near sea level during the Paleogene and has subsided since by ~1500 m. The drilling target, identified from seismic reflection data, is a buried flat-topped feature with ~100 m of relief above the regional unconformity surface. The feature has a positive polarity seismic reflection at its top but also has internal re-

flections. We hypothesized that it could be a coral reef or wave-cut surface formed during the Eocene. Rotary drilling was chosen because consideration of the seismic reflection amplitude and seismic refraction velocity (3.2–3.8 km/s) suggested the buried structure might be too hard for advanced piston corer (APC) or extended core barrel (XCB) coring.

Operations

Hole U1506A: 28°39.7180′S, 161°44.4240′E; water depth = 1495 m

Site U1506 was the first site occupied during Expedition 371. After an 1167 nmi transit from Townsville, Australia, the ship arrived at Site U1506 at 1912 h on 3 August 2017 (UTC + 10 h). At 1948 h, the drill floor was cleared for operations, beginning Hole U1506A.

The rotary core barrel (RCB) bottom-hole assembly (BHA) was assembled and deployed, and Hole U1506A was spudded at 0600 h on 4 August. Coring proceeded through Core 29R, where the expected hard formation was encountered at ~265 m drilling depth below seafloor (DSF). We recovered cores in half intervals (4.5–5.0 m length) below this depth to minimize the risk of core loss due to jams in the bit or inner barrel.

Coring stopped after Core 36R, which arrived on the rig floor at 1345 h on 5 August. Total recovery for the 306.1 m DSF cored in Hole U1506A was 192.38 m (63%) and included an average core recovery of 61% from Cores 1R through 28R and 79% from Cores 29R through 36R, which were recovered in half intervals (4.5–5.0 m). Hole U1506A operations ended at 1935 h, and the total time spent on Hole U1506A (and Site U1506) was 47.75 h or 2.0 days. At 2000 h, we departed for Site U1507.

Principal results

Site U1506 consists of ~265 m of Pleistocene–middle Eocene nannofossil ooze and chalk (lithostratigraphic Unit I) overlying ~40 m of volcanic rocks (lithostratigraphic Unit II; Figures **F10**, **F11**). Unit I sediments are further divided into three subunits.

Subunit Ia (0–258.2 m) consists of relatively homogeneous Pleistocene to upper Miocene white nannofossil ooze and chalk with foraminifers, with carbonate content ranging from 88% to 95%. Faint decimeter-scale white and grayish white color banding and rare blebs of pyrite (generally framboidal under the scanning electron microscope [SEM]) occur in this subunit. The ooze–chalk transition occurs across an interval that includes Cores 371-U1506A-24R through 26R (~260 m). Fine structures and texture, including bioturbation with slightly darker *Zoophycos, Planolites, Skolithos*, and *Chondrites* burrows, are better preserved and visible in the chalk than in the ooze.

Subunit Ib (258.2–264.3 m) is a ~6 m thick interval of pale yellow to white upper Oligocene nannofossil chalk with foraminifers. The Subunit Ia/Ib boundary is marked by a color change from white gray to pale yellow and a slight increase in magnetic susceptibility (MS). It also represents a ~10 My hiatus separating the late Oligocene from the late Miocene. Additionally, Subunit Ib is moderately bioturbated with common *Zoophycos* and *Planolites* trace fossils.

Subunit Ic (264.3–264.6 m) is a 34 cm thick interval of middle Eocene glauconitic nannofossil chalk with foraminifers. The Subunit Ib/Ic boundary, defined by the appearance of glauconite and a coincident color change to light greenish gray, represents a ~20 My hiatus between the middle Eocene and late Oligocene. Subunit Ic is intensely bioturbated, with burrows filled with pale yellow Oligocene nannofossil chalk from the overlying Subunit Ib.

Lithostratigraphic Unit II (264.6–305.3 m) represents the uppermost ~41 m of a volcanic rock sequence. It consists of microcrystalline to fine-grained basalt with facies alternating in ~10 m couplets of (1) dark reddish brown microcrystalline, highly vesicular, and amygdaloidal basalt with common veins and (2) dark gray fine-grained massive aphyric basalt with rare carbonate veins. Thin sections and X-ray diffraction (XRD) measurements show the basalt is dominated by Ca-plagioclase and clinopyroxene alongside various alteration minerals such as Fe-Ti oxides and chlorite. The carbonate veins and vesicle fills display a variety of composition and texture, including large (>1 cm grain size) fibrous calcite crystals and fine-grained bioclastic packstone.

Nannofossil and planktic foraminifer biostratigraphy assign a Pleistocene to late Oligocene age to lithostratigraphic Subunits Ia and Ib. Higher resolution sampling identified a condensed interval between Samples 371-U1506A-28R-3, 75 cm, and 28R-4, 75 cm (257.25–258.75 m), that represents ~10 My. Subunit Ic is of middle Eocene age. A sample of a burrow fill in Subunit Ic (Sample 29R-2, 70 cm; 264.36 m) is late Oligocene in age, indicating erosion or nondeposition of middle Eocene to upper Oligocene sediment.

Microfossil assemblages consist of well-preserved calcareous nannofossils, planktic and benthic foraminifers, and ostracods, indicating a depositional depth well above the lysocline. The middle Eocene benthic foraminifers are characteristic of an upper bathyal environment, about 500–1000 m shallower than the late Oligocene and younger intervals. The ostracod assemblages indicate a deep-water setting throughout Subunits Ia and Ib (representing late Oligocene and younger age) but an upper bathyal setting for Subunit Ic (middle Eocene).

Rare, heavily recrystallized reworked radiolarians were found in some core catcher samples from this site. No other siliceous microfossils were found in samples examined from this site.

A palynological reconnaissance study carried out on five samples from Hole U1506A, including one sample from the middle Eocene glauconite-rich layer in Section 29R-2, yielded no palynomorphs.

Paleomagnetic measurements from ooze samples, representing most of lithostratigraphic Subunit Ia, yielded unstable paleomagnetic directions, largely due to reworking of sediments (bioturbation) and drilling disturbance associated with the RCB coring system. Integration with discrete sample–derived directions does not allow reliable correlation with the geomagnetic polarity timescale (GPTS). However, stable paleomagnetic directions with several polarity reversals were obtained in the chalk interval (below ~245 m), and clarity was improved by alternating field (AF) demagnetization at 20 mT. Principal component analysis of paleomagnetic directions after stepwise AF demagnetization of discrete samples reveals a stable remanent magnetization component above 10–20 mT, confirming observations from superconducting rock magnetometer measurements.

Lithostratigraphic Unit II yields a stable paleomagnetic signal after removing the overprint with AF demagnetization at 20 mT. A normal polarity was obtained from most volcanic rock samples. Some intervals not affected by AF demagnetization showed a reversed polarity after 20 mT demagnetization. Further analyses (e.g., thermal demagnetization) are required to investigate the paleomagnetic signal of the volcanic materials.

Gamma ray attenuation (GRA) bulk density, MS, color, and natural gamma radiation (NGR) exhibit small amplitude variations in lithostratigraphic Unit I and significantly greater amplitude variations in Unit II.

Figure F10. Lithostratigraphic comparison of sites cored during Expedition 371. Arrows = approximate location of ooze–chalk transition.

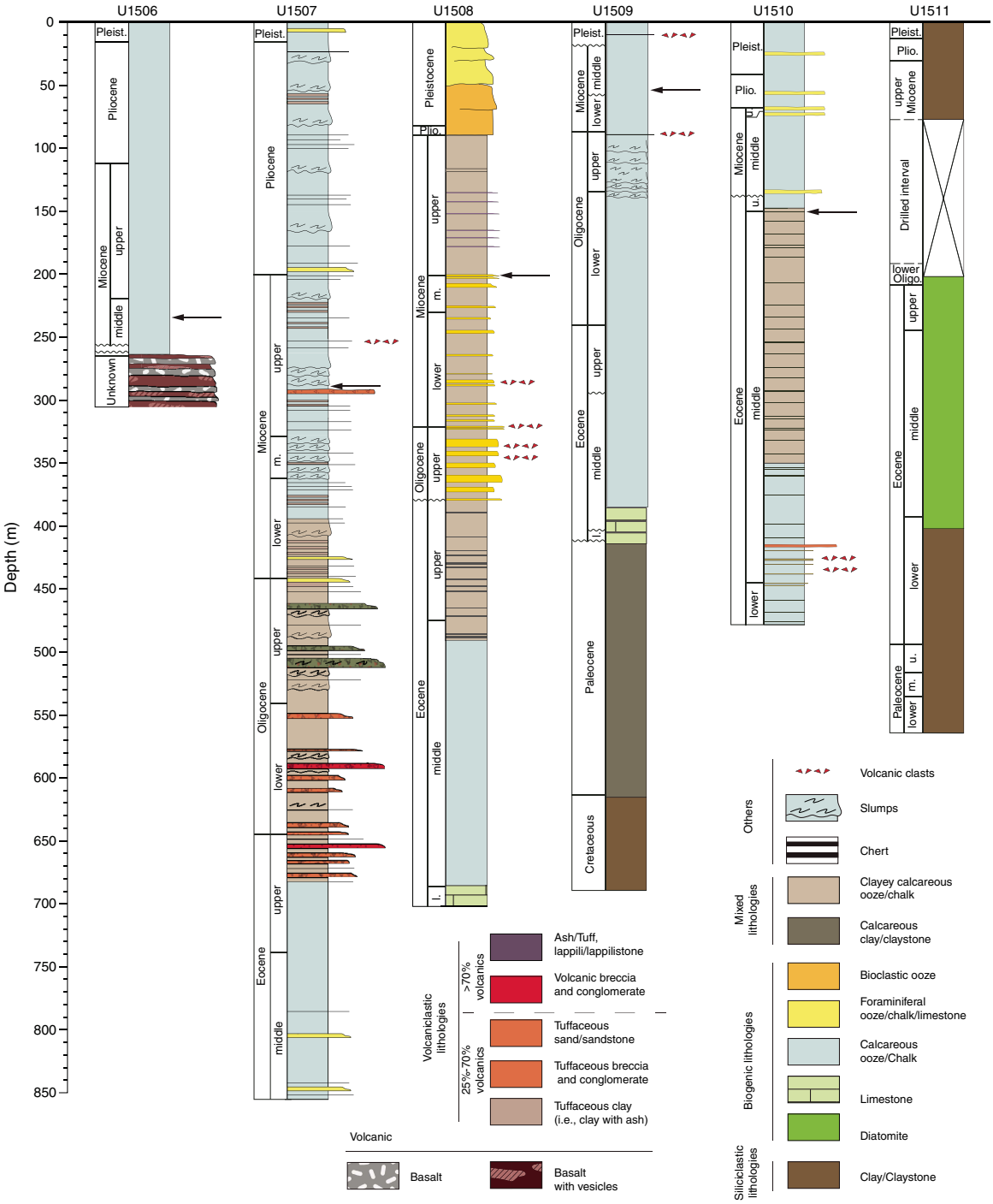

In Unit I, GRA bulk density varies between 1.6 and 1.8 g/cm^3, and porosity decreases from ~63% to 52% from the seafloor to the base of Unit I, typical of calcareous ooze and chalk. *P*-wave velocity increases gradually with depth from ~1600 to ~2000 m/s. Intermittently higher *P*-wave velocity values of ~2200 m/s in Cores 371-U1506A-26R and 27R reflect the diagenetic transition of ooze to chalk. MS is low throughout the sedimentary section, with a few local MS spikes as high as 100 instrument units (IU). NGR is also generally low (1–4 counts/s) but increases to ~25 counts/s in glauconitic Subunit Ic.

Thermal conductivity shows a gradual and increasing trend with depth from 1.1 to 1.4 W/(m·K) over the uppermost ~250 m, consistent with expected values for calcareous ooze and chalk. Vane shear strength increases from ~18 kPa near the seafloor to ~40 kPa at 190 m. Compressive strength from penetrometer measurements shows very low strength in the top ~72 m of Unit I and then increases and becomes variable (~60 to ~100 kPa) to 186 m.

The most significant change in physical properties spans the lithostratigraphic Unit I/II boundary. This sediment/rock contact at 265 m corresponds to major increases in bulk density (as high as 2.8

Figure F11. Age-depth models for each site drilled during Expedition 371.

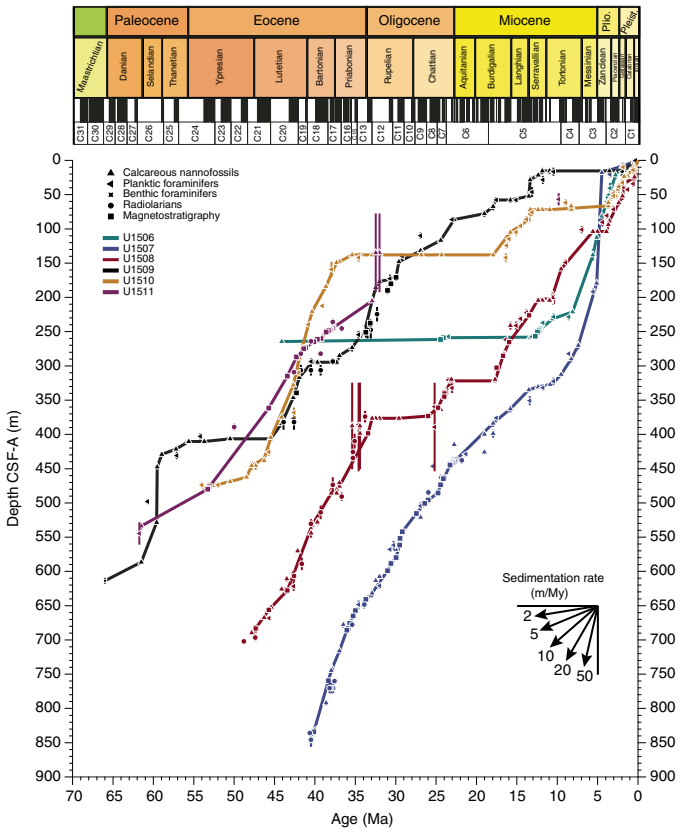

g/cm^3) and *P*-wave velocity (4400–6500 m/s). This impedance contrast can be correlated with the major reflection seen in the multichannel seismic (MCS) profiles used in the site surveys (2.29 s two-way traveltime [TWT]). MS (0–1500 IU), NGR (~3–9 counts/s), bulk density, and color reflectance show much higher amplitude variations in Unit II than in Unit I. Porosity drops to 9%–20% in Unit II.

A total of 15 interstitial water (IW) samples were collected from Cores 371-U1506A-4R through 28R (26–261 m; lithostratigraphic Unit I). Sulfate concentration decreases from ~29 mM at the "mudline" to ~20 mM at depth. The ammonium profile somewhat mirrors that of sulfate, increasing from 0 to 150 µM, which suggests sulfate reduction of particulate organic carbon in the sediments. The product of this reaction, H_2S, once reacting with Fe, also explains the abundant iron sulfide mineral horizons observed in the cores. From the top to the bottom of the sedimentary section, Ca increases from 10.6 to 18.3 mM and Mg decreases from 52.9 to 36.2 mM, which could reflect reactions between pore water and basement rock. Si and Mn increase from 160 to 200 mM and from 0.4 to 3 mM, respectively, at the transition from ooze to chalk.

Headspace gas samples were collected from each core. Hydrocarbon gas concentrations in all samples were below detection limits.

Carbonate ($CaCO_3$) content is high (>88 wt%) throughout Unit I and increases with depth in the uppermost 70 m, with the highest values (~95 wt%) between 85 and 143 m and between 200 and 228 m. Total organic carbon (TOC) percentages are low, with values ranging between 0.2 and 0.4 wt% in the top ~210 m and between 0.6 and 1.0 wt% from 219 to 247 m. Trace amounts of nitrogen are present in the uppermost two samples (0.65 and 14.32 m). No samples were taken for bulk sediment geochemistry from Subunit Ic or Unit II.

Site U1507 (northern New Caledonia Trough)

Background and objectives

Site U1507 (proposed Site NCTN-8A) is located in the New Caledonia Trough, ~460 km south of New Caledonia, ~620 km north of DSDP Site 206, and ~530 km east of Sites 208 and 588. Trending northwest–southeast and north–south, the New Caledonia Trough delineates a ~1700 km long bathymetric low on northern Zealandia (Figure **F2**). The northern and central parts of the feature were not drilled prior to Expedition 371. On the basis of evidence from Site 206 and the Taranaki Basin, it was inferred that the New Caledonia Trough formed during Cretaceous rifting and subsequent subsidence. However, recent analysis of high-quality seismic reflection data led to an alternate hypothesis: the present physiography was created mainly during Eocene subduction zone initiation. Site U1507 was chosen to determine the timing of deformation and uplift of Norfolk Ridge, constrain the age of trough formation and sedimentary fill, and obtain a record of regional volcanism (Sutherland et al., 2016). The intent was to core Site U1507 using the APC/XCB system to sample a downlapping sequence (at ~500–700 meters below seafloor [mbsf]) that was inferred to represent an influx of sediment from the Norfolk Ridge and hence date emergence of the ridge.

Operations

Hole U1507A: 26°29.3158′S, 166°31.7039′E; water depth = 3568 m
Hole U1507B: 26°29.3158′S, 166°31.7155′E; water depth = 3568 m

Hole U1507A was cored with the APC and XCB systems. The first was used to retrieve Cores 1H through 26H with an average recovery of 106%. Temperature measurements were taken at the bottom of Cores 4H, 7H, 10H, 13H, 16H, and 19H. Deployment of orientation and temperature tools was discontinued after Core 20H, and APC coring was discontinued after Core 26H. Coring continued with the XCB system, retrieving Cores 27X through 46X with an average recovery of 55%. Total recovery for Hole U1507A was 352.7 m (83%), and the total time spent on Hole U1507A was 3.6 days.

Hole U1507B was first drilled without coring from 0 to 376 m DSF and then cored (Cores 2R through 53R) with a recovery of 371.5 m (76%). The total time spent on Hole U1507B was 8.1 days.

After dropping the coring bit at the bottom of the hole and replacing the hole with heavy mud, three logging passes were made with a modified triple combo tool string between 75.2 and 864 m wireline log depth below seafloor (WSF): a downhole log, a 125 m uphole log for calibration, and a main log up the entire hole. The modified triple combo logging tool string included MS, electrical resistivity, sonic, bulk density, and NGR tools.

Principal results

The sedimentary sequence at Site U1507 consists of ~685 m of biogenic ooze and chalk interbedded with calcareous and volcaniclastic turbidites (lithostratigraphic Unit I) overlying ~170 m of more homogeneous clayey nannofossil chalk (lithostratigraphic Unit II; Figures **F10**, **F11**). Unit I sediments are further divided into three subunits based on changes in lithology and sedimentological features as identified by macroscopic and microscopic (smear slide, thin section, and SEM) core description.

Subunit Ia (0–401.2 m) mostly consists of white nannofossil ooze and chalk. This dominant lithology is accompanied by light greenish gray nannofossil-rich clay with volcanic ash, white gray normally graded foraminiferal ooze or limestone beds, and a re-

stricted ~2 m thick interval of very dark greenish gray volcanic breccia and tuffaceous sandstone. Soft-sediment deformation is widespread but particularly common in the lowermost part of the subunit.

Subunit Ib (401.2–542.9 m) is primarily composed of greenish gray clayey nannofossil chalk with volcanic ash that shows significant soft-sediment deformation and is interbedded with dark gray clayey tuffaceous sandstone and greenish gray clayey foraminiferal limestone with volcanic clasts. This subunit differs from Subunit Ia because of an overall increase in clay and volcanic content.

Subunit Ic (542.9–685.5 m) consists of dark greenish gray coarse- to fine-grained tuffaceous conglomerate, sandstone, and tuff alternating with light greenish gray clayey nannofossil chalk with volcanic ash. The boundary with Subunit Ib is defined by the first occurrence of a thick-bedded tuffaceous conglomerate. Volcaniclastic lithologies display a range of sedimentary facies that point to deposition from various gravity flow processes from debris flows to turbidity currents. Thin sections and XRD measurements on the volcaniclastics reveal that clast lithologies consist of variable percentages of basaltic minerals such as pyroxene, plagioclase, and olivine phenocrysts, as well as volcanic glass shards, vesicular pumice, and large benthic foraminifers.

Lithostratigraphic Unit II (685.5–855.7 m) consists of homogeneous light greenish gray bioturbated clayey nannofossil chalk with common *Zoophycos, Nereites*, and *Spirophyton* burrows and rare foraminiferal limestone beds. The lithology is consistent with hemipelagic-dominated sedimentation. Very rare foraminiferal limestone beds with few volcanic grains are still encountered in this subunit. Between 826 and 836 m, the lithology changes to a greenish gray nannofossil claystone, possibly reflecting increased carbonate dissolution.

Nannofossils and foraminifers are present throughout Holes U1507A and U1507B, providing a robust stratigraphy (Figure **F11**): Pliocene–Pleistocene (6.2–177.8 m), Miocene (187.0–432.6 m), late Oligocene (449.9–520.0 m), early Oligocene (523.1–639.1 m), and late to middle Eocene (642.3–855.7 m). The Oligocene/Miocene boundary was approximated using the top of *Sphenolithus delphix* (~442.5 m). The Eocene/Oligocene boundary was approximated using the top of planktic foraminifer *Globigerina euapertura*, the benthic foraminifer *Nuttallides truempyi*, the base acme of calcareous nannofossil *Clausicoccus subdistichus*, and the top of rosette discoasters.

The occurrence of *Orbulinoides beckmanni* in samples from 835.5 to 836.1 m constrains these depths to planktic foraminiferal Zone E12 (40.03–40.43 Ma), which effectively marks the Middle Eocene Climatic Optimum (MECO). For calcareous nannofossils, the base of *Dictyococcites bisectus* at ~836.1 m and the top of *Sphenolithus obtusus* at ~825.6 m indicate the post-MECO interval was recovered in this interval. However, Core 371-U1507B-51R (835.7–836.1 m) only recovered 38 cm (4%), so most of the MECO was washed away or lost during coring.

Radiolarians have a patchy record. Well-preserved Neogene radiolarians are found in samples from 6.2 to 54.1 m. The interval from 63.4 to 380.6 m is barren of radiolarians. The interval from 380.6 to 523.2 m contains varying amounts of radiolarians, ranging from trace to common, with some samples barren of radiolarians. Low-latitude index species are absent or rare.

Benthic foraminifers indicate paleodepths that gradually range from abyssal in the most recent part of the sequence to lower bathyal in the Oligocene and Eocene. In some intervals (e.g., ~205.6 m), their assemblages contain a mixture of deep-water and relatively shallow-water taxa with different preservation states. A palynological reconnaissance study carried out on 10 core catcher samples throughout the sedimentary sequence showed that deposits at Site U1507 are effectively barren of palynomorphs. Ostracods are rare to common between 6.2 and 279.7 m in Hole U1507A and absent in Hole U1507B, except for one sample.

The quality of paleomagnetic measurements on section halves from Holes U1507A and U1507B varies for different lithostratigraphic units. In Hole U1507A, the natural remanent magnetization (NRM) intensity is in the range of 10^{-2} A/m and increases from 234 m downhole by about one order of magnitude. NRM inclination is mostly positive, likely the effect of a present-day geomagnetic overprint. After AF demagnetization cleaning at 20 mT, the interval from 0 to 54.1 m is characterized by dominantly normal polarity with some intervals of reversed polarity. Between 53.7 and 215.6 m, some swings between positive and negative inclination without a clear bimodal clustering were observed, and from 216 m downhole inclinations are less stable. This instability may reflect some combination of drilling-related deformation, depositional processes, and weak magnetization. The average inclination for Hole U1507A is around −20°, and no reliable shipboard magnetostratigraphy could be obtained for this hole.

High-quality paleomagnetic data were obtained on sediments from Hole U1507B, including a well-defined series of normal and reversed polarity intervals in lithostratigraphic Unit I. Inclination values for Unit I after 20 mT AF demagnetization are clustered in two clear peaks around −40° and 45°. The overall high-quality paleomagnetic data from Hole U1507B can be attributed to the high NRM intensity and good recovery of lithified sediment cores. Integration with biostratigraphic results shows that the interval between 433.3 and 682.9 m contains most polarity chrons from Chron C6Br in the early Miocene through Chron C16n in the late Eocene.

Lithostratigraphic Unit II sediments generally show scattered inclination values without recognizable bimodal distribution. Two inclination changes at 759.3 and 834.0 m are tentatively correlated with the bases of Chrons C17n and C18n, respectively.

Anisotropy of magnetic susceptibility (AMS) was measured on 123 discrete samples from Site U1507, which were collected in the most undisturbed intervals and often on top of turbidite layers. The soft and magnetically weak sediments from Hole U1507A did not yield well-defined orientations of the AMS tensor. Cube samples from lithified sediment, however, show a clear oblate magnetic fabric in which the minimum axis of the AMS ellipsoid is statistically oriented perpendicular to the bedding.

Cores recovered from Holes U1507A and U1507B were analyzed with the full suite of physical properties measurements. Downhole temperature measurements were made in Hole U1507A, and wireline logging was completed using a modified triple combo tool string in Hole U1507B.

Bulk density increases with depth from the seafloor (1.5 g/cm^3) to the bottom of the hole (2.4 g/cm^3) with local decreases to ~1.6 g/cm^3 observed between ~420 and ~500 m. Moisture and density–derived porosity values correspondingly decrease from ~70% in nannofossil ooze at the top of Hole U1507A to ~25% in nannofossil chalk at the base of Hole U1507B. Grain density is ~2.71 g/cm^3 to ~300 m and then varies between 2.7 and 2.8 g/cm^3 to ~700 m, except for the interval from ~420 to 500 m, where grain density conspicuously drops to 2.6–2.7 g/cm^3. In lithostratigraphic Unit II, grain density decreases again to ~2.5–2.7 g/cm^3.

P-wave velocity measured on cores gradually increases downhole in Subunit Ia, with a more rapid increase around 290 m corre-

sponding to the diagenesis of ooze to chalk. From ~400 to 520 m, *P*-wave velocity increases from 2000 to 2500 m/s and then stays at similar values to the base of the hole. *P*-wave velocity from wireline logging increases from 2300 to 2700 m/s in Unit II, with a negative excursion to ~2400 m/s associated with the MECO at ~835 m.

Thermal conductivity increases gradually with depth from 1.1 to 1.8 W/(m·K) in Subunit Ia and decreases in Subunits Ib and Ic. In Hole U1507A, six temperature measurements were made with the advanced piston corer temperature tool (APCT-3), yielding a temperature gradient of 46.9°C/km.

MS is low (<50 IU) in Subunits Ia and Ib and as high as 1000 IU in Subunit Ic. Below 680 m, values decrease to ~40 IU and are constant in the lowermost part of the hole. NGR measured on cores and by wireline logging show matching downhole variations. NGR is low, except for positive excursions of ~20–40 counts/s between 400 and 520 m and between 520 and 680 m.

Changes in color reflectance occur at the base of Subunit Ia, where all parameters decrease, reflecting the darker and greener clay-rich sediments. A slight increase in lightness (L*) was observed at the top of Unit II.

Headspace gas samples were routinely collected from each core from Holes U1507A and U1507B. Hydrocarbon gas concentrations in all samples were below detection limits.

A total of 56 IW samples were collected from Cores 371-U1507A-1H through 45X (51 samples) and 371-U1507B-6R through 14R (5 samples). The results show a distinctive difference between above and below 250 m, corresponding to the change from APC to XCB or rotary coring. The IW constituent profiles are smooth in the upper 250 m and become scattered below 250 m. Despite this issue, Mg, K, and SO_4^{2-} generally decrease downhole, whereas Ca increases downhole. Dissolved Sr increases smoothly in the upper 160 m and then remains approximately constant with depth. The negative correlation between dissolved Ca and Mg concentrations suggests reactions between volcanic material and pore water in the sediment column. The downhole decrease in SO_4^{2-} suggests sulfate reduction of particulate organic carbon, which also explains the rise in dissolved NH_4^+ with depth.

Samples for solid sediment analysis were taken at a sampling resolution of at least one sample per core from Holes U1507A and U1507B. Carbonate content is very high (>90 wt%) throughout Subunit Ia. Decreasing carbonate content (30–70 wt%) toward the middle of Subunit Ib and Ic correlates well with changes in other properties, such as decreasing reflectance L*, increasing MS, and increasing NGR. Interbedded darker colored layers are represented by lower total carbon and carbonate contents (~20 wt%). Carbonate content in Unit II is high, varying between 50 and 80 wt%. TOC content is low (averaging 0.4 wt%) throughout the sediment column and does not differ significantly between units.

Linear sedimentation rates (LSRs) and mass accumulation rates (MARs) were calculated for Site U1507 using paleomagnetic and calcareous nannofossil datums (Figure **F11**). The record recovered at Site U1507 is remarkably continuous despite numerous turbidite deposits and seismic reflectors, and it includes the entirety of the Oligocene. LSRs in the mid- to late Eocene vary between ~30 and 60 m/My but decrease near the Eocene–Oligocene transition to ~15–20 m/My. An extended duration of low LSRs (~12 m/My) characterizes the Oligocene to middle Miocene, except for two short time intervals of enhanced LSRs (30–29 and 25–23 Ma). After 9.5 Ma, LSRs stepwise increase to 40 m/My at 7.4 Ma and remain at these high values until 4.0 Ma. This pulse in sedimentation, which is characterized by constant high carbonate contents, may correspond to the late Miocene to early Pliocene biogenic bloom as documented at other sites. The uppermost 4 My at Site U1507 are represented by a relatively condensed section with LSRs <4 m/My.

Sediment MARs follow the trend observed in LSRs and vary between 2 and 12 g/cm^2/ky.

Site U1508 (Reinga Basin)

Background and objectives

Site U1508 (proposed Site REIS-2A) is located ~130 km west of Cape Reinga, the northern tip of Northland, New Zealand. The location is on the northeast margin of Reinga Basin (Bache et al., 2012), which contains folded Eocene strata that have been dredged but never drilled (Browne et al., 2016). The site was chosen to sample a record of deformation, uplift, subsidence, and early arc volcanism in a southern region proximal to Tonga-Kermadec subduction initiation (Sutherland et al., 2016). The overall objective was to sample Miocene–Eocene strata that includes an onlap surface that marks the onset of deformation. A high-amplitude seismic reflector near the base of the borehole has regional significance for stratigraphic correlation and was hypothesized to represent a major change in sedimentation during the Eocene.

Operations

Hole U1508A: 34°26.8902′S, 171°20.6073′E; water depth = 1609 m
Hole U1508B: 34°26.8975′S, 171°20.5990′E; water depth = 1609 m
Hole U1508C: 34°26.8905′S, 171°20.5889′E; water depth = 1609 m

We completed the 546 nmi transit from Site U1507 to Site U1508 and arrived at 2300 h on 20 August 2017 (UTC + 10 h). An APC/XCB BHA was made up, and APC coring in Hole U1508A started at 0900 h on 21 August. Temperature measurements were taken on Cores 7H, 9H, 10H, 12H, 14H, and 17H. Core 23H had to be drilled over for 40 min to release it from the formation, and Hole U1508A was ended at 1140 h on 22 August. Total recovery for the 210.3 m DSF cored was 201.1 m (96%). The time spent on Hole U1508A was 36.0 h or 1.5 days.

The ship was offset ~20 m to the southwest. An RCB BHA was made up, and drilling without coring in Hole U1508B started at 1745 h on 22 August, reaching the target (186.6 m DSF) at 2245 h on 22 August. Coring in Hole U1508B began with Core 2R. While retrieving Core 38R (503.4 m DSF) at 0700 h on 24 August, we stopped operations because of a medical emergency and began recovering the drill string. Cores 2R through 38R penetrated from 186.6 to 503.4 m DSF and recovered 133.32 m (42%). The time spent on Hole U1508B was 49.5 h or 2.1 days.

The 302 nmi transit to Auckland began at 1354 h on 24 August. During the trip, the clock was advanced twice (to UTC + 12 h; Auckland time). On the way back from the medical evacuation, the clock was set back 1 h to UTC + 11 h and remained that way for the rest of the Expedition 371 drilling operations. The trip back to Site U1508 was completed at 0600 h on 27 August. An RCB BHA was deployed, and Hole U1508C was initiated ~20 m northwest of Hole U1508B at 1150 h. The uppermost 450 m of Hole U1508C was drilled without coring, except for two spot-cored intervals at 278.0–292.6 m DSF (Cores 2R through 4R) and 316.0–330.7 m DSF (Cores 6R and 7R) to better recover key intervals. At 0730 h on 28 August, we resumed RCB coring until penetration rates slowed to ~2 m/h. Although short of the desired target depth, we decided to stop coring and conduct wireline logging at 0300 h on 31 August. Collec-

tively, Cores 2R through 38R and the two drilled intervals penetrated from 278.0 to 704.5 m DSF and recovered 185.04 m of sediment (65% of cored intervals).

The bit was dropped at the bottom of the hole at 0325 h on 31 August, the hole was displaced with 194 bbl of 11.0 lb/gal mud, and the open end of the drill string was set at 86.7 m DSF. At 0900 h, we deployed the same modified triple combo logging tool string configuration as the one used in Hole U1507B, but no source was installed in the density tool. Logging went well until ~1230 h, when the tool string became stuck at ~270 m WSF. The logging line was cut at the rig floor and terminated with connectors that would allow assembly of drill pipe over the logging line to wash down and over the logging tools with the open-ended BHA. After the logging tools were free at 2105 h, the tool string arrived back on the rig floor at 0315 h on 1 September. After the drill string was recovered, the ship began the transit to Site U1509 at 0730 h on 1 September.

Principal results

The sedimentary sequence at Site U1508 consists of ~700 m of heterogeneous strata divided into three lithostratigraphic units (I, II, and III).

Lithostratigraphic Unit I (0.0–90.1 m) consists of ~90 m of foraminiferal ooze with varying amounts of nannofossils and coarse-grained bioclasts. An increase in the occurrence of millimeter-sized bioclasts composed mainly of bryozoans starts at ~49 m and extends to the bottom of the unit. The Unit I/II boundary at 90.1 m is defined by an abrupt change from foraminiferal ooze with bioclasts to clayey nannofossil ooze with biosilica.

Lithostratigraphic Unit II (90.1–379.3 m) consists of ~290 m of calcareous ooze and chalk with varying amounts of clay and is divided into two subunits. Subunit IIa (90.1–200.6 m) comprises light greenish clayey nannofossil ooze with varying contents of foraminifers and sponge spicules. Subunit IIb (200.6–379.3 m) is nannofossil-rich foraminiferal ooze and chalk with lithic and volcanic grains increasing to ~336 m and then decreasing downhole, resulting in a pure foraminiferal chalk in the lowermost 30 m of the subunit.

The lithostratigraphic Unit II/III boundary at 379.3 m was identified by an abrupt downhole decrease in grain size to nannofossil chalk with varying amounts of foraminifers. Unit III (379.3–701.9 m) is composed of moderately bioturbated nannofossil chalk, which is further divided into two subunits. Subunit IIIa (379.3–491.6 m) consists of moderately to heavily bioturbated clayey nannofossil chalk and contains at least 50 sporadic centimeter-scale cherty limestone intervals. Subunit IIIb (493.8–701.9 m) is characterized by a downhole decrease in clay content and color brightening, with cherty limestone last observed at ~503 m. Subunit IIIb comprises nannofossil chalk, and from ~685 m downhole it is sufficiently lithified to be classified as nannofossil limestone.

Calcareous nannofossils are abundant in most of the studied samples. Planktic foraminifers dominate over benthic foraminifers, which are present in most samples. Radiolarians are few to rare in most samples, barren in some samples from Holes U1508A and U1508B, and few to abundant in the lower half of Hole U1508A. Ostracods are abundant to common in Unit I and Subunit IIb and rare to barren in Subunits IIa, IIIa, and IIIb. Preservation of all fossil groups decreases downhole, ranging from excellent to good in the upper part of Hole U1508A and from moderate to poor in Hole U1508C.

Calcareous nannofossil and planktic foraminiferal datums, occasionally supplemented by radiolarian biostratigraphy, allow age assignments for all studied samples (Figure **F11**). Lithostratigraphic Unit I is Pleistocene–Pliocene in age. The interval between 96 and 210 m, nearly coincident with lithostratigraphic Subunit IIa, is Miocene in age. Samples between 187 and 373 m are Miocene to Oligocene in age. Nannofossil biostratigraphy points to an early Miocene to late Oligocene hiatus (Zones NN4–NN1) of ~6 My in both Holes U1508B (312–321 m) and U1508C (316–321 m). The interval from 379 to 497 m in Hole U1508B is late to middle Eocene in age. In Hole U1508C, the interval from 450 to 480 m is late Eocene in age and the interval from 484 to 686 m is middle Eocene in age. Nannofossils, planktic foraminifers, and radiolarians indicate an early Eocene age near the bottom of the sequence (686–702 m). Age-diagnostic dinocyst species corroborate the age constraints determined by nannofossils and planktic foraminifers.

Benthic microfossils (ostracods and foraminifers) indicate a lower bathyal paleoenvironment throughout most of the sedimentary sequence and at slightly shallower paleodepths (deep middle bathyal) during the Oligocene and late Eocene. Palynological assemblages contain moderately to well-preserved palynomorphs, which are predominantly inner neritic to pelagic dinocysts. Terrestrial palynomorph content is much higher in the Pliocene to late Oligocene than in the early Oligocene to Eocene, indicating a significant change in offshore transport. Reworked microfossils, particularly those of early Paleogene age, commonly occur downhole from the mid-Miocene in all fossil groups.

Pass-through paleomagnetic measurements from Unit I (0–90 m) are affected by core disturbance and have extremely weak magnetization (~10^{-5}–10^{-3} A/m), resulting in random NRM inclinations. NRM inclinations in Subunit IIa (~90–210 m) show a series of polarity swings but no clear polarity pattern. In contrast, high-quality paleomagnetic data were obtained from Subunit IIb from ~250 to 380 m with well-defined geomagnetic reversals. From lithostratigraphic Subunit IIb to Unit III, the NRM intensity drops to ~10^{-4}–10^{-3} A/m, resulting in poor paleomagnetic behavior for many cores. Reliable paleomagnetic data were obtained from some intervals in Hole U1508C, including 278–324 and ~650–700 m. Integration with biostratigraphy allows a series of paleomagnetic reversals in Holes U1508B and U1508C (Subunit IIb and Unit III) to be correlated with the GPTS back to ~48 Ma.

Samples from Hole U1508A have a poorly defined orientation of the AMS tensor, whereas most samples from Holes U1508B and U1508C exhibit a well-defined oblate AMS fabric with the minimum axis of the AMS ellipsoids statistically oriented perpendicular to the bedding plane.

Variations in physical properties define three distinctive boundaries at ~90, ~200, and ~500 m and are correlated with two strong reflections in the MCS data and three lithostratigraphic boundaries. The upper interval, corresponding to lithostratigraphic Unit I, is characterized by low density (~1.5 g/cm^3), high porosity (~65%–75%), and increasing velocity (~1500 to ~1700 m/s). All of these values show a baseline shift at the Unit I/II boundary (~90 m) to higher bulk density values (~1.65 g/cm^3), lower porosity values (~60%–65%), and lower velocity values (~1600 m/s) that remain constant throughout Subunit IIa to ~200 m. In the uppermost part of Subunit IIb (~200–250 m), bulk density decreases from ~1.75 to ~1.55 g/cm^3, porosity increases from ~60% to ~70%, and shear strength decreases from ~100 to ~30 kPa, whereas *P*-wave velocity increases from ~1600 to 1900 m/s. Below the Subunit IIIa/IIIb boundary at 500 m, bulk density gradually increases from 2.0 to 2.3 g/cm^3, porosity gradually decreases to ~25%, and *P*-wave velocity increases from ~2200 to 2600 m/s. At the very base of Subunit IIIb where the

transition from chalk to limestone occurs (680–700 m), velocity and bulk density sharply increase to ~3600 m/s and 2.45 g/cm^3, respectively.

NGR and color reflectance data reveal complementary trends to the density, porosity, and velocity measurements, including the three distinctive boundaries at ~90, ~200, and ~500 m. NGR increases and the color changes at ~90 m. NGR decreases and then increases around ~200 m. MS from wireline logging and core measurements are low throughout the entire section, except for the interval from ~240 to ~380 m (Subunit IIb), which contains lithic constituents. This interval also has higher amplitude (as high as ~20 counts/s) NGR variations.

Five in situ temperature measurements in Hole U1508A revealed a gradient of ~55°C/km.

Headspace gas samples were routinely collected from each Hole U1508A core and from deeper Hole U1508C cores. Methane was above the detection limit from ~460 m downhole and progressively increased below ~500 m. At the base of Hole U1508C, methane concentration was ~6000 ppmv and ethane concentration was 36 ppmv.

A total of 75 IW samples were collected from Site U1508 by three different methods: whole-round squeezing, Rhizon sampling, and half-round squeezing. The latter were ~15 cm intervals taken from core working halves 1–2 days after recovery and crushed in plastic bags. These half-round samples yield reasonable results for some dissolved species, notably sulfate. Rhizon results generally lie close to those from squeezed samples at nearby depths. The manganese concentration profile does not show a peak in the uppermost meter or so, which suggests the true mudline is missing. Adjacent samples from the upper ~100 m of the section have large variance because the sediment is unconsolidated foraminiferal sand, which makes collection of uncontaminated pore water difficult. Nonetheless, most constituents do not vary much in concentration over the uppermost 275 m. Below 275 m, sulfate concentrations decrease downhole linearly and ammonium, barium, and strontium concentrations increase linearly or exponentially. The concomitant loss of sulfate and rise in methane from ~500 m downhole suggests a deep zone of anaerobic oxidation of methane (AOM), which also may explain the abundant macroscopic pyrite at this depth interval.

Bulk sediment carbonate content varies considerably with depth, with 100 m scale fluctuations between highs of ~95 wt% and lows of ~40 wt% that relate to the lithostratigraphic units. TOC content is 0.76 ± 0.36 wt% without any consistent downhole trend.

All cores from Holes U1508A–U1508C were correlated with the downhole logging data (on the wireline log matched depth below seafloor [WMSF] depth scale) using one tie per core. An offset table allows users to approximate depths of core data on the core depth below seafloor (CSF-A) depth scale to the WMSF depth scale of the downhole logging data.

LSRs were calculated for Site U1508 using calcareous nannofossil datums and polarity chron boundaries from 0 to 48 Ma (Figure **F11**). LSRs in the Pliocene–Pleistocene vary between ~10 and 80 m/My, and they average ~20 m/My during the early to late Miocene. The succession is condensed for most of the Oligocene despite a short interval from 23 to 26 Ma. LSRs for the late to middle Eocene are steady at ~20 m/My.

Site U1509 (southern New Caledonia Trough)

Background and objectives

Site U1509 (proposed Site NCTS-2A) is located ~640 km west of the northern tip of New Zealand, ~300 km south of Site 206, and ~200 km north of DSDP Site 592. The location is on the western margin of the New Caledonia Trough at the base of the Lord Howe Rise slope near the mouth of a canyon that drains around the northeast end of a small submerged spur (Sutherland et al., 2016). This spur, inferred to have been created by deformation, is underlain by the northeast-dipping limb of a west-verging fold that exposes strata that can be traced beneath the axis of the New Caledonia Trough. Site U1509 was chosen to determine the timing of Cenozoic folding in the southern New Caledonia Trough and to obtain stratigraphic constraints on the timing of vertical tectonic movements and volcanism.

Operations

Hole U1509A: 34°39.1312′S, 165°49.6599′E; water depth = 2911 m

We arrived at Site U1509 at 1030 h on 2 September 2017 (UTC + 11 h), completing the 273 nmi transit from Site U1508. RCB coring in Hole U1509A was initiated at 2145 h on 2 September. The decision to use the RCB system was made after considering target depth, time constraints, and success at previous sites. Coring continued until 2345 h on 6 September and reached 690.7 m DSF (Core 74R). Total recovery in Hole U1509A was 462.86 m (67%).

Planned wireline logging in Hole U1509A was canceled because of ship heave exceeding 3.0 m. Hole U1509A was ended at 1434 h after a total of 127.5 h or 5.3 days. At 1630 h on 7 September, the ship began a ~200 nmi transit to the north to avoid severe weather forecast for 9–10 September; this weather also impacted operations at the remaining drilling sites.

Principal results

The sedimentary sequence at Site U1509 consists of ~415 m of calcareous ooze, chalk, and limestone (Unit I) overlying ~275 m of claystone (Unit II).

Lithostratigraphic Unit I is divided into three subunits. Subunit Ia (0–99.6 m) consists of calcareous ooze and chalk with rare tuffaceous beds. RCB coring led to soupy and mousse-like drilling disturbance in the soft sediments of the upper ~50 m of this subunit, followed by biscuiting, horizontal cracking, fracturing, and pulverization in the more indurated lower sediment of the unit. The ooze–chalk transition was observed at a remarkably shallow depth of ~55 m. Subunit Ib (99.6–139.28 m) comprises calcareous chalk showing significant soft-sediment deformation (i.e., slumps). Subunit Ic (139.28–414.57 m) consists of calcareous chalk and limestone with biosilica and several silicified (chert) intervals. Subunit Ic is characterized distinctively by tilted bedding (apparent dip of ~20°). From Subunit Ic downhole, preferential fracturing of cores was seen along primary deformation structures such as shear zones, microfaults, and tilted bedding. The chalk–limestone transition occurs in Subunit Ic at around 385 m.

Lithostratigraphic Unit II is divided into two subunits. Subunit IIa (414.57–614.2 m) consists of claystone with nannofossils and silt. Subunit IIb (614.2–689.68 m) consists of massive brown claystone with minor bioturbation and agglutinated benthic foraminifers. Similar to Subunit Ic, tilted bedding was observed throughout Unit II.

Nannofossil and planktic foraminifer preservation and abundance generally decrease downhole, with these groups absent below 617.6 and 536.0 m, respectively. Radiolarians are rare to abundant and well preserved in the upper 393 m but are rare and poorly preserved farther downhole. Benthic foraminifer abundance is low, and preservation decreases downhole in the upper 249 m and remains

poor below. Only agglutinated taxa are found in sediments below 617.6 m. Ostracods are common to rare with moderate to poor preservation in the upper 178 m and are rare to barren below. A palynological reconnaissance study focused on Unit II and recovered rich and well-preserved assemblages.

Nannofossil and foraminifer datums yielded Miocene (22.41–82.47 m), Oligocene (90.13–248.63 m), Eocene (259.98–407.07 m), and Paleocene (418.53–609.27 m) ages for the sequence in Hole U1509A (Figure **F11**). The interval from 617.6 to 689.6 m is barren of age-diagnostic nannofossils and planktic foraminifer taxa but contains Late Cretaceous dinocysts and agglutinated benthic foraminifers. Benthic foraminifers indicate deposition in a lower bathyal–abyssal environment during the Pleistocene to Eocene and at middle bathyal depths during the Paleocene and Cretaceous.

The NRM intensity of most sediment cores from Hole U1509A is weak, mostly around 10^{-4} A/m, which results in generally noisy paleomagnetic data from the pass-through magnetometer. However, step-wise AF demagnetization of some discrete samples gives reliable paleomagnetic data. Integrating these data with biostratigraphy, the observed magnetic polarity values at 110 to ~260 m are tentatively correlated with Chrons C9 through C13 of GPTS2012. The claystone interval of Subunit IIb produces higher quality pass-through data compared with intervals above. Subunit IIb cores have a normal magnetic polarity.

Physical properties measurements on Hole U1509A cores exhibit gradual changes in bulk density and *P*-wave velocity with depth, except across a layer of limestone between ~390 and 415 m. Through the ooze and chalk, above the limestone, *P*-wave velocity and bulk density increase with depth from 1500 to 1900 m/s and from 1.55 to 1.90 g/cm^3, respectively. The transition from ooze to chalk is shallow (~55 m) and correlates with a *P*-wave velocity increase of ~100 m/s. The limestone of Subunit Ic represents a discrete interval where *P*-wave velocity and density increase by ~40% and porosity decreases sharply. *P*-wave velocity, bulk density, and MS are approximately constant in the Unit II claystone below the limestone. A gradual decrease in porosity with depth was also observed. NGR values show high variance in Unit II (from 8 to 30 counts/s), reflecting changes in clay composition and abundance.

A total of 23 IW samples were collected from Hole U1509A. Profiles of some species show trends similar to those at Site U1508. For example, sulfate concentrations decrease and ammonium concentrations increase downhole, suggesting sulfate reduction of particulate organic matter and release of nitrogen to pore water. Furthermore, at ~370 m, sulfate concentrations drop below 1.0 mM and methane concentrations start to rise, suggesting further sulfate consumption by AOM at a deep sulfate–methane transition (SMT). Sulfate reduction leads to the production of hydrogen sulfide, which reacts with iron to form pyrite (Snyder et al., 2007), which is present in many cores from this hole. Below the SMT, headspace methane concentrations increase to 15,000 ppmv and dissolved Ba concentrations increase to 0.4 mM. Such values are common to slope environments of many continental margins.

Bulk sediment chemistry corresponds to lithostratigraphic units. Unit I is characterized by carbonate content that decreases downhole from ~94 wt% at 20 m to ~65 wt% between 360 and 380 m. Carbonate content varies little in the uppermost 200 m but by more than 10% in the lower part of the unit. Carbonate content drops drastically across the Unit I–II transition (415 m) to average values of 18 and 0.5 wt% in Subunits IIa and IIb, respectively. TOC content is ~0.3 wt% in Unit I and Subunit IIa and ~1.0 wt% in Upper Cretaceous Subunit IIb.

Site U1510 (southern Lord Howe Rise)

Background and objectives

Site U1510 (proposed Site LHRS-3A) is located on the southern Lord Howe Rise, ~850 km west of northern New Zealand and ~495 km south of Site 206. Site U1510 is ~80 km west of Site 592 and ~105 km northwest of Site 207. Seismic reflection data can be used to tie stratigraphy at the three sites but with some uncertainty caused by unconformities and deformation (Sutherland et al., 2016). Site U1510 was chosen to determine the timing of Cenozoic folding on the southern Lord Howe Rise and to constrain the timing of regional tectonic movements and volcanism. The primary drilling objectives at Site U1510 were to (1) constrain the depths and ages for the top and base of the syntectonic seismic unit, (2) determine the nature of the lowest seismic unit and pretectonic state of the southern Lord Howe Rise, and (3) collect evidence for volcanism or vertical movements, especially including sediments representing nearby shallow water of any age. A secondary objective was to collect a continuous late Neogene record for paleoceanographic studies.

Operations

Hole U1510A: 36°19.7385′S, 164°33.5220′E; water depth = 1238 m
Hole U1510B: 36°19.7392′S, 164°33.5347′E; water depth = 1238 m

After the 380 nmi transit in heavy winds and seas from a waiting on weather location, the ship arrived at Site U1510 at 0918 h on 12 September 2017 (UTC + 11 h).

An APC/XCB BHA was deployed, and coring in Hole U1510A started at 1915 h on 12 September. Cores 1H through 17H penetrated from 0 to 150.5 m DSF and recovered 147.9 m (98%). We stopped deploying the orientation tool after Core 15H. Temperature measurements were taken on Cores 4H, 7H, 10H, 13H, and 17H. We continued with XCB coring until 1930 h on 14 September. Cores 18X through 52X penetrated from 150.5 to 483.4 m DSF and recovered 108.1 m (32%). Recovery over portions of this depth interval was seriously compromised because of frequent chert layers. Coring in Hole U1510A concluded on 14 September with a total penetration to 483.4 m DSF and total recovery of 260.0 m (53%). The time spent on Hole U1510A was 60 h or 2.5 days.

The ship was offset 20 m to the east, and APC coring in Hole U1510B began at 2300 h on 14 September and ended at 0215 h on 15 September. Cores 1H through 7H penetrated from 0 to 66.3 m DSF and recovered 64.7 m (98%). An APCT-3 temperature measurement was taken on Core 7H. Operations in Hole U1510B and at Site U1510 ended at 0815 h on 15 September. The time spent on Hole U1510B was 10.75 h or 0.4 days. At 0842 h, the ship began the transit to Site U1511.

Principal results

Lithostratigraphic Unit I (0–138.0 m) is composed of calcareous ooze and is divided into two subunits. Subunit Ia (0–60.0 m) consists of subtle color banding between light gray and white calcareous ooze. Subunit Ib (60.0–138.0 m) is white homogeneous calcareous ooze. The Unit I/II boundary is defined by the first occurrence of chert at 138 m.

Lithostratigraphic Unit II (138.0–418.1 m) consists of ~340 m of calcareous ooze and chalk interbedded with cherty limestone and chert. Unit II is divided into three subunits. Subunit IIa is a ~9.5 m thick white homogeneous nannofossil ooze with bioclasts. The upper ~30 cm of Subunit IIa consists of centimeter-sized extraclasts composed of chert, cherty limestone, and lithic clasts. Although this interval could be affected by drilling disturbance (i.e., "fall-in" at the

top of the core), it also contains the first occurrence of chert; similar material had not been found in the cores above. Subunit IIb (147.5–349.4 m) is a 201.9 m thick interval of light gray moderately bioturbated clayey calcareous chalk with scattered shallow-water bioclasts interbedded with cherty limestone. Subunit IIc (349.4–478.1 m) is a 128.7 m thick homogeneous white nannofossil chalk interbedded with chert and sparse volcaniclastic beds in the lower portion of the subunit.

Core recovery in Unit I was near 100%, with coring disturbance limited to up-arching and soupy sediments. Recovery dropped to ~20% in Subunits IIa and IIb because of the presence of chert and cherty limestone and the use of the XCB coring system, and drilling disturbance included severe fracturing of chert and cherty limestone intervals and moderate to severe biscuiting of calcareous chalk intervals.

Nannofossils are generally abundant with moderate preservation. Planktic foraminifer abundance and preservation decrease downhole (from 215 and 187 m, respectively), with a few barren samples. Radiolarians are rare throughout, except for a short middle Miocene interval (109.6 to 119.7 m) where radiolarians are common. Radiolarian preservation is good in the upper 135 m and poor farther downhole. Benthic foraminifers were recovered at generally low abundance from all cores, with very good preservation for the Neogene and generally poor preservation for the Paleogene. Ostracods are very abundant in most samples, with good preservation from 0 to ~150 m and poor preservation below. Because of weather constraints on processing, no samples from Site U1510 were analyzed for palynology. Paleodepth was lower bathyal from the Pleistocene through the Eocene. During the late and middle Eocene, a significant component of the benthic fauna appears to be derived from shallower (shelf, upper bathyal, and middle bathyal) sources.

Based on nannofossil and foraminifer biostratigraphy, the following ages were determined for the sequence in Hole U1510A: Pleistocene (5.0–33.5 m), Pliocene (43.1–70.3 m), Miocene (72.3–135.4 m), and late, middle, and early Eocene (138.8–147.7, 150.5–438.9, and 448.9–478.2 m, respectively).

The low NRM intensity of most cores, low core recovery, and significant core disturbance from XCB coring make it difficult to establish shipboard magnetostratigraphy at Site U1510.

Physical properties measurements show a gradual increase in bulk density and *P*-wave velocity with depth in the nannofossil and foraminiferal ooze of Unit I. In Subunits IIa and IIb, from 140 to ~350 m, physical properties measurements are less reliable and sparse because of drilling disturbance and low recovery, respectively. Bulk density (~1.75 g/cm^3) and *P*-wave velocity (~1750 m/s) increase downhole to 300 m and then decrease again to the base of Subunit IIb, where fewer chert layers were observed. MS and NGR both increase downhole in these two subunits and then decrease toward the base of Subunit IIb. *P*-wave velocity peaks and spikes in NGR in Subunit IIc correlate with sandstone and claystone. Near the base of the hole (~470 m), where sediments become more lithified, density and velocity increase and porosity decreases.

Headspace samples from Site U1510 yielded hydrocarbon gas concentrations below detection limits.

A total of 118 IW samples were taken from Site U1510 by squeezing whole-round sediment and Rhizon sampling (Dickens et al., 2007). Ca concentrations increase downhole and Mg and K concentrations decrease, similar to Sites U1506 and U1507. These profiles may result from the reaction of pore water with volcanic material in the sediment. Sulfate and ammonium concentration profiles mirror each other, suggesting sulfate reduction of organic matter. Dissolved Sr, Si, Li, and B concentrations increase downhole, likely reflecting dissolution of biogenic carbonate and silica. Dissolved Mn and Fe concentrations decrease in the uppermost 1 m, suggesting the true mudline is missing. Dissolved Fe concentrations in Rhizon samples decrease rapidly over the upper 8 to 10 m, consistent with the odor of H_2S at ~10 m.

Carbonate content is >90 wt% in Unit I and in Subunits IIa and IIc, corresponding to calcareous ooze and chalk lithologies. In Subunit IIb, carbonate content decreases downhole toward the middle of the subunit, and L* decreases and NGR increases. Interbedded cherty and tuffaceous layers are distinguished by carbonate contents of <50 and <20 wt%, respectively. TOC content is mostly below the detection limit but is represented by somewhat higher values (0.35 wt%) below 400 m.

Coring in Hole U1510B was monitored in near real time through out-of-sequence measurement of whole-round sections. Using primarily NGR data, Hole U1510A and U1510B cores were depth shifted to construct a composite depth scale. A spliced record was generated using the composite scale, which provides a continuous record of the top ~44 m of sediment at Site U1510.

Site U1511 (Tasman Abyssal Plain)

Background and objectives

Site U1511 (proposed Site TASS-2A) is located on the Tasman Abyssal Plain, ~945 km east of Australia and ~990 km northwest of New Zealand. Site U1511 lies west of Lord Howe Rise on oceanic crust of Late Cretaceous age that is thought to have formed during Chron C33 (74–84 Ma). Regional seismic reflection data reveal a thick (>800 m) sequence of sediments deformed by reverse faults and folds (Sutherland et al., 2016). Site U1511 was chosen to find the age of this deformation and provide the second comprehensive record of sedimentation on the Tasman Abyssal Plain. The primary drilling objectives at Site U1511 were to sample (1) the top of the middle seismic unit to constrain the age of folding and (2) the rest of the sedimentary sequence to develop an understanding of this significant abyssal location. The only previous scientific borehole into Tasman Abyssal Plain sediments was drilled in 1973 at DSDP Site 283, 870 km to the southwest and on conjugate crust of Late Cretaceous age east of southeast Australia.

Operations

Hole U1511A: 37°33.6665′S, 160°18.9380′E; water depth = 4847 m
Hole U1511B: 37°33.6656′S, 160°18.9379′E; water depth = 4847 m

The ship completed the transit from Site U1510 and arrived at Site U1511 at 1248 h on 16 September 2017 (UTC + 11 h). RCB coring in Hole U1511A began at 0425 h on 17 September. After retrieving Core 3R, the drill string had to be pulled clear of the seafloor because of excessive heave and wind. Cores 1R through 3R penetrated from 0 to 26.6 m DSF and recovered 7.9 m (30%). A total of 19.25 h or 0.8 days were spent on Hole U1511A.

After waiting 17 h because of weather, Hole U1511B was initiated at 0145 h on 18 September by washing down (i.e., drilling without coring and without a center bit installed) to 19.8 m DSF. Coring resumed at 0215 h on 18 September, and Cores 2R through 7R penetrated from 19.8 to 77.2 m DSF. A center bit was deployed, and the interval from 77.2 to 192.2 m DSF was drilled without coring to ensure we could reach the target depth in the remaining time of the expedition. Coring resumed at 1500 h on 18 September, and Cores 9R through 41R penetrated from 192.2 to 508.8 m DSF. At 1600 h on 20 September, coring was suspended because of excessive heave,

and the drill string was raised above the bottom of the hole. As the swell began to subside at 1030 h on 21 September, the drill string was lowered back to the bottom of the hole. After pumping a 25 bbl mud sweep, coring resumed at 1600 h on 21 September and ended with the recovery of the last core (47R) at 0450 h on 22 September. The total cored interval in Hole U1511B was 431.4 m DSF, and recovery was 279.3 m (65%). Two intervals were drilled without coring for a total of 134.8 m.

The rig floor was secured for transit to Hobart at 1630 h on 22 September, ending Hole U1511B and Site U1511. A total of 110.75 h or 4.6 days were spent on Hole U1511B. The total time at Site U1511 was 130.0 h or 5.4 days, including 40.5 h lost because of weather.

Principal results

The three lithostratigraphic units described are differentiated by the presence or absence of microfossils. Unit I (0–77.2 m) is ~80 m of gray to brown clay with calcareous nannofossils restricted to the lowermost 40 cm of the unit. Unit II (201.9–403.4 m) is separated from Unit I by a ~120 m drilled interval and consists of ~200 m of greenish gray to yellowish brown diatomite with minor abundances of clay and other siliceous microfossils (radiolarians, sponge spicules, ebridians, and silicoflagellates). Unit III (403.4–560.7 m) is ~150 m of claystone. A ~30 m reddish brown interval near the top of Unit III contains minor abundances of radiolarians. A ~40 m grayish green interval near the bottom of the unit contains minor abundances of calcareous nannofossils.

A variety of secondary minerals are present throughout Site U1511, attesting to diagenesis and alteration. Manganese nodules and black specks of sulfides occur in Unit I, whereas sporadic centimeter-scale nodules and specks of pink rhodochrosite occur in Unit II. Several centimeter-scale intervals of greenish gray claystone in Units II and III contain sand-sized grains of native copper surrounded by dark green halos. The lower part of Unit II also contains cristobalite and an interval of red and pink fluorapatite. Furthermore, a color gradient across Unit III from red and reddish brown at the top of the unit to greenish gray toward the base, with alternations of the two colors in the intervening interval, seems to be related to trace amounts of redox-sensitive metal oxides. These minerals suggest a complex history of diagenesis and alteration, the latter possibly mediated by past fluid flow.

Calcareous nannofossils and planktic foraminifers are generally absent throughout Site U1511. When present, their abundances and preservation states are varied. Radiolarians are present from 192 to 547 m and are abundant from 209 to 394 m, with good preservation. Below, radiolarians are less abundant and poorly preserved.

Benthic foraminifers are sparse in the Pliocene to lower Eocene interval, where a low-diversity agglutinated assemblage was recognized. The transition to a higher diversity Paleocene to lowermost Eocene assemblage was observed at the contact between lithostratigraphic Units II and III. The Paleocene interval contains both agglutinated and calcareous taxa. Samples are barren of ostracods and palynomorphs. Given the overall microfossil assemblages, the location of Site U1511 has probably been abyssal and beneath or near the calcite compensation depth (CCD) since the Paleocene.

Rare nannofossils and planktic foraminifers found through the Pliocene, Miocene, lower Oligocene, and Paleocene intervals were used to constrain age where possible (Figure **F11**). Based on planktic foraminifers, Pliocene (7.5–7.6 m), lower Pliocene to upper Miocene (7.5–47.6 m), and possible Miocene (65.6–65.7 m) strata were recognized. Based on calcareous nannofossils, the lower Oligocene (192.2–204.0 m) was identified; however, sediments from this level may have come from the drilled interval and may not be in situ.

Based on radiolarian biostratigraphy, upper Eocene (209–235 m), lower to middle Eocene (235–389 m), and Paleocene (432–539 m) strata were recognized. The lower to middle Paleocene (538.8–539.4 m) was also identified based on nannofossil biostratigraphy.

High-quality paleomagnetic data were obtained across intervals of Units II and III. In Cores 371-U1511B-14R through 30R (~240–400 m), all polarity reversals from the base of Chron C17n.3n to Chron C21n were identified, indicating that Unit II in Hole U1511B spans from ~38 to 47.5 Ma (Bartonian–Lutetian). Four magnetic polarity reversals in Core 38R can be successfully correlated with Chrons C24n.1n to C24.2n (~53 Ma).

The remanence intensity of sediments from Units II and III exhibits possible cycles. These variations appear related to lithologic color changes, where brown intervals generally have a higher magnetization compared with the lower magnetization in the gray sediment intervals. Such changes may be related to magnetic mineral diagenesis. Many samples in Unit III show magnetically hard NRM behavior that is resistant to AF demagnetization. Such a hard remanence component is carried by hematite, which probably contributes to the reddish sediment color in Unit III.

Cube samples from Units II and III show reliable AMS data and distinct patterns for Units II and III. Samples from Unit II indicate a random orientation of the AMS tensor, which probably reflects a random deposition of minerals without sediment compaction. In contrast, sediments from Unit III exhibit a well-defined oblate AMS fabric, which is typical for compacted sedimentary rocks.

Porosity decreases downhole from 80% to 65% in Unit I along a trend typical for pelagic clay. This trend continues in Unit III (from 60% to 45%). In Unit II, however, porosity is offset to extremely high values (70%–83%). This general profile is mirrored in bulk density and is attributed to the diatomite with clay in Unit II. *P*-wave velocity increases linearly downhole, except for two peaks, one in the lower part of Unit II (1750 m/s) and the other in the middle part of Unit III (1850 m/s). MS values vary between 5 and 50 IU in Unit I and near the top of Unit III and are much lower in Unit II and in the lower part of Unit III. NGR has a similar trend, and both MS and NGR appear to correspond to clay content. All color reflectance parameters (L*, a*, and b*) increase downhole from 200 to 300 m and then decrease from 300 to 400 m, corresponding to the diatomite in Unit II. A step increase in bulk density (1.50–1.75 g/cm^3), MS, NGR, and a* and b*, associated with a decrease in porosity (from 70% to 52%), is attributed to a red claystone interval in the top of Unit III (~410 m).

Headspace samples from Site U1511 yielded no light hydrocarbon gas concentrations above detection limits.

Low carbonate (<15 wt%) and TOC (<0.4 wt%) contents prevail throughout the sedimentary column at Site U1511. Carbonate content only rises >1 wt% in samples from two intervals: at the bottom of Unit I (71–77 m) and in the lower half of Unit III (490–539 m).

A total of 50 IW samples were collected at Site U1511 by two methods: squeezing and Rhizon sampling. At the precision required to understand basic processes at Site U1511, squeeze and Rhizon samples give similar profiles for most dissolved species. These profiles show some general trends and some unusual features, reflecting a combination of lithology and multiple processes.

As also observed at other Expedition 371 sites, modest oxidation of particulate organic carbon leads to production of alkalinity and NH_4^+ and removal of SO_4^{2-}. Limited dissolution of biogenic silica occurs, which increases dissolved H_4SiO_4 (particularly in Unit

II). Dissolved Ca increases downhole and dissolved Mg and K decrease, suggesting reactions with silicate minerals. However, the change in Ca relative to Mg with respect to depth is much greater at Site U1511 than at other Expedition 371 sites, which probably results from reactions with underlying basalt rather than sediment or continental crust. Many species display an inflection in concentrations at ~200 m and a major drop in concentrations at ~400 m. The first change probably results from the major increase in porosity associated with diatomite; the latter change probably represents the conversion of biosilica to cristobalite and the release of water. Dissolved Mn increases slightly in the upper 80 m but sharply below 200 m, reaching an extreme of 357 µM at 421 m. Such high values suggest dissolution of Mn oxides in the lower layer of the sediment column. Ammonium concentrations are below the detection limit across the uppermost 20 m, which may indicate a deep horizon of ammonia oxidation.

Physical properties, paleomagnetic, and biostratigraphic data were compiled to locate middle Eocene climate events in Hole U1511B. Interpretation of magnetic inclination and radiolarian assemblages indicates the MECO was recovered in Core 371-U1511B-16R. The putative Chron C19r hyperthermal event (Edgar et al., 2007) may be present in Core 18R, based on natural magnetic remanence data.

Summary of scientific results

Results compared with objectives

Expedition 371 targeted Paleogene sediment sequences across an extensive area of northern Zealandia with multiple objectives. The main goal was to obtain stratigraphic records of subduction zone initiation in the southwest Pacific and hence complement results from Expeditions 350, 351, and 352 in the northwest Pacific. We successfully completed this objective by coring at six sites that were optimally located on the basis of local and regional seismic reflection lines and from consideration of regional structure and plate motion history. A summary of spatial and temporal relationships discovered is shown in Figure **F12**.

Secondary objectives were designed to address aspects of regional paleoceanography. Three previous scientific drilling expeditions to the Tasman Sea (Legs 21, 29, and 90) focused on Cenozoic paleoceanography of the region and led to several key insights. However, this work, as nicely summarized by Kennett and von der Borch (1986), also highlights biases in the paleoceanographic literature: (1) the proportion of text that discusses the Paleogene as compared with the Neogene is approximately 26%, whereas the Paleogene represents ~65% of the combined geological time; (2) conclusions come from extrapolations across a vast and poorly mapped area; and (3) the detailed records come without full consideration of diagenetic reactions. Expedition 371 was an opportunity to address each of these issues: (1) our focus was on understanding Paleogene stratigraphy; (2) our site selection was grounded by a greatly expanded geophysical data set; and (3) our shipboard chemistry and physical properties measurements were far more extensive than possible when the previous drilling was conducted more than 30 years ago. Under very high atmospheric pCO_2 conditions or high climate sensitivity, global climate models (Huber and Caballero, 2011; Lunt et al., 2012) can reasonably simulate early Eocene warming in many regions (Douglas et al., 2014; Tripati et al., 2003) but not the extreme warmth inferred for the southwest Pacific and Southern Ocean (Bijl et al., 2009; Hollis et al., 2009, 2012; Pross et al., 2012), making it important to gain better-resolved SST reconstructions from this region. Furthermore, because this mismatch could be related to errors in paleogeographic reconstructions, the primary tectonic science objective of Expedition 371 relates to secondary objectives.

Figure F12. Summary of spatial and temporal relationships discovered during Expedition 371.

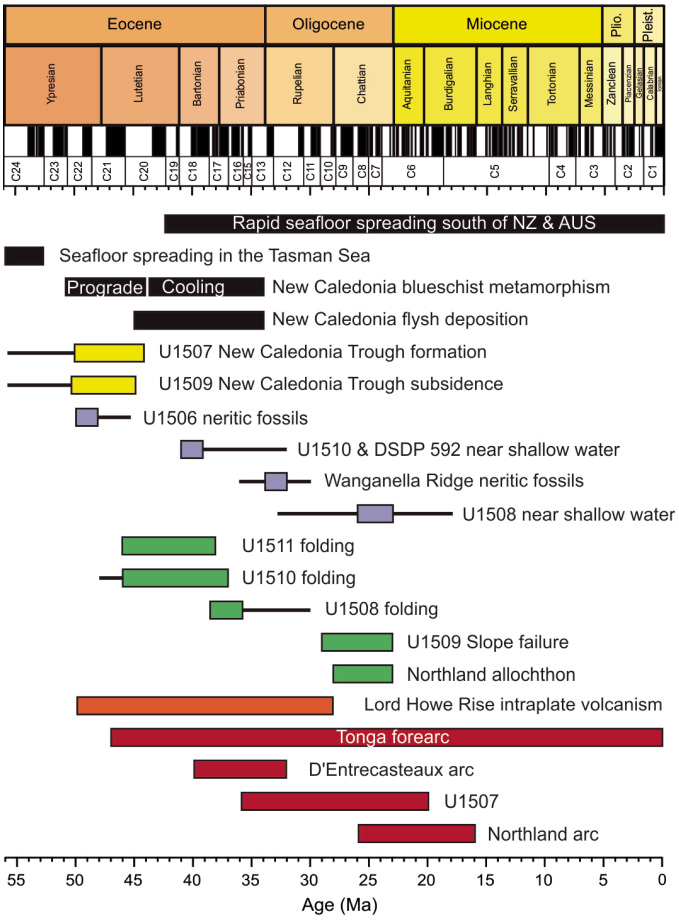

Our results advance our understanding of compaction and diagenesis of bathyal sediment. We find that sediment accumulation and diagenesis across the Tasman Sea were variable in space and time and can be related to differences in sedimentation type and tectonic history. Our data sets of physical properties, chemistry, burial depth, and sediment composition provide a diverse view of bathyal sediments deposited on oceanic rises distant from land. Empirical relationships may be derived from these data that can be applied elsewhere and used to understand underlying processes of compaction and diagenesis.

Observations made at our six sites represent a substantial gain in knowledge about northern Zealandia, a large underexplored region. The only previous boreholes that penetrated strata older than late Eocene were at Sites 206, 207, and 208 (Shipboard Scientific Party, 1973a, 1973b, 1973c), and these sites were drilled in 1971 (Leg 21), before regional seismic reflection data were available and the context of sites was understood. It was widely accepted that the stratigraphic development of the region was simple: Cretaceous rift to drift processes created the first-order physiography and initial subsidence; additional subsidence during the Cenozoic only secondarily affected the region (Figure **F13**).

Expedition 371 was founded on high-quality seismic reflection data that raised new ideas about how the region had evolved, specifically the recently discovered Tectonic Event of the Cenozoic in the Tasman Area (TECTA) (Sutherland et al., 2010, 2017; Collot et al., 2008, 2009; Bache et al., 2012, 2014a; Baur et al., 2014; Rouillard et al., 2017; Etienne et al., 2018). We drilled six sites to test these ideas by focusing on the timing of deformation, the uplift and subsidence history, and the presence of past volcanism. The sites greatly increased the available material from Eocene and older strata on submerged portions of Zealandia (Figure **F14**). Only two continents on Earth remain largely unexplored: Antarctica and Zealandia. Therefore, our new regional stratigraphic knowledge, which has significance for understanding regional paleogeographic, climatic, and biotic evolution, is of global interest.

Figure F13. A widely held hypothesis for stratigraphic development of the region studied during Expedition 371 is that Cretaceous rifting (bottom) was followed by transgression (middle) and development of deep water (top) before the end of the Cretaceous. Further subsidence then led to the existing geography. This hypothesis is not consistent with our finding of Eocene fossils indicative of shallow water on the crest of the Lord Howe Rise, extensive Paleogene erosion surfaces, and widespread reverse faulting of Eocene age.

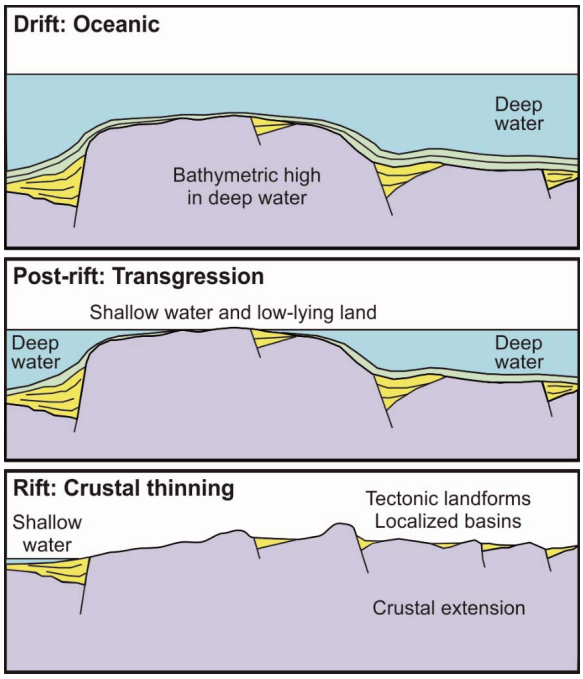

Subduction zone initiation

Timing and style of deformation

Observations at Sites U1508–U1511 place age constraints on the timing of convergent plate failure at the southern end of the subduction system in the southwest Pacific. Results from Site U1507 provide a unique new insight into subduction initiation adjacent to New Caledonia. Conclusions presented here are based on high-quality age models tied to seismic reflection images at each site.

At Site U1507, we collected the first record of sedimentation in the northern New Caledonia Trough. Almost all previous publications have assumed that this part of the sedimentary basin was created during Cretaceous rifting (e.g., Auzende et al., 2000; Lafoy et al., 2005; Schellart et al., 2006; Cluzel et al., 2012; Matthews et al., 2015). In our predrilling analysis of seismic reflection data, we identified three seismic units: (1) an upper onlapping unit, (2) a downlapping middle unit that indicated a period of high sediment supply from Norfolk Ridge, and (3) a lower unit of continuous reflectors with subunits in its lower part and a normal-faulted base. The hypothesis we tested by drilling was that the lower unit was formed by Cretaceous rifting and then postrift subsidence, the middle unit corresponded to deformation of Norfolk Ridge during subduction initiation, and the upper unit represented sediment accumulation under conditions similar to the present. We discovered that the middle unit (lithostratigraphic Subunits Ib and Ic at Site U1507) was composed of clayey chalk with volcaniclastic deposits ranging in age

Figure F14. Site locations in relation to regional seismic stratigraphic relationships. Pink layers are interpreted to be those deposited during times of active uplift, erosion, volcanism, and reverse faulting. In the northern New Caledonia Trough (Site U1507), the basal layer was assumed to be Cretaceous to Eocene in age, as indicated by drilling elsewhere, but our new results indicate it may be entirely Eocene in age.

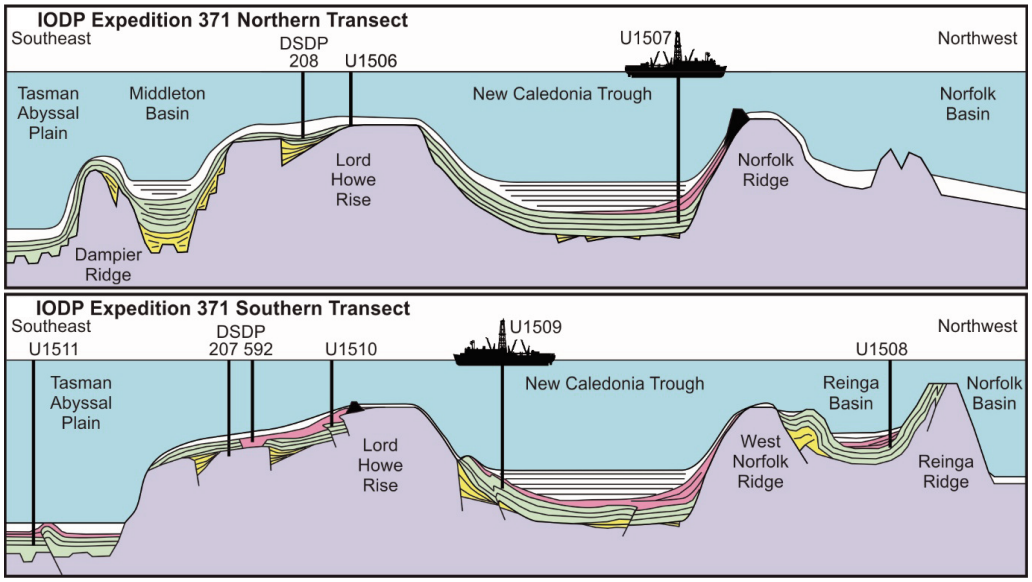

from 36 to 20 Ma. Basement rock was not reached, but the 170 m of clayey nannofossil chalk cored (lithostratigraphic Unit II) from the lower seismic unit is Eocene age and much younger than expected. Additional chemical analyses are required to test whether the influx of volcaniclastic sediments starting in the late Eocene is a signal of early arc development.

At Site U1508, folding in Reinga Basin is interpreted from onlap relationships in seismic reflection data (indicating deposition against tilted strata) to have started during the transition from deposition of lithostratigraphic Subunit IIIb (bioturbated nannofossil chalk and limestone) to Subunit IIIa (bioturbated clayey nannofossil chalk with centimeter-scale siliceous intervals). The lithostratigraphic transition is dated from radiolarians and calcareous nannofossils to have occurred at 39–38 Ma (late middle Eocene). Evidence for reworking of middle Eocene to Paleocene microfossils in the Subunit IIIa upper Eocene strata supports the seismic stratigraphic interpretation. The age of folding cessation is not clear from stratigraphic relationships at Site U1508, but undeformed limestone caps the eroded crest of a fold in Reinga Basin (western basin margin, Wanganella Ridge) and constrains folding to have stopped there by 36–30 Ma (Sutherland et al., 2017). These conclusions are consistent with 53–43 Ma ages of the youngest deformed rocks exposed at the seabed near fold crests elsewhere in the Reinga Basin (Browne et al., 2016; Sutherland et al., 2017).

Site U1509 is located on the flank of a reverse-faulted fold at the western margin of southern New Caledonia Trough. Chalk from lithostratigraphic Subunit Ib is characterized by slumped intervals containing overturned folds and sharp-based, convoluted to parallel-laminated beds. A brecciated and severely faulted interval occurs at the base of Subunit Ib (~137–139 m). Strata of Subunit Ic chalk and limestone with biosilica are tilted, with an average apparent dip of ~22°. The age of transition is 29–26 Ma from lithostratigraphic Subunit Ic to Subunit Ib and 24–23 Ma from Subunit Ib to Subunit Ia. Reworked late to middle Eocene nannofossils and foraminifers were identified in Subunit Ib and the basal part of Subunit Ia (61.68–135.22 m; lower Miocene to upper Oligocene). The reworking of sediment and structural relationships indicates that a local slope failure occurred during deposition of Subunit Ib (29–23 Ma). Seismic stratigraphic relationships show Unit II claystone is parallel-bedded and affected by deep-seated deformation. Detachment surfaces imaged on seismic reflection data in Paleocene claystone (Subunit IIa) may represent basal surfaces of local slope failure. Slope failure may have been synchronous with deep-seated folding and faulting, or folding may have occurred and been draped with some (or all) Subunit Ic strata before slope failure occurred. Therefore, the age of folding has a poorly constrained Eocene to Oligocene age.

Site U1510 is on the southern Lord Howe Rise, where reverse faults offset a sequence characterized by parallel continuous reflections. Lithostratigraphic Unit II was rapidly deposited (LSR = 20–50 m/My) during 46–37 Ma, and rapid sedimentation may have started as early as 48 Ma. Seismic stratigraphic relationships and evidence in cores for volcanism and sediment reworking indicate that high sedimentation rate was linked with tectonic activity.

Site U1511 is on the Tasman Abyssal Plain adjacent to a reverse-faulted fold that deforms the sedimentary sequence. The unit we infer from seismic interpretation to be syntectonic in its upper part is highly reflective, and the correlative lithostratigraphic Unit II is composed of diatomite and clay. The age of the upper part of Unit II indicates fault activity occurred during 46–38 Ma.

Uplift and subsidence of ridges

Bathyal Late Cretaceous and Paleocene sediments were sampled at Sites 207 and 208 on Lord Howe Rise (Shipboard Scientific Party, 1973b, 1973c), and Late Cretaceous magnetic anomalies were identified on marginal ocean crust of the Tasman Sea (Hayes and Ringis, 1973). These observations, combined with interpretations of sparse seismic reflection data, have led almost all previous workers to conclude that Cretaceous rift (crustal thinning) and postrift (thermal diffusion) subsidence processes were primary controls on the physiographic evolution of Lord Howe Rise and New Caledonia Trough (e.g., Auzende et al., 2000; Lafoy et al., 2005; Schellart et al., 2006; Cluzel et al., 2012; Matthews et al., 2015) (Figure **F13**).

Paleogene stratigraphy from Legs 21, 29, and 90 was used to infer dramatic changes in oceanography during the Paleogene associated with thermal isolation of Antarctica by seafloor spreading and hence development of the modern system of thermohaline circulation (Kennett, 1977). A prominent Eocene–Oligocene unconformity is recognized in the southwest Pacific and interpreted by many authors to have formed in deep water during the onset of the ACC (Edwards, 1973; Kennett et al., 1975; Kennett and von der Borch, 1986). Sutherland et al. (2010) mapped this unconformity on Lord Howe Rise and noted concordant (flat) erosional unconformities that were tentatively interpreted to be surfaces produced by sea level–modulated erosion. Such a model requires that Lord Howe Rise was transiently uplifted to sea level during the Paleogene and subsequently subsided by >1 km.

Results from Site U1506 confirm that at least at this locality the northern Lord Howe Rise was near sea level during the Eocene. Sediment cored at Site U1506 is composed of nannofossil ooze and chalk with foraminifers (264.6 m thick). The thick (258.2 m) Pleistocene to middle Miocene (0–14 Ma) subunit contains lower bathyal benthic microfossil assemblages that indicate paleowater depths similar to the present (1495 m), with an unconformity at the base of this subunit. A thin (6.1 m), upper Oligocene (25–23 Ma) chalk beneath this unconformity contains lower bathyal assemblages but transitions at its base into a highly condensed (0.4 m), burrowed glauconitic chalk containing an upper bathyal (200–600 m water depth) assemblage, with ostracod and benthic foraminifer species indicative of shelf depths also present but inferred to have been transported downslope. The glauconitic base of the sedimentary sequence is middle Eocene age (~45 Ma). Underlying basalt flows contain many calcite-filled amygdules and a Neptunian dike (~10 m below the top contact) with a diverse fossil assemblage. These assemblages indicate a neritic environment existed during or shortly after the early Eocene (after ~50 Ma), and the glauconitic layer shows that rapid subsidence at the site occurred during the middle Eocene.

At Site U1510 on the southern Lord Howe Rise, Pleistocene to lower Eocene ooze and chalk with cherty layers and volcanic detritus contain three unconformities. A hiatus occurs between the middle Pliocene and late Miocene (~4.4 My duration), and a second hiatus occurs between the late Miocene and middle Miocene (5.25 My duration). A third hiatus separates the early Miocene from the late Eocene with a duration of ~17.5 My. Benthic foraminifer and ostracod assemblages indicate a lower or middle bathyal depositional environment at Site U1510 (present water depth is 1238 m) since the early Eocene; however, the upper ~100 m of the Eocene section (41–37 Ma) contains microfossils and large (<4 cm) bioclasts transported from much shallower water (neritic), and reworked fossils of early and middle Eocene age are present. In this

anomalous interval, sighted ostracods are common, as well as shallow-water (<50 m) benthic foraminifers, and nannofossils indicate a nearby neritic environment. The base of the Miocene sequence (~20 Ma) does not contain evidence for nearby shallow water.

Site U1510 is ~80 km from Site 592, where the present water depth is 1088 m and an unconformity separates lower Miocene (23–19 Ma) chalk from lower Oligocene (33–32 Ma) ooze. Microfossils indicate a lower or middle bathyal environment since the Eocene at Site 592, but the Oligocene contains several layers of coarse (1–4 cm) mollusk (*Ostrea*) fragments consistent with findings at Site U1510 of material redeposited from shallow water in the unit just beneath the regional unconformity.

The Eocene–Oligocene uplift history at Site U1510 has some similarity with that of the western margin of Reinga Basin (Wanganella Ridge; West Norfolk Ridge), which is on the opposite side of New Caledonia Trough (Figure **F14**). Bioclastic limestone dredged from ~1750 m water depth (Reinga Basin Dredge TAN1312-d19; Wanganella Scarp; Bache et al., 2014b) contains neritic (<100 m water depth) benthic foraminifers with a depositional age of 36–30 Ma, and the same samples contain reworked Eocene (43–38 Ma) planktic species (Browne et al., 2016; Sutherland et al., 2017).

At Site U1508 (1609 m water depth) on the northeast margin of Reinga Basin, biostratigraphy reveals significant hiatuses in sedimentation at 33–26 and 23–18 Ma. The upper Oligocene unit between these unconformities contains volcaniclastic detritus and a concentration of shallow-water ostracods and benthic foraminifers, as well as a palynoflora that indicates nearby land. Benthic foraminifers indicate a middle to lower bathyal (600–2000 m water depth) environment of deposition for upper Oligocene strata, so the abundant neritic and terrestrial fossils were transported into deeper water. Seismic reflection interpretation reveals an extensive flat angular unconformity that truncates folded strata immediately east of Site U1508 (Figure **F14**) that may have been the source of neritic and terrestrial fossils. Late Oligocene rocks containing terrestrial fossils are rare in New Zealand, so the find has biogeographic significance (Mildenhall, 2014).

It is clear from these combined observations (Figure **F12**) that Lord Howe Rise, West Norfolk and Wanganella Ridges, and the northeastern margin of Reinga Basin experienced Cenozoic uplift to near or above sea level and then substantial (>1 km) subsidence. However, the timing of uplift and subsidence varies between the northern and southern sites. The northern Lord Howe Rise at Site U1506 was at sea level at (or after) 50 Ma and subsided to upper bathyal depths (200–600 m) by 45 Ma and then to lower bathyal depths (1000–2000 m) by 25 Ma. In contrast, the southern Lord Howe Rise and West Norfolk and Wanganella Ridges rose to near sea level during 41–30 Ma and subsided back to lower bathyal depths by 23–19 Ma. The northeastern margin of Reinga Basin contains evidence for a similar late Eocene to Oligocene uplift event. All sites contain evidence for local volcanic activity of Eocene to Miocene age.

New Caledonia Trough

New Caledonia Trough underwent substantial vertical motions during the Paleogene. At Site U1507, the basal sediments drilled show that lower bathyal to abyssal depths were established by 41 Ma. Extrapolation of sedimentation rates using seismic reflection data to the base of the sedimentary fill suggests a Paleogene age for the basin (Figure **F14**). The apparent lack of Cretaceous sediment suggests an elevation near or above sea level when the basin started to form. Either the region was previously covered in Cretaceous sediment that was eroded before basin formation, or older sediment was never deposited (e.g., it corresponded to a Late Cretaceous island or sediment-starved basin).

At Site U1509 in the southern New Caledonia Trough (Figure **F14**), Paleogene tectonic movements are overprinted on a Cretaceous sedimentary basin that can be traced with seismic reflection data into Fairway Basin to the north and Taranaki Basin to the south (Collot et al., 2009). Pleistocene to Oligocene ooze and chalk contain lower bathyal to abyssal (>1000 m, probably >2000 m) benthic foraminifer assemblages consistent with water depths similar to the present (2911 m). Lower bathyal (1000–2000 m) Eocene assemblages indicate slightly shallower conditions than the present but with some uncertainty. Paleocene and Cretaceous middle to lower bathyal (600–2000 m) assemblages indicate a most likely paleowater depth of ~1000 m. Cretaceous claystones contain abundant plant fragments and fern spores that indicate a nearby shoreline. The combined data suggest ~2000 m of subsidence at Site U1509, with most of it being accomplished during 60–45 Ma.

Volcanic history

At Site U1506 on the northern Lord Howe Rise, basalt flows have a possible age of ~50 Ma based on fossils found in a Neptunian dike but could also be older (radiometric dating of basalt is in progress). Small basaltic cones are associated with the regional Eocene unconformity elsewhere on the northern Lord Howe Rise (Dadd et al., 2011). Preliminary X-ray fluorescence analysis shows volcanic rocks at Site U1506 to be tholeiitic, which is consistent with the mildly alkaline tholeiitic trend of other analyses from the northern Lord Howe Rise (Mortimer et al., 2017).

At Site U1510 on the southern Lord Howe Rise, Eocene (48–35 Ma) strata contain volcaniclastic layers. Based on interpretation of seismic reflection and bathymetric data, the strata have clear synvolcanic stratigraphic relationships with nearby volcanic cones. At Site 592, ~80 km from Site U1510 (Figure **F4**), green and brown laminations in the upper Eocene to lower Oligocene (37–32 Ma) ooze and chalk are interpreted to be volcaniclastic (Shipboard Scientific Party, 1986a). At DSDP Site 593 on Challenger Plateau, upper Eocene (37–34 Ma) volcaniclastic turbidites contain coarser material than that found at Site 592 (Shipboard Scientific Party, 1986b). Near Site U1509, which is east of Site U1510 on the margin of Lord Howe Rise with New Caledonia Trough, samples of mildly alkaline basalt dredged from the seabed yield ages of 30–28 Ma (Mortimer et al., 2017).

At Site U1507 in New Caledonia Trough, a thick (285 m) unit of Eocene–Miocene (36–20 Ma) clayey chalk contains volcaniclastic turbidites. Site U1507 is adjacent to one of a series of large submerged volcanoes exposed just west of the crest of Norfolk Ridge. Seabed dredging from the southern end of this volcanic chain recovered a shoshonite that is interpreted to be subduction-related (but not typical) and has an age of 26 Ma (Mortimer et al., 2007). At the northern end of d'Entrecasteaux Ridge, which is the structural extension of Norfolk Ridge north of New Caledonia (i.e., along strike), Mortimer et al. (2014) reported ages of 38–32 Ma from volcanic rocks with a clear subduction signature. Our preliminary interpretation is that the volcaniclastic sequence at Site U1507 records the onset of subduction-related volcanism at that location, but additional geochemical work is required.

At Site U1508 in Reinga Basin, volcaniclastic material is found in the upper Oligocene to middle Miocene (26–15 Ma). Extensive geochemical work on correlative rocks exposed onshore nearby (Northland region of northern New Zealand) shows this volcanic

phase was subduction-related (Booden et al., 2011). Ages of volcanic rocks in Northland range from 23 to 11 Ma with a general trend of younger ages to the southeast (Hayward et al., 2001). Seismic stratigraphic analysis of the offshore region west of Northland has identified many volcanic centers and ties to boreholes that confirm the arc was active there during the interval 23–16 Ma (Herzer, 1995). Results from Site U1508 are consistent with this previous work, but our preliminary analysis suggests the onset of volcanism may be slightly older (26 Ma). This difference may be because Site U1508 is north of all previous sites, or it may be that the record we sampled is more complete.

Tectonic synthesis

The modern Pacific Ring of Fire was mostly created during the Eocene when subduction initiated throughout the western Pacific. In the northwest Pacific, volcanic activity associated with the new subduction system started at ~52 Ma (Arculus et al., 2015b), and the associated change in Pacific plate motion was complete by ~44–43 Ma (Sharp and Clague, 2006). Expedition 371 provides new and precise age constraints on the deformation, uplift, and volcanic histories in the southwest Pacific (Figure **F12**) and hence broadens our understanding of the spatial and temporal patterns of various types of tectonic activity during a large-scale subduction initiation event.

The first signs of tectonic change in the southwest Pacific occur at about the same time as they do in the northwest Pacific. Seafloor spreading ended in the Tasman Sea at ~52 Ma (Gaina et al., 1998), and dolerite dikes and sills in oceanic crust now exposed in New Caledonia (Poya terrane) have radiometric ages that cluster at 54 ± 5 Ma (Cluzel et al., 2017). Boninites with ages of 55–50 Ma intrude ultramafic rocks now exposed in New Caledonia (Cluzel et al., 2016). In the Tonga fore arc, plagiogranites associated with ultramafic rocks have ages of 51–50 Ma (Meffre et al., 2012).

Blueschist rocks in New Caledonia provide direct evidence for high-pressure, low-temperature metamorphism that is likely associated with convergence and subduction initiation. The onset of blueschist metamorphism in New Caledonia is constrained by detrital zircons and prograde mica growth to be during 55–50 Ma (Pirard and Spandler, 2017; Vitale Brovarone et al., 2018). Zircon growth dates peak metamorphism at ~44 Ma (Spandler et al., 2005), and thermochronology reveals a subsequent phase of rapid exhumation and cooling that mostly terminated by ~34 Ma (Baldwin et al., 2007). Exhumation was associated with emplacement of the Poya and ultramafic nappes (Aitchison et al., 1995) and deposition of a thick flysch sequence that is now exposed on the southwest coast of New Caledonia (Maurizot, 2011; Cluzel et al., 2012; Dallanave et al., 2018).

Our observations demonstrate that paleogeography of the early Eocene and older times cannot easily be inferred from looking at the present physiography of northern Zealandia. Subduction initiation in the southwest Pacific changed the stress and thermal state, modified the crustal and lithospheric structure, and hence caused major changes in water depth.

Evidence from Site U1507 suggests the northern New Caledonia Trough formed during the early stages of Paleogene tectonic change (before 44 Ma). Paleowater depth estimates from Site U1509 are consistent with evidence for a drowned shelf in Taranaki Basin (Sutherland et al., 2010; Baur et al., 2014) and indicate that the Cretaceous Fairway-Aotea-Taranaki Basin (Collot et al., 2009) was dramatically deepened (~2000 m) at a similar time (i.e., early Eocene, but additional detailed stratigraphy is required in the southern region) to form southern New Caledonia Trough.

The northern Lord Howe Rise at Site U1506 rose to sea level at ~50 Ma and subsided back to upper bathyal depths (200–600 m) by 45 Ma. In contrast, the southern Lord Howe Rise near Site U1510 experienced its transient uplift peak at ~40–30 Ma. A pulse of convergent plate failure, named the TECTA event by Sutherland et al. (2017), took place across the southern part of the region (Tasman Abyssal Plain, Lord Howe Rise, New Caledonia Trough, and Reinga Basin) and is constrained by our observations to have occurred during ~45–35 Ma.

The volcanic history requires further analysis, but a preliminary interpretation is that uplift of Lord Howe Rise was associated with a prolonged phase of intraplate volcanism. A pulse of subduction-related volcanism appears to have migrated southward from d'Entrecasteaux Ridge to Norfolk Ridge to Northland at 38–32, 36–20, and 26–15 Ma, respectively. The oldest subduction-related rocks in the Tonga fore arc are dated at 48 Ma (Meffre et al., 2012).

Induced subduction initiation models predict a phase of convergent plate failure as the new slab starts to form (Gurnis et al., 2004), whereas spontaneous subduction models predict tensile stresses and back-arc opening early in the initiation process (Stern, 2004). In the context of western Pacific subduction initiation and plate motion change, events initiated at ~53–50 Ma, as evidenced by the age of the Emperor-Hawaii bend (Sharp and Clague, 2006) and the onset of volcanism in the Izu-Bonin-Mariana subduction system (Ishizuka et al., 2011; Arculus et al., 2015b). Further, the nature of faulting and volcanic products in the Izu-Bonin-Mariana system reveals tensile stress and seafloor spreading at a very early stage (53–50 Ma); hence, a spontaneous subduction initiation model is implicated (Arculus et al., 2015b), possibly caused by instability associated with juxtaposition of a buoyant relic arc against the old Pacific oceanic plate by a weak fault (Leng and Gurnis, 2015). Subduction initiation in the northwest Pacific and Pacific plate motion change was completed by ~44–43 Ma (Sharp and Clague, 2006).

Magnetic anomalies show that Tasman Sea spreading ended at ~52 Ma, and a new phase of rapid seafloor spreading started south of Australia and New Zealand at ~43 Ma to create the south Tasman Sea ocean crust (Sutherland, 1995; Gaina et al., 1998; Cande and Stock, 2004). Therefore, regional changes in plate motion can be linked to the observations of uplift, deformation, and volcanism described above. A clear temporal relationship exists between events in the northwest Pacific, the change in direction of the Pacific plate in a hotspot reference frame, and the sequence of events in the southwest Pacific.

Formation of the northern New Caledonia Trough was associated with the early phase of Cenozoic tectonic activity in the southwest Pacific and may be evidence for spontaneous subduction initiation in the north. However, no published subduction initiation model involves large-scale removal of crust and long-term basin formation. The onset of volcanism at ~38 Ma at Site U1507 is much later than the earliest signs of tectonic activity (~53 Ma). Transient vertical movements of Lord Howe Rise are not predicted by existing models and require a physical explanation. Convergent deformation in the southern part of the Tasman Frontier suggests an induced subduction initiation model (Sutherland et al., 2017), but deformation does not occur until 45–35 Ma. The spatial and temporal relationships we observed suggest it is not appropriate to simplify the subduction initiation processes in 2-D. Future work will focus on the development of a new class of subduction initiation geodynamic model that can fit all observations and will likely include 3-D considerations. For the first time, we have sufficient observations to constrain such a model.

Paleoceanography and climate

Quaternary sediment cycles and bryozoan fossils

Two sites provided Quaternary records amenable for paleoceanographic study. The upper section of Site U1510 on the southern Lord Howe Rise was recovered using APC coring in two holes that can be spliced together to form a 44.5 m continuous section spanning most of the late Pleistocene. The section contains calcareous ooze with obvious cycles in physical properties, such as color and grain size. Site U1508 northwest of northern New Zealand has a nearly 100 m thick Pleistocene section. Although rotary cored, layers with macroscopic fragments of bryozoans and other shallow-water organisms present an intriguing and unusual find. The site is at a "temperate carbonate" margin (Nelson and Hancock, 1984) that provides an opportunity to study coupling between sedimentology and large-amplitude variations in sea level.

Late Miocene to early Pliocene biogenic bloom

Four sites recovered carbonate-rich sediment in which to assess the so-called late Miocene–early Pliocene biogenic bloom (Dickens and Owen, 1999). This phenomenon, which is recognized from sediment sections at multiple ocean drilling sites, can be described as follows: beneath zones of surface water divergence and upwelling in the Indian and Pacific Oceans, accumulation rates of biogenic components to the seafloor increased significantly between about 8 and 3 Ma, suggesting significantly increased primary productivity and expansion of the oxygen minimum zone.

Similar to previously drilled DSDP sites from the Tasman Sea, carbonate accumulation rates rose dramatically at northern Sites U1506 and U1507 from 8 to 3 Ma. These records provide an excellent opportunity to assess variations in global nutrient cycling and look into a plausible explanation for this event. However, a condensed interval marks the stratigraphic records at southern Sites U1509 and U1510 and may indicate underlying changes in deep-water flow during the late Miocene and early Pliocene.

Biogenic silica in the Eocene to Oligocene interval

Previous drilling in the Tasman Sea recovered very little sediment deposited between the middle Eocene and middle Oligocene, which led to an idea of a regional unconformity caused by intensification of deep-water currents (Kennett et al., 1975; Edwards, 1973, 1975).

We recovered apparently complete Oligocene sections at Sites U1507 and U1509 in New Caledonia Trough, with all late Eocene and Oligocene calcareous biozones and most polarity chrons identified at the first site. However, a hiatus of variable duration was found at shallow sites on Lord Howe Rise between the upper Eocene and upper Oligocene at Site U1508 and between the upper Eocene and middle Miocene at Site U1510. Notably, the middle Eocene through lower Oligocene interval, where found, including at Site U1511 on the Tasman Abyssal Plain, contains biosilica or chert. Postexpedition effort might be placed on understanding whether these observations support unusual oceanography or a different paleogeography and how silica deposition here compares with other global locations.

Regional Paleogene climate records

Several Paleogene sediment sections exposed in New Zealand and New Caledonia have become the focus of paleoclimate research because, once placed onto accurate age models, lithologic variations at key sites, such as Mead Stream in South Island, correspond to established changes in global climate (e.g., Dallanave et al., 2015). Several Expedition 371 sites contain lithostratigraphic records where changes in sediment composition appear to correlate with those now uplifted on land, particularly Site U1508 in Reinga Basin.

Early Paleogene greenhouse world and hyperthermals

The late Paleocene through early Eocene greenhouse world started to warm in the late Paleocene, culminating in the warmest part of the Cenozoic (53–49 Ma), referred to as the EECO. This long-term evolution was punctuated by short, extreme warming events called hyperthermals. The PETM (~55.5 Ma) was the most extreme of these hyperthermals. Additional transient warming events include the MECO (~40 Ma).

These events generally were not recovered at most sites during Expedition 371. At Sites U1507 and U1508, poorly recovered horizons (probably rich in chert) may mark the MECO. Sites U1508 and U1510 terminated near the top of the lower Eocene because of operational time restraints. At Site U1509, almost the entire early Eocene appears to have slumped on a surface approximately coincident with the PETM. It is possible that lithologic changes associated with warm events, such as clay-rich horizons and surrounding chert, make them difficult to recover in deep holes. Despite the above difficulties, apparently complete MECO and EECO intervals were recovered from the Tasman Abyssal Plain at Site U1511. However, these intervals at Site U1511 lack carbonate constituents and were dated using radiolarians and paleomagnetism.

Paleocene and Maastrichtian claystones

Paleogene calcareous green claystone was found at Sites U1509 and U1511. At the former site, coring also recovered dark brown Maastrichtian claystone. Considering exposed sections on land and past drill sites in the region, Paleogene clays accumulated over a widespread area of Zealandia (Andrews et al., 1975). At Site U1509 and other locations, these clays contain modest organic carbon, whereas the Paleocene at Site U1511 yields slightly higher carbonate content than in the rest of the succession.

Sediment diagenesis and pore fluids

Sediment compaction and ooze–chalk transition

Calcareous ooze, dominantly comprising microscopic calcite shells, blankets a large area of the modern seafloor above the CCD. With time and burial, this ooze can become compacted and altered to chalk and ultimately limestone. Reduction in porosity (Figure **F15**) and lithification over the transition zone from ooze to chalk has long fascinated the marine geoscience community because it affects the velocity of seismic waves, the recovery of core, and the nature of calcareous components. Analysis of previous DSDP drilling emphasized the complex nature of the ooze–chalk transition in the Tasman Sea. Cores and data from Expedition 371 provide new empirical data to quantify relationships between sediment composition, burial history, compaction, and diagenesis and may help clarify our understanding of the underlying processes. The ooze–chalk transition was found at approximately 235, 290, 200, 55, and 150 m at Sites U1506, U1507, U1508, U1509, and U1510, respectively. The very shallow transition in middle Miocene sediment at Site U1509 probably reflects missing overburden that was lost by slumping. The range in depths at the other sites may reflect differences in age, compaction, and sediment composition.

Thermogenic gas

Routine headspace gas sampling revealed significant concentrations of light hydrocarbon gases in deep sediments at two locations.

Figure F15. Summary of porosity data collected during Expedition 371.

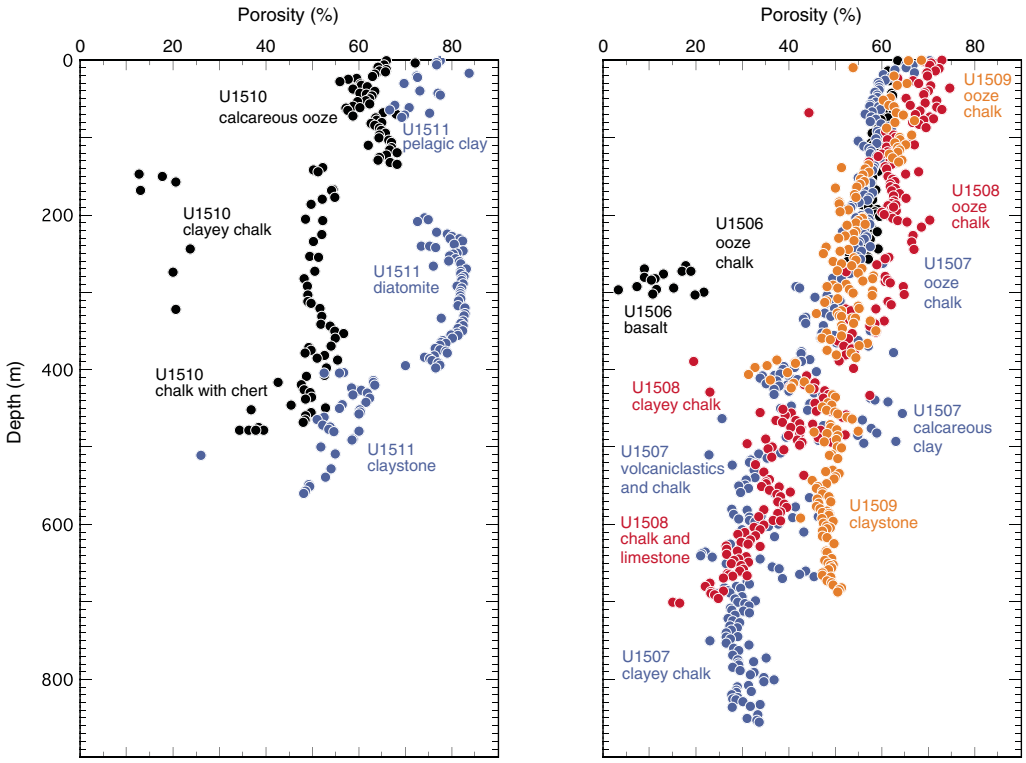

Methane concentrations began to increase below ~500 m in the middle Eocene nannofossil chalk at Site U1508 and below ~400 m in the Eocene calcareous claystone at Site U1509. At both locations, ethane and propane were also detected, although the C_1/C_2 ratio did not drop below 100. The suites of hydrocarbons measured were not classified as "anomalous" but do suggest burial of strata containing organic carbon and thermogenic hydrocarbon production in Reinga Basin and the southern New Caledonia Trough.

Deep anaerobic oxidation of methane

Upward-migrating gas at Sites U1508 and U1509 (above) impacts pore water chemistry significantly. At both sites, dissolved sulfate concentrations steadily decrease almost linearly from near seawater values at some shallow depth to zero at the depth where methane concentrations begin to rise. These deep SMT depths, ~500 m at Site U1508 and ~400 m at Site U1509, probably represent locations of AOM. Abundant pyrite is found in sediment near the SMTs, and dissolved Ba concentrations rise steeply beneath the SMTs. Interestingly, at Site U1508, sulfate concentrations begin decreasing at ~290 m rather than at the seafloor, possibly because of major changes in the porosity of sediment. In any case, these two Expedition 371 sites, along with a few other sites recently drilled elsewhere, significantly expand the subbottom depth range over which AOM can occur.

Iron oxide and copper mineralization

Vivid red-orange (2.5YR 5/6) claystone and native copper surrounded by dark green halos were found in multiple intervals of lower Eocene sediment at Site U1511. The striking color of the claystone comes from hematite, as determined from rock magnetic properties. Although the thickest and most striking horizon approximately coincides with the EECO (see above), both observations and theoretical arguments suggest the unusual mineralogy is not primary but the product of alteration. Presumably, saline fluids lacking dissolved oxygen and sulfur but carrying dissolved iron and copper precipitated minerals as they passed through the sediment, perhaps along fractures. Notably, seismic profiles show that Eocene and older strata at the site are folded and faulted. Native copper has been described at previous scientific drill sites (Dickens et al., 1995), and a commonality seems to be proximal folding and faulting.

An advance in pore water collection method

Coring with the APC system in multiple holes and the construction of spliced records has become a common approach for drilling expeditions with paleoceanography or biogeochemistry objectives. To achieve the Expedition 371 goals, which required deep drilling (in a time window shortened by weather, technical problems, and a medical emergency), the sedimentary records at most sites were recovered mostly in one hole, often using the RCB system. Although not ideal, good first-order sedimentary records and pore water profiles were generated at most sites. Notably, at sites where intervals were cored using both the XCB and RCB methods, the latter generally gave better quality cores in a shorter time period. To obtain reasonably good and detailed pore water profiles with minimal impact to the sedimentary record, Rhizon samples were taken at some sites and squeeze samples were taken from the bases of Sections 1, 6, or both. Such sampling generally avoids splice intervals (i.e., the core gaps created by IW sampling fall into "off-splice" intervals).

Regional stratigraphy

During Expedition 371, the sedimentary section was retrieved at six sites (Table **T1**) in a vast remote region (Figure **F2**). At five sites, we sampled nannofossil and foraminiferal ooze and chalk that contained volcanic or volcaniclastic intervals with variable clay content

Table T1. Hole summary, Expedition 371. Drilled intervals were purposefully drilled without collecting core. DSF = drilling depth below seafloor. APC = advanced piston corer, XCB = extended core barrel, RCB = rotary core barrel. **Download table in CSV format.**

Hole	Latitude	Longitude	Water depth (m)	Penetration DSF (m)	Cored interval (m)	Recovered length (m)	Recovery (%)	Drilled interval (m)	Total cores (*N*)	APC cores (*N*)	XCB cores (*N*)	RCB cores (*N*)	Time on hole (days)
U1506A	28°39.7180′S	161°44.4240′E	1495	306.1	306.1	192.5	63		36	0	0	36	2.1
U1507A	26°29.3158′S	166°31.7039′E	3568	425.4	425.4	352.7	83		46	26	20	0	3.6
U1507B	26°29.3158′S	166°31.7155′E	3568	864.4	488.4	371.5	76	376.0	52	0	0	52	8.1
U1508A	34°26.8902′S	171°20.6073′E	1609	210.3	210.3	201.1	96		23	23	0	0	1.5
U1508B	34°26.8975′S	171°20.5990′E	1609	503.4	316.7	133.3	42	186.7	37	0	0	37	2.1
U1508C	34°26.8905′S	171°20.5889′E	1609	704.5	283.8	184.8	65	420.7	35	0	0	35	5.0
U1509A	34°39.1312′S	165°49.6599′E	2911	690.7	690.7	462.8	67		74	0	0	74	5.2
U1510A	36°19.7385′S	164°33.5220′E	1238	483.4	483.4	255.9	53		52	17	35	0	2.5
U1510B	36°19.7392′S	164°33.5347′E	1238	66.3	66.3	64.7	98		7	7	0	0	0.4
U1511A	37°33.6665′S	160°18.9380′E	4847	26.6	26.6	7.9	30		3	0	0	3	0.8
U1511B	37°33.6656′S	160°18.9379′E	4847	566.2	431.4	279.3	65	134.8	45	0	0	45	5.1
			Totals:	4847.3	3729.1	2506.4	67	1118.2	410	73	55	282	36.4

(Figure **F10**). The Paleocene and Cretaceous sections are generally clay rich or predominantly claystone. At the final site (U1511), a sequence of abyssal clay and diatomite was recovered with only minor carbonate. The ages at the base of the deepest hole at each site varied from Eocene to Cretaceous, and sedimentation rates were moderate to high (5–20 m/My) for the lower bathyal and abyssal environments in which most sediments accumulated (Figures **F11**, **F16**). Our new results provide the first substantial basis for definition of formal lithostratigraphic units that can be mapped across a substantial part of northern Zealandia and related to onshore regions of New Caledonia and New Zealand, which will be the subject of future work. Rather than tectonic objectives, future Zealandia drilling can target expanded sections, and so on. For example, Site U1510 is located where the Neogene section pinches out and a much more expanded section could be drilled.

Figure F16. LSRs determined during Expedition 371 compared with previously drilled sites in the region.

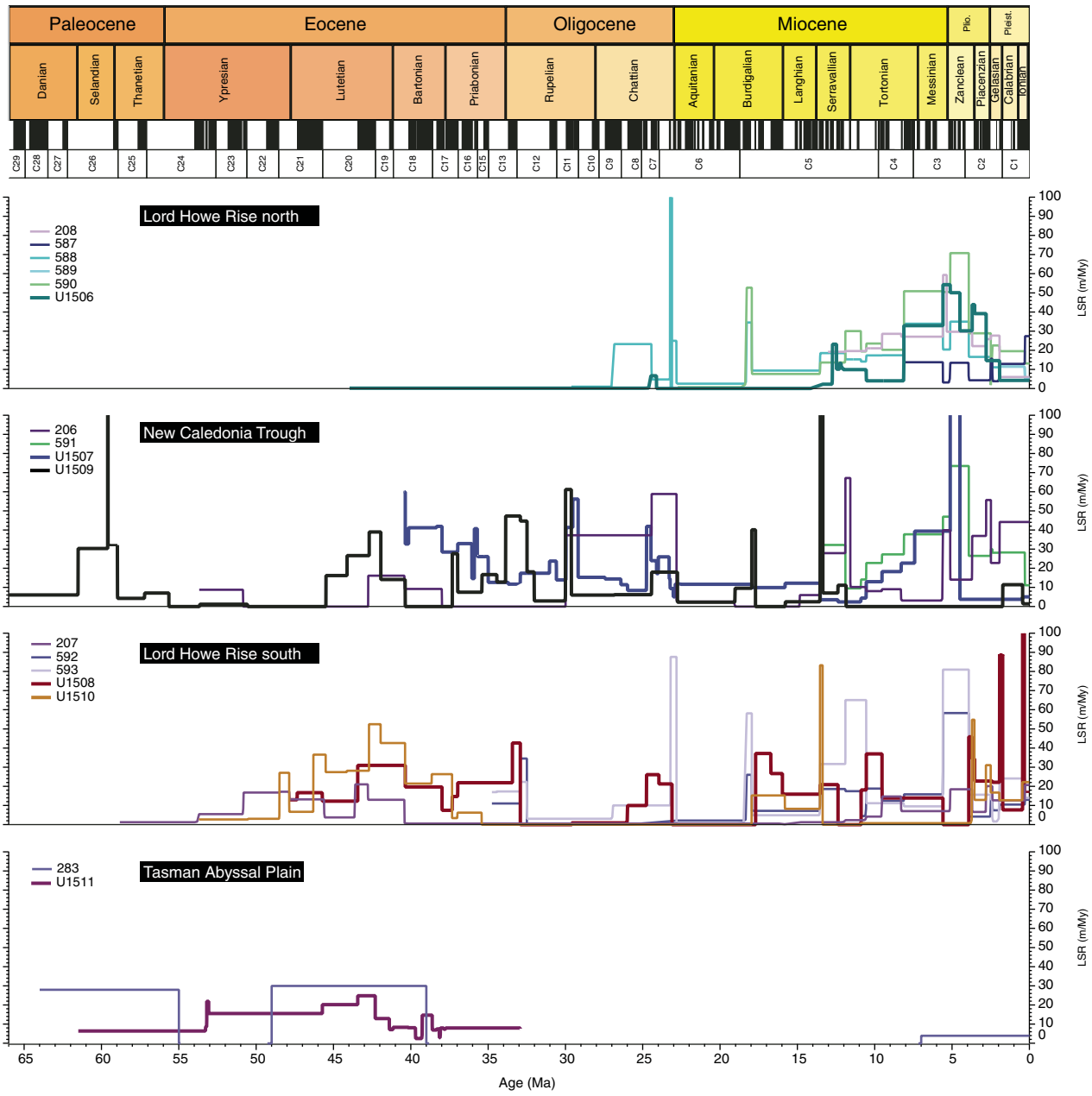

References

Adams, C.J., Cluzel, D., and Griffin, W.L., 2009. Detrital-zircon ages and geochemistry of sedimentary rocks in basement Mesozoic terranes and their cover rocks in New Caledonia, and provenances at the Eastern Gondwanaland margin. *Australian Journal of Earth Sciences,* 56(8):1023–1047. **https://doi.org/10.1080/08120090903246162**

Aitchison, J.C., Ali, J.R., and Davis, A.M., 2007. When and where did India and Asia collide? *Journal of Geophysical Research: Solid Earth,* 112(B5):B05423. **https://doi.org/10.1029/2006JB004706**

Aitchison, J.C., Clarke, G.L., Meffre, S., and Cluzel, D., 1995. Eocene arc-continent collision in New Caledonia and implications for regional southwest Pacific tectonic evolution. *Geology,* 23(2):161–164. **https://doi.org/10.1130/0091-7613(1995)023<0161:EAC-CIN>2.3.CO;2**

Aitchison, J.C., Ireland, T.R., Clarke, G.L., Cluzel, D., Davis, A.M., and Meffre, S., 1998. Regional implications of U/Pb SHRIMP age constraints on the tectonic evolution of New Caledonia. *Tectonophysics,* 299(4):333–343. **https://doi.org/10.1016/S0040-1951(98)00211-X**

Andrews, P.B, Gostin, V.A., Hampton, M.A., Margolis, S.V., and Ovenshine, A.T., 1975. Synthesis—sediments of the Southwest Pacific Ocean, Southeast Indian Ocean, and South Tasman Sea. *In* Kennett, J.P., Houtz, R.E. et al., *Initial Reports of the Deep Sea Drilling Project,* 29: Washington, DC (U.S. Govt. Printing Office), 1147–1153. **https://doi.org/10.2973/dsdp.proc.29.143.1975**

Andrews, P.B., and Ovenshine, A.T., 1975. Terrigenous silt and clay facies: deposits of the early phase of ocean basin evolution. *In* Kennett, J.P., Houtz, R.E. et al., *Initial Reports of the Deep Sea Drilling Project,* 29: Washington, DC (U.S. Government Printing Office), 1049–1063. **https://doi.org/10.2973/dsdp.proc.29.131.1975**

Arculus, R.J., Ishizuka, O., Bogus, K., Aljahdali, M.H., Bandini-Maeder, A.N., Barth, A.P., Brandl, P.A., do Monte Guerra, R., Drab, L., Gurnis, M.C., Hamada, M., Hickey-Vargas, R.L., Jiang, F., Kanayama, K., Kender, S., Kusano, Y., Li, H., Loudin, L.C., Maffione, M., Marsaglia, K.M., McCarthy, A., Meffre, S., Morris, A., Neuhaus, M., Savov, I.P., Sena Da Silva, C.A., Tepley, F.J., III, van der Land, C., Yogodzinski, G.M., and Zhang, Z., 2015a. Expedition 351 summary. *In* Arculus, R.J., Ishizuka, O., Bogus, K., and the Expedition 351 Scientists, *Proceedings of the International Ocean Discovery Program, Expedition 351: Izu-Bonin-Mariana Arc Origins:* College Station, TX (International Ocean Discovery Program). **https://doi.org/10.14379/iodp.proc.351.101.2015**

Arculus, R.J., Ishizuka, O., Bogus, K.A., Gurnis, M., Hickey-Vargas, R., Aljahdali, M.H., Bandini-Maeder, A.N., et al., 2015b. A record of spontaneous subduction initiation in the Izu-Bonin-Mariana arc. *Nature Geoscience,* 8:728–733. **https://doi.org/10.1038/ngeo2515**

Auzende, J.-M., Van de Beuque, S., Régnier, M., Lafoy, Y., and Symonds, P., 2000. Origin of the New Caledonian ophiolites based on a French–Australian seismic transect. *Marine Geology,* 162(2–4):225–236. **https://doi.org/10.1016/S0025-3227(99)00082-1**

Bache, F., Mortimer, N., Sutherland, R., Collot, J., Rouillard, P., Stagpoole, V., and Nicol, A., 2014a. Seismic stratigraphic record of transition from Mesozoic subduction to continental breakup in the Zealandia sector of eastern Gondwana. *Gondwana Research,* 26(3–4):1060–1078. **https://doi.org/10.1016/j.gr.2013.08.012**

Bache, F., Sutherland, R., Mortimer, N., Browne, G.H., Lawrence, M.J.F., Black, J., Flowers, M., et al., 2014b. Tangaroa TAN1312 voyage report: dredging Reinga and Aotea Basins to constrain seismic stratigraphy and petroleum systems (DRASP), NW New Zealand. *GNS Science Report,* 2014/05.

Bache, F., Sutherland, R., Stagpoole, V., Herzer, R., Collot, J., and Rouillard, P., 2012. Stratigraphy of the southern Norfolk Ridge and the Reinga Basin: a record of initiation of Tonga–Kermadec–Northland subduction in the southwest Pacific. *Earth and Planetary Science Letters,* 321–322:41–53. **https://doi.org/10.1016/j.epsl.2011.12.041**

Baldwin, S.L., Rawling, T., and Fitzgerald, P.G., 2007. Thermochronology of the New Caledonian high-pressure terrane: implications for middle Tertiary plate boundary processes in the southwest Pacific. *Special Paper - Geological Society of America,* 419:117–134. **https://doi.org/10.1130/2006.2419(06)**

Baur, J., Sutherland, R., and Stern, T., 2014. Anomalous passive subsidence of deep-water sedimentary basins: a prearc basin example, southern New Caledonia Trough and Taranaki Basin, New Zealand. *Basin Research,* 26(2):242–268. **https://doi.org/10.1111/bre.12030**

Becker, T.W., and O'Connell, R.J., 2001. Predicting plate velocities with mantle circulation models. *Geochemistry, Geophysics, Geosystems,* 2(12):1060. **https://doi.org/10.1029/2001GC000171**

Beerling, D.J., and Royer, D.L., 2011. Convergent Cenozoic CO_2 history. *Nature Geoscience,* 4(7):418–420. **https://doi.org/10.1038/ngeo1186**

Berner, R.A., 1994. GEOCARB II: a revised model of atms. CO_2 over Phanerozoic time. *American Journal of Science,* 294:56–91.

Berner, R.A., and Kothavala, Z., 2001. Geocarb III: a revised model of atmospheric CO_2 over Phanerozoic time. *American Journal of Science,* 301(2):182–204.

Bijl, P.K., Schouten, S., Sluijs, A., Reichart, G.-J., Zachos, J.C., and Brinkhuis, H., 2009. Early Palaeogene temperature evolution of the southwest Pacific Ocean. *Nature,* 461(7265):776–779. **https://doi.org/10.1038/nature08399**

Billen, M.I., and Gurnis, M., 2005. Constraints on subducting plate strength within the Kermadec Trench. *Journal of Geophysical Research: Solid Earth,* 110(B5):B05407. **https://doi.org/10.1029/2004JB003308**

Booden, M.A., Smith, I.E.M., Black, P.M., and Mauk, J.L., 2011. Geochemistry of the early Miocene volcanic succession of Northland, New Zealand, and implications for the evolution of subduction in the Southwest Pacific. *Journal of Volcanology and Geothermal Research,* 199(1–2): 25–37. **https://doi.org/10.1016/j.jvolgeores.2010.10.006**

Browne, G.H., Lawrence, M.J.F., Mortimer, N., Clowes, C.D., Morgans, H.E.G., Hollis, C.J., Beu, A.G., Black, J.A., Sutherland, R., and Bache, F., 2016. Stratigraphy of Reinga and Aotea basins, NW New Zealand: constraints from dredge samples on regional correlations and reservoir character. *New Zealand Journal of Geology and Geophysics,* 59(3):396–415. **https://doi.org/10.1080/00288306.2016.1160940**

Brummer, G.J.A., and van Eijden, A.J.M., 1992. "Blue-ocean" paleoproductivity estimates from pelagic carbonate mass accumulation. *Marine Micropaleontology,* 19(1–2):99–117. **https://doi.org/10.1016/0377-8398(92)90023-D**

Bryan, S.E., Constantine, A.E., Stephens, C.J., Ewart, A., Schön, R.W., and Parianos, J., 1997. Early Cretaceous volcano-sedimentary successions along the eastern Australian continental margin: implications for the break-up of eastern Gondwana. *Earth and Planetary Science Letters,* 153(1–2):85–102. **https://doi.org/10.1016/S0012-821X(97)00124-6**

Buffett, B.A., 2006. Plate force due to bending at subduction zones. *Journal of Geophysical Research: Solid Earth,* 111(B9):B09405. **https://doi.org/10.1029/2006JB004295**

Burns, R.E., and Andrews, J.E., 1973. Regional aspects of deep sea drilling in the southwest Pacific. *In* Burns, R.E., Andrews, J.E., et al., *Initial Reports of the Deep Sea Drilling Project,* 21: Washington, DC (U.S. Government Printing Office), 897–906. **https://doi.org/10.2973/dsdp.proc.21.128.1973**

Cande, S.C., Patriat, P., and Dyment, J., 2010. Motion between the Indian, Antarctic and African plates in the early Cenozoic. *Geophysical Journal International,* 183(1):127–149. **https://doi.org/10.1111/j.1365-246X.2010.04737.x**

Cande, S.C., and Stock, J.M., 2004. Pacific–Antarctic–Australia motion and the formation of the Macquarie plate. *Geophysical Journal International,* 157(1):399–414. **https://doi.org/10.1111/j.1365-246X.2004.02224.x**

Cande, S.C., Stock, J.M., Müller, R.D., and Ishihara, T., 2000. Cenozoic motion between east and west Antarctica. *Nature,* 404(6774):145–150. **https://doi.org/10.1038/35004501**

Caress, D.W., Menard, H.W., and Hey, R.N., 1988. Eocene reorganization of the Pacific-Farallon spreading center north of the Mendocino Fracture Zone. *Journal of Geophysical Research: Solid Earth,* 93(B4):2813–2838. **https://doi.org/10.1029/JB093iB04p02813**

Carter, R.M., McCave, I.N., and Carter, L., 2004. Leg 181 synthesis: fronts, flows, drifts, volcanoes, and the evolution of the southwestern gateway to the Pacific Ocean, eastern New Zealand. *In* Richter, C. (Ed.), *Proceedings of the Ocean Drilling Program, Scientific Results,* 181: College Station, TX (Ocean Drilling Program), 1–111. **https://doi.org/10.2973/odp.proc.sr.181.210.2004**

Cluzel, D., Adams, C.J., Meffre, S., Campbell, H., and Maurizot, P., 2010. Discovery of Early Cretaceous rocks in New Caledonia: new geochemical and U-Pb zircon age constraints on the transition from subduction to marginal breakup in the southwest Pacific. *Journal of Geology,* 118(4):381–397. **https://doi.org/10.1086/652779**

Cluzel, D., Aitchison, J.C., and Picard, C., 2001. Tectonic accretion and underplating of mafic terranes in the late Eocene intraoceanic fore-arc of New Caledonia (southwest Pacific): geodynamic implications. *Tectonophysics,* 340(1–2):23–59. **https://doi.org/10.1016/S0040-1951(01)00148-2**

Cluzel, D., Maurizot, P., Collot, J., and Sevin, B., 2012. An outline of the geology of New Caledonia: from Permian–Mesozoic Southeast Gondwanaland active margin to Cenozoic obduction and supergene evolution. *Episodes,* 35(1):72–86. **https://hal-brgm.archives-ouvertes.fr/hal-00861251**

Cluzel, D., and Meffre, S., 2002. The Boghen Terrane (New Caledonia, SW Pacific): a Jurassic accretionary complex. Preliminary U-Pb radiochronological data on detrital zircon. *Comptes Rendus Geoscience,* 334(11):867–874. **https://doi.org/10.1016/S1631-0713(02)01823-0**

Cluzel, D., Meffre, S., Maurizot, P., and Crawford, A.J., 2006. Earliest Eocene (53 Ma) convergence in the southwest Pacific: evidence from pre-obduction dikes in the ophiolite of New Caledonia. *Terra Nova,* 18(6):395–402. **https://doi.org/10.1111/j.1365-3121.2006.00704.x**

Cluzel, D., Ulrich, M., Jourdan, F., Meffre, S., Paquette, J.-L., Audet, M.-A., Secchiari, A., and Maurizot, P., 2016. Early Eocene clinoenstatite boninite and boninite-series dikes of the ophiolite of New Caledonia: a witness of slab-derived enrichment of the mantle wedge in a nascent volcanic arc. *Lithos,* 260:429–442. **https://doi.org/10.1016/j.lithos.2016.04.031**

Cluzel, D., Whitten, M., Meffre, S., Aitchison, J.C., and Maurizot, P., 2017. A reappraisal of the Poya Terrane (New Caledonia): accreted Late Cretaceous–Paleocene marginal basin upper crust, passive margin sediments, and early Eocene E-MORB sill complex. *Tectonics,* 37(1):48–70. **https://doi.org/10.1002/2017TC004579**

Collot, J., Geli, L., Lafoy, Y., Vially, R., Cluzel, D., Klingelhoefer, F., and Nouzé, H., 2008. Tectonic history of northern New Caledonia Basin from deep offshore seismic reflection: relation to late Eocene obduction in New Caledonia, southwest Pacific. *Tectonics,* 27(6):TC6006. **https://doi.org/10.1029/2008TC002263**

Collot, J., Herzer, R., Lafoy, Y., and Géli, L., 2009. Mesozoic history of the Fairway-Aotea Basin: implications for the early stages of Gondwana fragmentation. *Geochemistry, Geophysics, Geosystems,* 10(12):Q12019. **https://doi.org/10.1029/2009GC002612**

Collot, J., Vendé-Leclerc, M., Rouillard, P., Lafoy, Y., and Géli, L., 2012. Map helps unravel complexities of the southwestern Pacific Ocean. *Eos, Transactions of the American Geophysical Union,* 93(1):1–2. **https://doi.org/10.1029/2012EO010001**

Cramwinckel, M.J., Huber, M., Kocken, I.J., Agnini, C., Bijl, P.K., Bohaty, S.M., Frieling, J., et al., 2018. Synchronous tropical and polar temperature evolution in the Eocene. *Nature,* 559(7714):382–386. **https://doi.org/10.1038/s41586-018-0272-2**

Crawford, A.J., Meffre, S., and Symonds, P.A., 2003. 120 to 0 Ma tectonic evolution of the southwest Pacific and analogous geological evolution of the 600 to 220 Ma Tasman fold belt system. *In* Hillis, R.R., and Müller, R.D. (Eds.), *Evolution and Dynamics of the Australian Plate.* Special Paper - Geological Society of America, 372:383–403. **https://doi.org/10.1130/0-8137-2372-8.383**

Dadd, K.A., Locmelis, M., Higgins, K., and Hashimoto, T., 2011. Cenozoic volcanism of the Capel-Faust Basins, Lord Howe Rise, SW Pacific Ocean. *Deep Sea Research, Part II: Topical Studies in Oceanography,* 58(7–8):922–932. **https://doi.org/10.1016/j.dsr2.2010.10.048**

Dallanave, E., Agnini, C., Bachtadse, V., Muttoni, G., Crampton, J.S., Strong, C.P., Hines, B.R., Hollis, C.J., and Slotnick, B.S., 2015. Early to middle Eocene magneto-biochronology of the southwest Pacific Ocean and climate influence on sedimentation: insights from the Mead Stream section, New Zealand. *Geological Society of America Bulletin,* 127(5–6):643–660. **https://doi.org/10.1130/B31147.1**

Dallanave, E., Agnini, C., Pascher, K.M., Maurizot, P., Bachtadse, V., Hollis, C.J., Dickens, G.R., Collot, J., and Monesi, E., 2018. Magneto-biostratigraphic constraints of the Eocene micrite–calciturbidite transition in New Caledonia: tectonic implications. *New Zealand Journal of Geology and Geophysics,* 61(2):145–163. **https://doi.org/10.1080/00288306.2018.1443946**

Davy, B., Hoernle, K., and Werner, R., 2008. Hikurangi Plateau: crustal structure, rifted formation, and Gondwana subduction history. *Geochemistry, Geophysics, Geosystems,* 9(7):Q07004. **https://doi.org/10.1029/2007GC001855**

DeConto, R.M., and Pollard, D., 2003. Rapid Cenozoic glaciation of Antarctica induced by declining atmospheric CO_2. *Nature,* 421(6920):245–249. **https://doi.org/10.1038/nature01290**

Dickens, G.R., Castillo, M.M., and Walker, J.C.G., 1997. A blast of gas in the latest Paleocene: simulating first-order effects of massive dissociation of oceanic methane hydrate. *Geology,* 25(3):259–262. **https://doi.org/10.1130/0091-7613(1997)025<0259:ABOGIT>2.3.CO;2**

Dickens, G.R., Koelling, M., Smith, D.C., Schneiders, L., and the IODP Expedition 302 Scientists, 2007. Rhizon sampling of pore waters on scientific drilling expeditions: an example from the IODP Expedition 302, Arctic Coring Expedition (ACEX). *Scientific Drilling,* 4:22–25. **https://doi.org/10.2204/iodp.sd.4.08.2007**

Dickens, G.R., and Owen, R.M., 1999. The latest Miocene–early Pliocene biogenic bloom: a revised Indian Ocean perspective. *Marine Geology,* 161(1):75–91. **https://doi.org/10.1016/S0025-3227(99)00057-2**

Dickens, G.R., Owen, R.M., and Pedersen, T.F., 1995. Copper mineralization at Site 884 in the North Pacific. *In* Rea, D.K., Basov, I.A., Scholl, D.W., and Allan, J.F. (Eds.), *Proceedings of the Ocean Drilling Program, Scientific Results,* 145: College Station, TX (Ocean Drilling Program), 389–397. **https://doi.org/10.2973/odp.proc.sr.145.129.1995**

Douglas, P.M.J., Affek, H.P., Ivany, L.C., Houben, A.J.P., Sijp, W.P., Sluijs, A., Schouten, S., and Pagani, M., 2014. Pronounced zonal heterogeneity in Eocene southern high-latitude sea surface temperatures. *Proceedings of the National Academy of Sciences of the United States of America,* 111(18):6582–6587. **https://doi.org/10.1073/pnas.1321441111**

Edgar, K.M., Wilson, P.A., Sexton, P.F., and Suganuma, Y., 2007. No extreme bipolar glaciation during the main Eocene calcite compensation shift. *Nature,* 448(7156):908–911. **https://doi.org/10.1038/nature06053**

Edwards, A.R., 1973. Southwest Pacific regional unconformities encountered during Leg 21. *In* Burns, R.E., Andrews, J.E., et al., *Initial Reports of the Deep Sea Drilling Project,* 21: Washington, DC (U.S. Government Printing Office), 701–720. **https://doi.org/10.2973/dsdp.proc.21.120.1973**

Edwards, A.R., 1975. Further comments on the Southwest Pacific Paleogene regional unconformities. *In* Andrews, J.E., Packham, G., et al., *Initial Reports of the Deep Sea Drilling Project,* 30: Washington (U.S. Government Printing Office), 663–666. **https://doi.org/10.2973/dsdp.proc.30.122.1975**

Etienne, S., Collot, J., Sutherland, R., Patriat, M., Bache, F., Rouillard, P., Henrys, S., Barker, D., and Juan, C., 2018. Deepwater sedimentation and Cenozoic deformation in the southern New Caledonia Trough (northern Zealandia, SW Pacific). *Marine and Petroleum Geology,* 92:764–779. **https://doi.org/10.1016/j.marpetgeo.2017.12.007**

Exon, N.F., Brinkhuis, H., Robert, C.M., Kennett, J.P., Hill, P.J., and Macphail, M.K., 2004a. Tectono-sedimentary history of uppermost Cretaceous through Oligocene sequences from the Tasmanian region: a temperate Antarctic margin. *In* Exon, N.F., Kennett, J.P., and Malone, M. (Eds.), *The Cenozoic Southern Ocean: Tectonics, Sedimentation, and Climate Change between Australia and Antarctica.* Geophysical Monograph, 151:319–344. **https://doi.org/10.1029/151GM18**

Exon, N.F., Kennett, J.P., and Malone, M. (Eds.), 2004b. *The Cenozoic Southern Ocean: Tectonics, Sedimentation, and Climate Change between Australia and Antarctica*. Geophysical Monograph, 151.

Farrell, J.W., Raffi, I., Janecek, T.R., Murray, D.W., Levitan, M., Dadey, K.A., Emeis, K.-C., Lyle, M., Flores, J.-A., and Hovan, S., 1995. Late Neogene sedimentation patterns in the eastern equatorial Pacific Ocean. *In* Pisias, N.G., Mayer, L.A., Janecek, T.R., Palmer-Julson, A., and van Andel, T.H. (Eds.), *Proceedings of the Ocean Drilling Program, Scientific Results,* 138: College Station, TX (Ocean Drilling Program), 717–756. **https://doi.org/10.2973/odp.proc.sr.138.143.1995**

Gaina, C., Müller, D.R., Royer, J.-Y., Stock, J., Hardebeck, J., and Symonds, P., 1998. The tectonic history of the Tasman Sea: a puzzle with 13 pieces. *Journal of Geophysical Research: Solid Earth,* 103(B6):12413–12433. **https://doi.org/10.1029/98JB00386**

Grant, K.M., and Dickens, G.R., 2002. Coupled productivity and carbon isotope records in the southwest Pacific Ocean during the late Miocene–early Pliocene biogenic bloom. *Palaeogeography, Palaeoclimatology, Palaeoecology,* 187(1–2):61–82. **https://doi.org/10.1016/S0031-0182(02)00508-4**

Gurnis, M., Hall, C., and Lavier, L., 2004. Evolving force balance during incipient subduction. *Geochemistry, Geophysics, Geosystems,* 5(7):Q07001. **https://doi.org/10.1029/2003GC000681**

Hall, C.E., Gurnis, M., Sdrolias, M., Lavier, L.L., and Dietmar Müller, R., 2003. Catastrophic initiation of subduction following forced convergence across fracture zones. *Earth and Planetary Science Letters,* 212(1–2):15–30. **https://doi.org/10.1016/S0012-821X(03)00242-5**

Hancock, H.J.L., Dickens, G.R., Strong, C.P., Hollis, C.J., and Field, B.D., 2003. Foraminiferal and carbon isotope stratigraphy through the Paleocene–Eocene transition at Dee Stream, Marlborough, New Zealand. *New Zealand Journal of Geology and Geophysics,* 46(1):1–19. **https://doi.org/10.1080/00288306.2003.9514992**

Hayes, D.E., and Ringis, J., 1973. Seafloor spreading in the Tasman Sea. *Nature,* 243(5408):454–458. **https://doi.org/10.1038/243454a0**

Hayward, B.W., Black, P.M., Smith, I.E.M., Ballance, P.F., Itaya, T., Doi, M., Takagi, M., et al., 2001. K-Ar ages of early Miocene arc-type volcanoes in northern New Zealand. *New Zealand Journal of Geology and Geophysics,* 44(2):285–311. **https://doi.org/10.1080/00288306.2001.9514939**

Herzer, R.H., 1995. Seismic stratigraphy of a buried volcanic arc, Northland, New Zealand and implications for Neogene subduction. *Marine and Petroleum Geology,* 12(5):511–531. **https://doi.org/10.1016/0264-8172(95)91506-K**

Herzer, R.H., Chaproniere, G.C.H., Edwards, A.R., Hollis, C.J., Pelletier, B., Raine, J.I., Scott, G.H., Stagpoole, V., Strong, C.P., Symonds, P., Wilson, G.J., and Zhu, H., 1997. Seismic stratigraphy and structural history of the Reinga Basin and its margins, southern Norfolk Ridge system. *New Zealand Journal of Geology and Geophysics,* 40: 425–451. **https://doi.org/10.1080/00288306.1997.9514774**

Herzer, R.H., Davy, B.W., Mortimer, N., Quilty, P.G., Chaproniere, G.C.H., Jones, C.M., Crawford, A.J., and Hollis, C.J., 2009. Seismic stratigraphy and structure of the Northland Plateau and the development of the Vening Meinesz transform margin, SW Pacific Ocean. *Marine Geophysical Researches,* 30(1):21–60. **https://doi.org/10.1007/s11001-009-9065-1**

Herzer, R.H., and Mascle, J., 1996. Anatomy of a continent-backarc transform—the Vening Meinesz Fracture Zone northwest of New Zealand. *Marine Geophysical Researches,* 18(2):401–427. **https://doi.org/10.1007/BF00286087**

Herzer, R.H., Sykes, R., Killops, S.D., Funnell, R.H., Burggraf, D.R., Townend, J., Raine, J.I., and Wilson, G.J., 1999. Cretaceous carbonaceous rocks from the Norfolk Ridge system, southwest Pacific: implications for regional petroleum potential. *New Zealand Journal of Geology and Geophysics,* 42(1):57–73. **https://doi.org/10.1080/00288306.1999.9514831**

Higgins, K., Hashimoto, T., Fraser, G., Rollet, N., and Colwell, J., 2011. Ion microprobe (SHRIMP) U-Pb dating of Upper Cretaceous volcanics from the northern Lord Howe Rise, Tasman Sea. *Australian Journal of Earth Sciences,* 58(2):195–207. **https://doi.org/10.1080/08120099.2011.543150**

Hollis, C.J., 2006. Radiolarian faunal turnover through the Paleocene–Eocene transition, Mead Stream, New Zealand. *Eclogae Geologicae Helvetiae,* 99(1):S79–S99. **https://doi.org/10.1007/s00015-006-0604-3**

Hollis, C.J., Dickens, G.R., Field, B.D., Jones, C.M., and Strong, C.P., 2005. The Paleocene–Eocene transition at Mead Stream, New Zealand: a southern Pacific record of early Cenozoic global change. *Palaeogeography, Palaeoclimatology, Palaeoecology,* 215(3–4):313–343. **https://doi.org/10.1016/j.palaeo.2004.09.011**

Hollis, C.J., Handley, L., Crouch, E.M., Morgans, H.E.G., Baker, J.A., Creech, J., Collins, K.S., Gibbs, S.J., Huber, M., Schouten, S., Zachos, J.C., and Pancost, R.D., 2009. Tropical sea temperatures in the high latitude South Pacific during the Eocene. *Geology,* 37(2):99–102. **https://doi.org/10.1130/G25200A.1**

Hollis, C.J., Taylor, K.W.R., Handley, L., Pancost, R.D., Huber, M., Creech, J.B., Hines, B.R., Crouch, E.M., Morgans, H.E.G., Crampton, J.S., Gibbs, S., Pearson, P.N., and Zachos, J.C., 2012. Early Paleogene temperature history of the Southwest Pacific Ocean: reconciling proxies and models. *Earth and Planetary Science Letters,* 349–350:53–66. **https://doi.org/10.1016/j.epsl.2012.06.024**

Huber, M., Brinkhuis, H., Stickley, C.E., Döös, K., Sluijs, A., Warnaar, J., Schellenberg, S.A., and Williams, G.L., 2004. Eocene circulation of the Southern Ocean: was Antarctica kept warm by subtropical waters? *Paleoceanography,* 19(4):PA4026. **https://doi.org/10.1029/2004PA001014**

Huber, M., and Caballero, R., 2011. The early Eocene equable climate problem revisited. *Climate of the Past,* 7(2):603–633. **https://doi.org/10.5194/cp-7-603-2011**

Ishizuka, O., Tani, K., Reagan, M.K., Kanayama, K., Umino, S., Harigane, Y., Sakamoto, I., Miyajima, Y., Yuasa, M., and Dunkley, D.J., 2011. The timescales of subduction initiation and subsequent evolution of an oceanic island arc. *Earth and Planetary Science Letters,* 306(3–4):229–240. **https://doi.org/10.1016/j.epsl.2011.04.006**

Karas, C., Nürnberg, D., Tiedemann, R., and Garbe-Schönberg, D., 2011. Pliocene climate change of the Southwest Pacific and the impact of ocean gateways. *Earth and Planetary Science Letters,* 301(1–2):117–124. **https://doi.org/10.1016/j.epsl.2010.10.028**

Keller, W.R., 2003. Cenozoic plate tectonic reconstructions and plate boundary processes in the southwest Pacific [Ph.D. dissertation]. California Institute of Technology. **http://resolver.caltech.edu/CaltechETD:etd-01102005-223039**

Kennett, J.P., 1977. Cenozoic evolution of Antarctic glaciation, the circum-Antarctic Ocean, and their impact on global paleoceanography. *Journal of Geophysical Research: Oceans and Atmospheres,* 82(27):3843–3860. **https://doi.org/10.1029/JC082i027p03843**

Kennett, J.P., and Exon, N.F., 2004. Paleoceanographic evolution of the Tasmanian seaway and its climatic implications. *In* Exon, N.F., Kennett, J.P., and Malone, M.J. (Eds.), *The Cenozoic Southern Ocean: Tectonics, Sedimentation, and Climate Change between Australia and Antarctica*. Geophysical Monograph, 151:345–367. **https://doi.org/10.1029/151GM19**

Kennett, J.P., Houtz, R.E., Andrews, P.B., Edwards, A.R., Gostin, V.A., Hajós, M., Hampton, M., Jenkins, D.G., Margolis, S.V., Ovenshine, A.T., and Perch-Nielsen, K., 1975. Cenozoic paleoceanography in the southwest Pacific Ocean, Antarctic glaciation, and the development of the Circum-Antarctic Current. *In* Kennett, J.P., Houtz, R.E., et al., *Initial Reports of the Deep Sea Drilling Project,* 29: Washington, DC (U.S. Government Printing Office), 1155–1169. **https://doi.org/10.2973/dsdp.proc.29.144.1975**

Kennett, J.P., and Shackleton, N.J., 1976. Oxygen isotopic evidence for the development of the psychrosphere 38 Myr ago. *Nature,* 260(5551):513–515. **https://doi.org/10.1038/260513a0**

Kennett, J.P., and von der Borch, C.C., 1986. Southwest Pacific Cenozoic paleoceanography. *In* Kennett, J.P., von der Borch, C.C., et al., *Initial Reports of the Deep Sea Drilling Project,* 90: Washington, DC (U.S. Government Printing Office), 1493–1517. **https://doi.org/10.2973/dsdp.proc.90.148.1986**

Kent, D.V., and Muttoni, G., 2008. Equatorial convergence of India and early Cenozoic climate trends. *Proceedings of the National Academy of Sciences of the United States of America,* 105(42):16065–16070. **https://doi.org/10.1073/pnas.0805382105**

King, P.R., and Thrasher, G.P., 1996. Cretaceous–Cenozoic geology and petroleum systems of the Taranaki Basin, New Zealand. *Institute of Geological & Nuclear Sciences Monograph,* 2.

Klingelhoefer, F., Lafoy, Y., Collot, J., Cosquer, E., Géli, L., Nouzé, H., and Vially, R., 2007. Crustal structure of the basin and ridge system west of New Caledonia (southwest Pacific) from wide-angle and reflection seismic data. *Journal of Geophysical Research: Solid Earth,* 112(B11):B11102. **https://doi.org/10.1029/2007JB005093**

Lafoy, Y., Brodien, I., Vially, R., and Exon, N.F., 2005. Structure of the basin and ridge system west of New Caledonia (southwest Pacific): a synthesis. *Marine Geophysical Research,* 26(1):37–50. **https://doi.org/10.1007/s11001-005-5184-5**

Laird, M.G., 1993. Cretaceous continental rifts: New Zealand region. *In* Ballance, P.F. (Ed.), *Sedimentary Basins of the World* (Volume 2): *South Pacific Sedimentary Basins*: Amsterdam (Elsevier), 37–49.

Lauretano, V., Hilgen, F.J., Zachos, J.C., and Lourens, L.J., 2016. Astronomically tuned age model for the early Eocene carbon isotope events: a new high-resolution $\delta^{13}C_{benthic}$ record of ODP Site 1263 between ~49 and ~54 Ma. *Newsletters on Stratigraphy,* 49(2):383–400. **https://doi.org/10.1127/nos/2016/0077**

Lee, C.-T.A., Shen, B., Slotnick, B.S., Liao, K., Dickens, G.R., Yokoyama, Y., Lenardic, A., Dasgupta, R., Jellinek, M., Lackey, J.S., et al., 2013. Continental arc–island arc fluctuations, growth of crustal carbonates, and long-term climate change. *Geosphere,* 9(1):21–36. **https://doi.org/10.1130/GES00822.1**

Leng, W., and Gurnis, M., 2015. Subduction initiation at relic arcs. *Geophysical Research Letters,* 42(17):7014–7021. **https://doi.org/10.1002/2015GL064985**

Lithgow-Bertelloni, C., and Richards, M.A., 1998. The dynamics of Cenozoic and Mesozoic plate motions. *Reviews of Geophysics,* 36(1):27–78. **https://doi.org/10.1029/97RG02282**

Lunt, D.J., Dunkley Jones, T., Heinemann, M., Huber, M., LeGrande, A., Winguth, A., Loptson, C., Marotzke, J., Roberts, C.D., Tindall, J., Valdes, P., et al., 2012. A model-data comparison for a multi-model ensemble of

early Eocene atmosphere-ocean simulations: EoMIP. *Climate of the Past,* 8(2):1716–1736. **https://doi.org/10.5194/cpd-8-1229-2012**

Matthews, K.J., Williams, S.E., Whittaker, J.M., Müller, R.D., Seton, M., and Clarke, G.L., 2015. Geologic and kinematic constraints on Late Cretaceous to mid Eocene plate boundaries in the southwest Pacific. *Earth-Science Reviews,* 140:72–107. **https://doi.org/10.1016/j.earscirev.2014.10.008**

Maurizot, P., 2011. First sedimentary record of the pre-obduction convergence in New Caledonia: formation of an early Eocene accretionary complex in the north of Grande Terre and emplacement of the "Montagnes Blanches" nappe. *Bulletin de la Société Géologique de France,* 182(6):479–491. **https://doi.org/10.2113/gssgfbull.182.6.479**

Maurizot, P., 2012. Palaeocene age for the Adio Limestone, New Caledonia: stratigraphic and regional context. *New Zealand Journal of Geology and Geophysics,* 56(1):16–26. **https://doi.org/10.1080/00288306.2012.735677**

McInerney, F.A., and Wing, S.L., 2011. The Paleocene–Eocene Thermal Maximum: a perturbation of carbon cycle, climate, and biosphere with implications for the future. *Annual Review of Earth and Planetary Sciences,* 39(1):489–516. **https://doi.org/10.1146/annurev-earth-040610-133431**

McKenzie, D.P., 1977. The initiation of trenches: a finite amplitude instability. *In* Talwani, M., and Pitman, W.C., III (Eds.), *Island Arcs, Deep Sea Trenches and Back-Arc Basins*. Maurice Ewing Series, 1:57–61. **https://agupubs.onlinelibrary.wiley.com/doi/10.1029/ME001p0057**

Meffre, S., Falloon, T.J., Crawford, T.J., Hoernle, K., Hauff, F., Duncan, R.A., Bloomer, S.H., and Wright, D.J., 2012. Basalts erupted along the Tongan fore arc during subduction initiation: evidence from geochronology of dredged rocks from the Tonga fore arc and trench. *Geochemistry, Geophysics, Geosystems,* 13(12):Q12003. **https://doi.org/10.1029/2012GC004335**

Mildenhall, D.C., Mortimer, N., Bassett, K.N., and Kennedy, E.M., 2014. Oligocene paleogeography of New Zealand: maximum marine transgression. *New Zealand Journal of Geology and Geophysics,* 57(2):107–109. **https://doi.org/10.1080/00288306.2014.904387**

Mortimer, N., 2004a. Basement gabbro from the Lord Howe Rise. *New Zealand Journal of Geology and Geophysics,* 47(3):501–507. **https://doi.org/10.1080/00288306.2004.9515072**

Mortimer, N., 2004b. New Zealand's geological foundations. *Gondwana Research,* 7(1):261–272. **https://doi.org/10.1016/S1342-937X(05)70324-5**

Mortimer, N., Campbell, H.J., Tulloch, A.J., King, P.R., Stagpoole, V.M., Wood, R.A., Rattenbury, M.S., et al., 2017. Zealandia: Earth's hidden continent. *GSA Today,* 27(3):27–35. **https://doi.org/10.1130/GSATG321A.1**

Mortimer, N., Gans, P.B., Palin, J.M., Herzer, R.H., Pelletier, B., and Monzier, M., 2014. Eocene and Oligocene basins and ridges of the Coral Sea–New Caledonia region: tectonic link between Melanesia, Fiji, and Zealandia. *Tectonics,* 33(7):1386–1407. **https://doi.org/10.1002/2014TC003598**

Mortimer, N., Hauff, F., and Calvert, A.T., 2008. Continuation of the New England orogen, Australia, beneath the Queensland Plateau and Lord Howe Rise. *Australian Journal of Earth Sciences,* 55(2):195–209. **https://doi.org/10.1080/08120090701689365**

Mortimer, N., Herzer, R.H., Gans, P.B., Laporte-Magoni, C., Calvert, A.T., and Bosch, D., 2007. Oligocene–Miocene tectonic evolution of the South Fiji Basin and Northland Plateau, SW Pacific Ocean: evidence from petrology and dating of dredged rocks. *Marine Geology,* 237(1–2):1–24. **https://doi.org/10.1016/j.margeo.2006.10.033**

Mortimer, N., Herzer, R.H., Gans, P.B., Parkinson, D.L., and Seward, D., 1998. Basement geology from Three Kings Ridge to West Norfolk Ridge, southwest Pacific Ocean: evidence from petrology, geochemistry and isotopic dating of dredge samples. *Marine Geology,* 148(3–4):135–162. **https://doi.org/10.1016/S0025-3227(98)00007-3**

Mortimer, N., Tulloch, A.J., Spark, R.N., Walker, N.W., Ladley, E., Allibone, A., and Kimbrough, D.L., 1999. Overview of the Median Batholith, New Zealand: a new interpretation of the geology of the Median Tectonic Zone and adjacent rocks. *Journal of African Earth Sciences,* 29(1):257–268. **https://doi.org/10.1016/S0899-5362(99)00095-0**

Müller, R.D., Gaina, C., Tikku, A., Mihut, D., Cande, S.C., and Stock, J.M., 2000. Mesozoic/Cenozoic tectonic events around Australia. *In* Richards, M.A., Gordon, R.G., and Van Der Hilst, R.D. (Eds.), *The History and Dynamics of Global Plate Motions.* Geophysical Monograph, 121:161–188. **https://doi.org/10.1029/GM121p0161**

Nelson, C.S., and Cooke, P.J., 2001. History of oceanic front development in the New Zealand sector of the Southern Ocean during the Cenozoic—a synthesis. *New Zealand Journal of Geology and Geophysics,* 44(4):535–553. **https://doi.org/10.1080/00288306.2001.9514954**

Nelson, C.S., and Hancock, G.E., 1984. Composition and origin of temperate skeletal carbonate sediments on South Maria Ridge, northern New Zealand. *New Zealand Journal of Marine and Freshwater Research,* 18(2):221–239. **https://doi.org/10.1080/00288330.1984.9516044**

Nicolo, M.J., Dickens, G.R., Hollis, C.J., and Zachos, J.C., 2007. Multiple early Eocene hyperthermals: their sedimentary expression on the New Zealand continental margin and in the deep sea. *Geology,* 35(8):699–702. **https://doi.org/10.1130/G23648A.1**

Pagani, M., Caldeira, K. Archer, D., and Zachos, J.C., 2006. An ancient carbon mystery. *Science,* 314(5805):1556–1557. **https://doi.org/10.1126/science.1136110**

Pagani, M., Huber, M., Liu, Z., Bohaty, S.M., Henderiks, J., Sijp, W., Krishnan, S., and DeConto, R.M., 2011. The role of carbon dioxide during the onset of Antarctic glaciation. *Science,* 334(6060):1261–1264. **https://doi.org/10.1126/science.1203909**

Pearson, P.N., Foster, G.L., and Wade, B.S., 2009. Atmospheric carbon dioxide through the Eocene–Oligocene climate transition. *Nature,* 461(7267):1110–1113. **https://doi.org/10.1038/nature08447**

Pearson, P.N., and Palmer, M.R., 2000. Atmospheric carbon dioxide concentrations over the past 60 million years. *Nature,* 406(6979):695–699. **https://doi.org/10.1038/35021000**

Pirard, C., and Spandler, C., 2017. The zircon record of high-pressure metasedimentary rocks of New Caledonia: implications for regional tectonics of the south-west Pacific. *Gondwana Research,* 46:79–94. **https://doi.org/10.1016/j.gr.2017.03.001**

Pross, J., Contreras, L., Bijl, P.K., Greenwood, D.R., Bohaty, S.M., Schouten, S., Bendle, J.A., et al., 2012. Persistent near-tropical warmth on the Antarctic continent during the early Eocene epoch. *Nature,* 488(7409):73–77. **https://doi.org/10.1038/nature11300**

Rait, G., Chanier, F., and Waters, D.W., 1991. Landward- and seaward-directed thrusting accompanying the onset of subduction beneath New Zealand. *Geology,* 19(3):230–233. **https://doi.org/10.1130/0091-7613(1991)019<0230:LASDTA>2.3.CO;2**

Raymo, M.E., and Ruddiman, W.F., 1992. Tectonic forcing of late Cenozoic climate. *Nature,* 359(6391):117–122. **https://doi.org/10.1038/359117a0**

Rea, D.K., Basov, I.A., Krissek, L.A., and the Leg 145 Scientific Party, 1995. Scientific results of drilling the North Pacific transect. *In* Rea, D.K., Basov, I.A., Scholl, D.W., and Allan, J.F. (Eds.), *Proceedings of the Ocean Drilling Program, Scientific Results,* 145: College Station, TX (Ocean Drilling Program), 577–596. **https://doi.org/10.2973/odp.proc.sr.145.146.1995**

Reagan, M.K., McClelland, W.C., Girard, G., Goff, K.R., Peate, D.W., Ohara, Y., and Stern, R.J., 2013. The geology of the southern Mariana fore-arc crust: implications for the scale of Eocene volcanism in the western Pacific. *Earth and Planetary Science Letters,* 380:41–51. **https://doi.org/10.1016/j.epsl.2013.08.013**

Ridgwell, A., and Zeebe, R.E., 2005. The role of the global carbonate cycle in the regulation and evolution of the Earth system. *Earth and Planetary Science Letters,* 234(3–4):299–315. **https://doi.org/10.1016/j.epsl.2005.03.006**

Rintoul, S.R., Hughes, C., and Olbers, D., 2001. The Antarctic circumpolar current system. *In* Siedler, G., Church, J., and Gould, J. (Eds.), *Ocean Circulation and Climate.* International Geophysics, 77:271–302. **https://doi.org/10.1016/S0074-6142(01)80124-8**

Rouillard, P., Collot, J., Sutherland, R., Bache, F., Patriat, M., Etienne, S., and Maurizot, P., 2017. Seismic stratigraphy and paleogeographic evolution of Fairway Basin, Northern Zealandia, Southwest Pacific: from Cretaceous Gondwana breakup to Cenozoic Tonga–Kermadec subduction. *Basin Research,* 29(S1):189–212. **https://doi.org/10.1111/bre.12144**

Royer, J.-Y., and Rollet, N., 1997. Plate-tectonic setting of the Tasmanian region. *In* Exon, N.F., and Crawford, A.J. (Eds.), *West Tasmanian Margin and Offshore Plateaus: Geology, Tectonic and Climatic History, and Resource Potential.* Australian Journal of Earth Sciences, 44(5):543–560. **https://doi.org/10.1080/08120099708728336**

Schellart, W.P., Lister, G.S., and Toy, V.G., 2006. A Late Cretaceous and Cenozoic reconstruction of the Southwest Pacific region: tectonics controlled by subduction and slab rollback processes. *Earth-Science Reviews,* 76(3–4):191–233. **https://doi.org/10.1016/j.earscirev.2006.01.002**

Seton, M., Müller, R.D., Zahirovic, S., Gaina, C., Torsvik, T., Shephard, G., Talsma, A., Gurnis, M., Turner, M., Maus, S., and Chandler, M., 2012. Global continental and ocean basin reconstructions since 200 Ma. *Earth-Science Reviews,* 113(3–4):212–270. **https://doi.org/10.1016/j.earscirev.2012.03.002**

Sharp, W.D., and Clague, D.A., 2006. 50-Ma initiation of Hawaiian-Emperor Bend records major change in Pacific plate motion. *Science,* 313(5791):1281–1284. **https://doi.org/10.1126/science.1128489**

Shaffer, G., Huber, M., Rondanelli, R., and Pepke Pedersen, J.O., 2016. Deep time evidence for climate sensitivity increase with warming. *Geophysical Research Letters,* 43(12):6538–6545. **https://doi.org/10.1002/2016GL069243**

Shipboard Scientific Party, 1973a. Site 206. With contributions by D. Burns and P.N. Webb. *In* Burns, R.E., Andrews, J.E., et al., *Initial Reports of the Deep Sea Drilling Project,* 21: Washington, DC (U.S. Government Printing Office), 103–195. **https://doi.org/10.2973/dsdp.proc.21.106.1973**

Shipboard Scientific Party, 1973b. Site 207. With contributions by D. Burns, W.A. Watters, and P.N. Webb. *In* Burns, R.E., Andrews, J.E., et al., *Initial Reports of the Deep Sea Drilling Project,* 21: Washington, DC (U.S. Government Printing Office), 197–269. **https://doi.org/10.2973/dsdp.proc.21.107.1973**

Shipboard Scientific Party, 1973c. Site 208. With contributions by D. Burns and P.N. Webb. *In* Burns, R.E., Andrews, J.E., et al., *Initial Reports of the Deep Sea Drilling Project,* 21: Washington, DC (U.S. Government Printing Office), 271–331. **https://doi.org/10.2973/dsdp.proc.21.108.1973**

Shipboard Scientific Party, 1986a. Site 592: Lord Howe Rise, 36°S. *In* Kennett, J.P., von der Borch, C.C., et al., *Initial Reports of the Deep Sea Drilling Project,* 90: Washington, DC (U.S. Government Printing Office), 139–252. **https://doi.org/10.2973/dsdp.proc.90.108.1986**

Shipboard Scientific Party, 1986b. Site 593: Challenger Plateau. *In* Kennett, J.P., von der Borch, C.C., et al., *Initial Reports of the Deep Sea Drilling Project,* 90: Washington, DC (U.S. Government Printing Office), 551–651. **https://doi.org/10.2973/dsdp.proc.90.109.1986**

Slotnick, B.S., Dickens, G.R., Nicolo, M.J., Hollis, C.J., Crampton, J.S., Zachos, J.C., and Sluijs, A., 2012. Large-amplitude variations in carbon cycling and terrestrial weathering during the latest Paleocene and earliest Eocene: the record at Mead Stream, New Zealand. *The Journal of Geology,* 120(5):487–505. **https://doi.org/10.1086/666743**

Snyder, G.T, Hiruta, A., Matsumoto, R., Dickens, G.R., Tomaru, H., Takeuchi, R., Komatsubara, J., Ishida, Y., and Yu, H., 2007. Pore water profiles and authigenic mineralization in shallow marine sediments above the methane-charged system on Umitaka Spur, Japan Sea. *Deep-Sea Research, Part II,* 54(11–13):1216–1239. **https://doi.org/10.1016/j.dsr2.2007.04.001**

Spandler, C., Rubatto, D., and Hermann, J., 2005. Late Cretaceous–Tertiary tectonics of the southwest Pacific: insights from U-Pb sensitive, high-resolution ion microprobe (SHRIMP) dating of eclogite facies rocks from New Caledonia. *Tectonics,* 24(3):TC3003. **https://doi.org/10.1029/2004TC001709**

Stadler, G., Gurnis, M., Burstedde, C., Wilcox, L.C., Alisic, L., and Ghattas, O., 2010. The dynamics of plate tectonics and mantle flow: from local to global scales. *Science,* 329(5995):1033–1038. **https://doi.org/10.1126/science.1191223**

Stagpoole, V., and Nicol, A., 2008. Regional structure and kinematic history of a large subduction back thrust: Taranaki Fault, New Zealand. *Journal of Geophysical Research: Solid Earth,* 113(B1):B01403. **https://doi.org/10.1029/2007JB005170**

Steinberger, B., Sutherland, R., and O'Connell, R.J., 2004. Prediction of Emperor–Hawaii Seamount locations from a revised model of global plate motion and mantle flow. *Nature,* 430(6996):167–173. **https://doi.org/10.1038/nature02660**

Stern, R.J., 2004. Subduction initiation: spontaneous and induced. *Earth and Planetary Science Letters,* 226(3–4):275–292. **https://doi.org/10.1016/j.epsl.2004.08.007**

Stern, R.J., and Bloomer, S.H., 1992. Subduction zone infancy: examples from the Eocene Izu-Bonin-Mariana and Jurassic California arcs. *Geological Society of America Bulletin,* 104(12):1621–1636. **https://doi.org/10.1130/0016-7606(1992)104<1621:SZIEFT>2.3.CO;2**

Sutherland, R., 1995. The Australia-Pacific boundary and Cenozoic plate motions in the SW Pacific: some constraints from Geosat data. *Tectonics,* 14(4):819–831. **https://doi.org/10.1029/95TC00930**

Sutherland, R., 1999. Basement geology and tectonic development of the greater New Zealand region: an interpretation from regional magnetic data. *Tectonophysics,* 308(3):341–362. **https://doi.org/10.1016/S0040-1951(99)00108-0**

Sutherland, R., Collot, J., Bache, F., Henrys, S., Barker, D., Browne, G., Lawrence, M., Morgans, H., Hollis, C., and Clowes, C., 2017. Widespread compression associated with Eocene Tonga-Kermadec subduction initiation. *Geology,* 45(4):355–358. **https://doi.org/10.1130/G38617.1**

Sutherland, R., Collot, J., Lafoy, Y., Logan, G.A., Hackney, R., Stagpoole, V., Uruski, C., et al., 2010. Lithosphere delamination with foundering of lower crust and mantle caused permanent subsidence of New Caledonia Trough and transient uplift of Lord Howe Rise during Eocene and Oligocene initiation of Tonga-Kermadec subduction, western Pacific. *Tectonics,* 29(2). **https://doi.org/10.1029/2009TC002476**

Sutherland, R., Dickens, G.R., and Blum, P., 2016. *Expedition 371 Scientific Prospectus: Tasman Frontier Subduction Initiation and Paleogene Climate.* International Ocean Discovery Program. **https://doi.org/10.14379/iodp.sp.371.2016**

Toth, J., and Gurnis, M., 1998. Dynamics of subduction initiation at preexisting fault zones. *Journal of Geophysical Research: Solid Earth,* 103(B8):18053–18067. **https://doi.org/10.1029/98JB01076**

Tripati, A.K., Delaney, M.L., Zachos, J.C., Anderson, L.D., Kelly, D.C., and Elderfield, H., 2003. Tropical sea-surface temperature reconstruction for the early Paleogene using Mg/Ca ratios of planktonic foraminifera. *Paleoceanography,* 18(4):1101–1113. **https://doi.org/10.1029/2003PA000937**

Tulloch, A.J., Kimbrough, D.L., and Wood, R.A., 1991. Carboniferous granite basement dredged from a site on the southwest margin of the Challenger Plateau, Tasman Sea. *New Zealand Journal of Geology and Geophysics,* 34(2):121–126. **https://doi.org/10.1080/00288306.1991.9514449**

Tulloch, A.J., Ramezani, J., Mortimer, N., Mortensen, J., van den Bogaard, P., and Maas, R., 2009. Cretaceous felsic volcanism in New Zealand and Lord Howe Rise (Zealandia) as a precursor to final Gondwana break-up. *In* Ring, U., and Wernicke, B. (Eds.), *Extending a Continent: Architecture, Rheology and Heat Budget.* Geological Society Special Publication, 321(1):89–118. **https://doi.org/10.1144/SP321.5**

Turcotte, D.L., Haxby, W.F., and Ockendon, J.R., 1977. Lithospheric instabilities. *In* Talwani, M., and Pitman, W.C., III (Eds.), *Island Arcs, Deep Sea Trenches and Back-Arc Basins.* Maurice Ewing Series, 1:63–69. **http://onlinelibrary.wiley.com/doi/10.1029/ME001p0063/summary**

Uruski, C., and Wood, R., 1991. A new look at the New Caledonia Basin, an extension of the Taranaki Basin, offshore North Island, New Zealand. *Marine and Petroleum Geology,* 8(4):379–391. **https://doi.org/10.1016/0264-8172(91)90061-5**

Uruski, C.I., 2008. Deepwater Taranaki, New Zealand: structural development and petroleum potential. *Exploration Geophysics,* 39(2):94–107. **https://doi.org/10.1071/EG08013**

van Andel, T.H., Heath, G.R., and Moore, T.C., Jr., 1975. Cenozoic history of the central equatorial Pacific Ocean: a synthesis based on Deep Sea Drilling Project data. *In* Sutton, G.H., Manghnani, M.H., Moberly, R., and Mcafee, E.U. (Eds.), *The Geophysics of the Pacific Ocean Basin and its Margin.* Geophysical Monograph, 19:281–295. **https://doi.org/10.1029/GM019p0281**

Vitale Brovarone, A., Agard, P., Monié, P., Chauvet, A., and Rabaute, A., 2018. Tectonic and metamorphic architecture of the HP belt of New Caledonia.

Earth-Science Reviews, 178:48–67. **https://doi.org/10.1016/j.earscirev.2018.01.006**

Weissel, J.K., and Hayes, D.E., 1977. Evolution of the Tasman Sea reappraised. *Earth and Planetary Science Letters,* 36(1):77–84. **https://doi.org/10.1016/0012-821X(77)90189-3**

Westerhold, T., Röhl, U., Donner, B., and Zachos, J.C., 2018. Global extent of early Eocene hyperthermal events: a new Pacific benthic foraminiferal isotope record from Shatsky Rise (ODP Site 1209). *Paleoceanography and Paleoclimatology,* 33(6):626–642. **https://doi.org/10.1029/2017PA003306**

Whattam, S.A., Malpas, J., Ali, J.R., and Smith, I.E.M., 2008. New SW Pacific tectonic model: cyclical intraoceanic magmatic arc construction and near-coeval emplacement along the Australia-Pacific margin in the Cenozoic. *Geochemistry, Geophysics, Geosystems,* 9(3):Q03021. **https://doi.org/10.1029/2007GC001710**

Whittaker, J.M., Müller, R.D., Leitchenkov, G., Stagg, H., Sdrolias, M., Gaina, C., and Goncharov, A., 2007. Major Australian-Antarctic plate reorganization at Hawaiian-Emperor Bend time. *Science,* 318(5847):83–86. **https://doi.org/10.1126/science.1143769**

Wood, R., and Woodward, D., 2002. Sediment thickness and crustal structure of offshore western New Zealand from 3D gravity modelling. *New Zealand Journal of Geology and Geophysics,* 45(2):243–255. **https://doi.org/10.1080/00288306.2002.9514971**

Wood, R.A., Lamarche, G., Herzer, R.H., Delteil, J., and Davy, B., 1996. Paleogene seafloor spreading in the southeast Tasman Sea. *Tectonics,* 15(5):966–975. **https://doi.org/10.1029/96TC00129**

Zachos, J.C., Dickens, G.R., and Zeebe, R.E., 2008. An early Cenozoic perspective on greenhouse warming and carbon-cycle dynamics. *Nature,* 451(7176):279–283. **https://doi.org/10.1038/nature06588**

Zachos, J.C., Röhl, U., Schellenberg, S.A., Sluijs, A., Hodell, D.A., Kelly, D.C., Thomas, E., Nicolo, M., Raffi, I., Lourens, L.J., McCarren, H., and Kroon, D., 2005. Rapid acidification of the ocean during the Paleocene–Eocene Thermal Maximum. *Science,* 308(5728):1611–1615. **https://doi.org/10.1126/science.1109004**

Zeebe, R.E., and Zachos, J.C., 2013. Long-term legacy of massive carbon input to the Earth system: Anthropocene versus Eocene. *Philosophical Transactions of the Royal Society A: Mathematical, Physical & Engineering Sciences,* 371(2001):20120006. **https://doi.org/10.1098/rsta.2012.0006**